CONVERSION OF CO_2 TO POLYCARBONATES AND OTHER MATERIALS: INSIGHTS THROUGH COMPUTATIONAL CHEMISTRY

A Dissertation

by

ANDREW D. YEUNG

Submitted to the Office of Graduate and Professional Studies of
Texas A&M University
in partial fulfillment of the requirements for the degree of

DOCTOR OF PHILOSOPHY

Chair of Committee	Donald J. Darensbourg
Committee Members	Marcetta Y. Darensbourg
	Michael B. Hall
	Oleg V. Ozerov
	Jamie C. Grunlan
Head of Department	David H. Russell

December 2014

Major Subject: Chemistry

ABSTRACT

The use of carbon dioxide as a chemical feedstock for the copolymerization with epoxides to give polycarbonates, and for coupling with hydrocarbons to give carboxylic acids, was probed using computational chemistry. Metal-free systems were modeled at high levels using composite methods that give "chemical accuracy", whereas metal-bound systems were studied using density functional theory, benchmarked to these high-accuracy results for confidence.

The thermodynamics of polymer vs. cyclic carbonate formation was calculated, and polymer is the exothermic product, whereas cyclic carbonate is the entropic product. The barriers for the metal-free carbonate and alkoxide backbiting reactions were also determined, carbonate backbiting having a higher barrier than alkoxide backbiting. The base degradation of polymers to epoxide co-monomers, and the acid- and base-catalyzed degradation of glycerol carbonate to glycidol were investigated too. Poly(cyclopentene carbonate) preferentially degrades to epoxide co-monomer instead of cyclic carbonate due to angle strain for alkoxide backbiting. Conversely, glycerol carbonate only yields glycidol instead of the isomeric 3-hydroxyoxetane because formation of the latter has a higher barrier.

The (salen)Cr(III)- and (salen)Co(III)-catalyzed copolymerization reactions were studied for a variety of epoxides, and the overall displacement of a polymeric carbonate by an epoxide, followed by ring-opening, was found to be rate limiting. Chromium(III)-catalyzed systems have higher free energy barriers than cobalt(III) systems due to enthalpy, which explains why such polymerization reactions have to be run at higher temperatures. The metal-bound polymer carbonate and alkoxide backbiting reactions generally have higher barriers than when unbound, due to the terminal oxygen atoms' reduced nucleophilicity.

The carboxylation of metal-hydride and metal-carbon bonds was studied for a series of *trans*-ML_2XY complexes, and thermodynamics of carboxylation of the M-X bond are influenced by M, L, and Y, in decreasing order. Similar *cis*-complexes did not exhibit as clear trends. Examination of these complexes indicated that the three steps for the overall conversion of hydrocarbons to carboxylic acids (oxidative addition of hydrocarbon, carboxylation, and reductive elimination of the carboxylic acid) must be optimized in parallel for the successful direct synthesis of carboxylic acids.

DEDICATION

I dedicate this dissertation to the memory of my mother. She taught me so much: to value education, to strive for excellence, and to reach for our goals through diligence.

ACKNOWLEDGMENTS

I am immensely appreciative toward my advisor, Professor Donald J. Darensbourg, for providing me with opportunities that led to my growth as a chemist and researcher. Being trained as a synthetic inorganic chemist, my learning curve for getting into computational chemistry was extremely steep. Don tolerated many months with little results as I grappled with this foreign environment. He could simply have told me to get back to the bench, but he did not. In Don's mentoring style, he pointed us in a general direction, and had us figure out what the problems were in that field, and how they might be solved. I took ownership of my research project, and it has made this dissertation stronger as a result. Don also gave me much time and funds to represent our group at various conferences, which has broadened my horizons, and provided me with much exposure. In fact, at this time of writing, I have just returned from the Gordon Research Conference on Green Chemistry in Hong Kong, which I fondly remember as "summer camp for chemists".

I would like to thank Professors Marcetta Y. Darensbourg, Michael B. Hall, Oleg V. Ozerov, and Jaime C. Grunlan for serving on my committee, for offering suggestions to my work, and for keeping me on my toes. I have also enjoyed my informal interactions with Marcetta, and thank her for her care and concern beyond the laboratory.

Professionally, my journey as a chemist started in Professor Han Vinh Huynh's laboratory in Singapore almost a decade ago. He personally taught me synthetic inorganic chemistry, including using Schlenk technique to handle air-sensitive compounds. While I do not do much of that type of work now, his excellent instruction allows me to continue to assist my experimentalist colleagues at the Darensbourg laboratory. Beyond these techniques, he taught me to think like a chemist, and write like

a chemist. This good grounding has allowed me to move around different areas of chemistry with relative ease.

When I left the Huynh laboratory for the Darensbourg laboratory, I expected to be performing synthetic inorganic and polymer chemistry like generations before me. Evidently, that plan did not come to fruition. Don had all of us take Dr. Hall's class entitled "Structure and Bonding" that utilized computational chemistry as a teaching aid. In that class, Dr. Hall made a comment about computational chemistry becoming as routinely performed by experimentalists as NMR (inaccuracies regretted). That comment and that course were the proximal causes for my change in direction.

The nuts and bolts of computational chemistry in Dr. Hall's course were taught by Dr. Lisa M. Pérez. I enjoyed that part of the course so much that I took Lisa's workshops and her standalone course over the summer. She helped me a great deal in my early work, and I would have failed without the foundation that she gave me. Other influences in my brief career in computational chemistry include Professors Steven E. Wheeler in our department, Edward N. Brothers at TAMU Qatar, and Angela K. Wilson at the University of North Texas; I am grateful for their comments and suggestions in my work.

I want to acknowledge the Darensbourgs' assistant, Ethel Mejia, for keeping my paperwork and duties straight. More importantly, I thank her for her friendship. My current and former colleagues have also made my time in the Darensbourg laboratory so much richer. My predecessors are Drs. Osit "Pop" Karroonnirun, Ross Poland, Sheng-Hsuan "Sunshine" Wei, and Stephanie Wilson. I joined the Darensbourg lab with Wan-Chun "Joanna" Chung, and Sam Kyran. I have known them the best, and the longest, and I am somewhat sore that they are *both* unavailable to attend my final defense. Lastly, we have Yanyan Wang, the baby of the group. I also wish to thank the various post-doctoral students and visiting scholars that cycle through our laboratory. I also

appreciate the presence of Marcetta's group; combined with ours, we have developed a great sense of community.

Beyond the Darensbourg hallway, I have made many other friends here. I will always remember the times we have had at various dining tables, restaurants, and swimming pools.

I was aided in this endeavor by encouragement by my father and brother in Singapore. They have always had faith in my abilities to accomplish what I intend, and have given me the confidence to choose the path less traveled. Here in College Station to celebrate my triumphs and guide me through my troubles was my ever-present wife, Melissa. Without her, this work would truly have been impossible.

TABLE OF CONTENTS

Page

LIST OF SCHEMES

Page

LIST OF FIGURES

Page

LIST OF TABLES

Page

CHAPTER I

INTRODUCTION AND LITERATURE REVIEW*

Introduction

Carbon dioxide is a product of burning carbonaceous fuel, and humans produce it on a grand scale: *ca.* 35 gigatonnes per year. As a greenhouse gas, its increasing concentration in the air is linked to global climate change. There are numerous strategies to reduce carbon dioxide's accumulation, and sequestration in geologic formations is viewed by some as a long-term solution.[1] CO_2 utilization is complementary to such efforts, and incorporation of this gas in useful products provides an opportunity for indirect storage. The production of polycarbonates from CO_2 and epoxides (**Scheme I-1**) is one of the focuses of the U.S. Department of Energy's Carbon Storage Program.[2] As significant energy costs are involved in mechanically compressing CO_2 for use,[3] efforts are being made toward the direct use of CO_2 within flue gas.[4-5]

This copolymerization reaction that was first reported by Inoue and coworkers in 1969[6] converts an otherwise undesirable waste product into a useful chemical feedstock. Some of these polycarbonates have been commercialized as packaging material and coatings,[7-8] while low molecular weight poly(propylene carbonate) serves as a drop-in replacement for poly(propylene oxide) used for preparing polyurethanes.[9] Catalytic systems that produce these polycarbonates have been comprehensively reviewed.[10-20]

In the general reaction, the polymerization reaction begins when an epoxide co-monomer displaces a metal-bound initiator ligand. The epoxide is activated by a Lewis

* Adapted from Darensbourg, D. J.; Yeung, A. D. *Polym. Chem.* **2014**, *5*, 3949. - Reproduced by permission of The Royal Society of Chemistry. This article is also located at http://pubs.rsc.org/en/Content/ArticleLanding/2014/PY/c4py00299g.

acidic metal center, and undergoes nucleophilic attack by a suitable initiator, undergoing ring-opening. The alkoxide formed reacts with CO_2 to form a carbonate (**Scheme I-2**). This carbonate serves as the nucleophile for subsequent epoxide ring-opening reactions (**Scheme I-3**), and the catalytic cycle continues. Along the way, the polymeric carbonate or alkoxide may backbite while metal-bound or metal-free to give the undesired cyclic carbonate.

Scheme I-1. Reaction between CO_2 and an epoxide to yield the desired copolymer, and cyclic carbonate side-product.

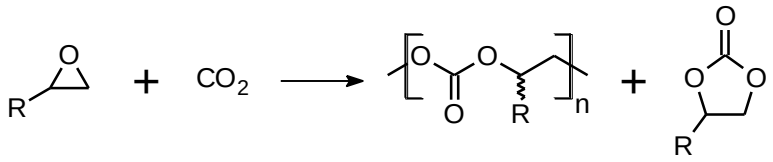

Scheme I-2. The initiation step for the general CO_2-epoxide copolymerization reaction.

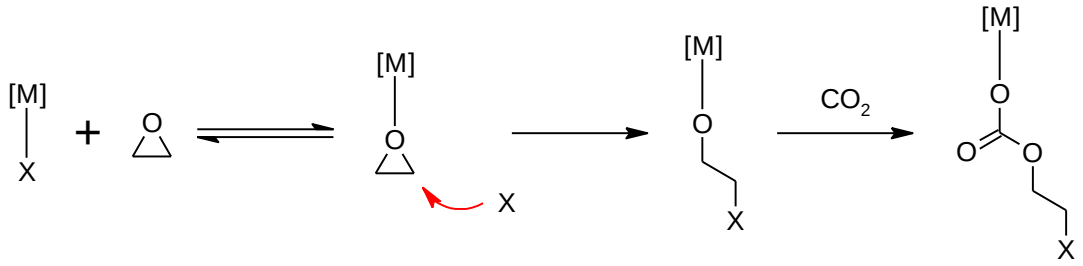

Scheme I-3. Propagation: Once the initial carbonate is formed, the copolymerization proceeds by successive epoxide ring-opening reactions, followed by CO_2 insertion into the metal-alkoxide bond. The polymeric carbonate (top) or alkoxide (bottom) may undergo backbiting while metal-bound or metal-free to produce, in this instance, the undesired cyclic carbonate side-product.

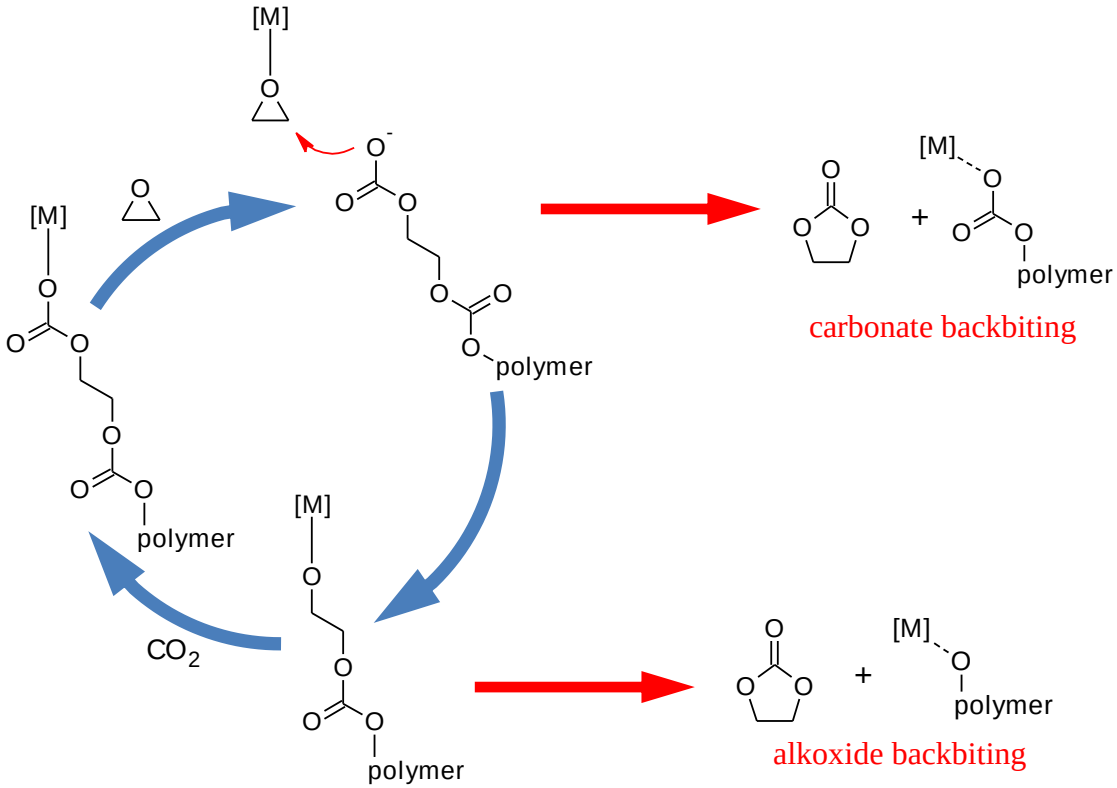

The first generation of catalysts comprises zinc complexes, such as zinc phenoxides,[21-22] that trace their lineage to Inoue's diethylzinc-water system. Coates *et al.* showed that the zinc-catalyzed reaction was second order in [Zn],[23] leading to the design of dizinc complexes by Coates' and Williams' groups (Figure I-1a). Early zinc catalysts were effective for copolymerizing cyclohexene oxide with carbon dioxide, but ineffective for the analogous reaction with propylene oxide. Due to zinc's Lewis acidity, some of these systems catalyzed the epoxide homopolymerization reaction too, resulting in polyether defects within the polycarbonate. The more mature systems are very active, and can

provide polyether-free polycarbonate at low CO_2 partial pressures.[24] Zinc catalysts are especially well covered in Williams *et al.*'s review.[17]

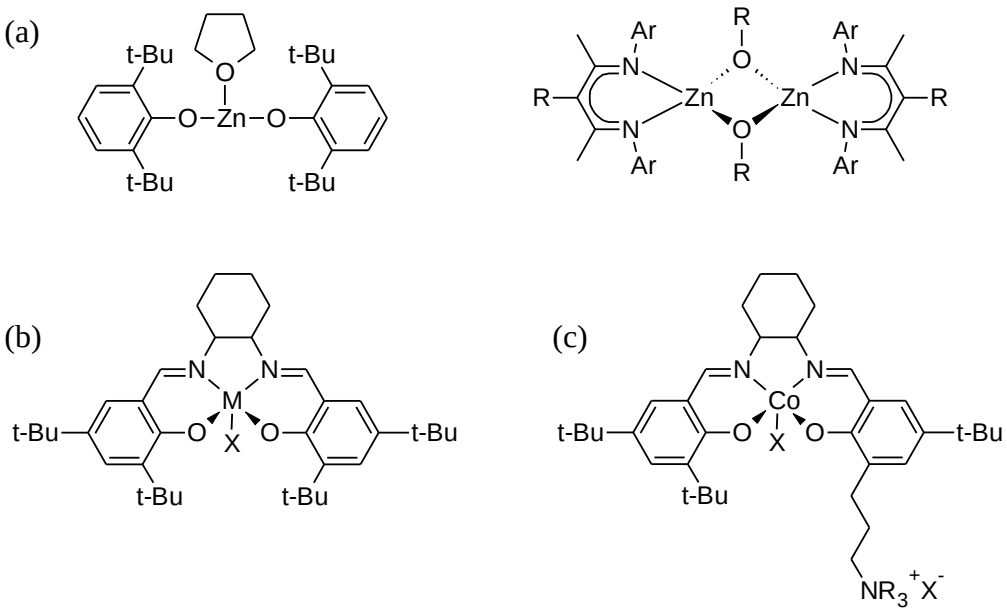

Figure I-1. Examples of catalysts for the CO_2-epoxide copolymerization: (a) First generation: a zinc phenoxide catalyst, and a (β-diiminate)zinc dizinc catalysts. (b) Second generation (salen)M(III)X catalysts, usually used with cocatalysts. (c) Third generation bifunctional salen-type catalyst that comes with its own cocatalyst.

Subsequently, a second generation of catalysts derived from porphyrin and salen complexes were developed (Figure I-1b). In the absence of an onium salt, these catalysts were second order in metal, reminiscent of the well-studied epoxide hydrolysis reaction.[25] Coates and coworkers' binap-linked dinuclear cobalt complex was an elegant response to the rate law.[26-28] However, the addition of cocatalysts converted the square pyramidal complexes to octahedral complexes that were first order in metal. Especially effective cocatalysts in use are the chloride, azide, and dinitrophenolate anions, and the N,N-dimethylaminopyridine (DMAP) and N-methyltriazabicyclodecene (mTBD) neutral amines. These catalysts required modest CO_2 pressures to operate, but yielded copolymers with perfect CO_2 incorporation. Unfortunately, these systems generate cyclic

carbonates in addition to the desired polymer. These second generation salen-type catalysts have been comprehensively reviewed by Darensbourg.[15]

Third generation cobalt catalysts featuring built-in cocatalysts emerged thereafter (Figure I-1c). Those bearing quaternary onium cation arms had the added benefit, in that the dissociated anionic polymer chain was kept from being lost to the bulk of the reaction mixture. Proximity allows the polymeric carbonate to quickly return to ring-open the epoxide that displaced it from the metal center. Furthermore, the tethered polymer is prevented from attacking itself, thereby reducing monomer wastage through cyclic carbonate formation. Since they contain their own built-in cocatalyst, they are also named bifunctional catalysts, as opposed to prior binary catalyst/cocatalyst systems. These third generation cobalt catalysts are some of the best to date, and they operate at high temperatures (70-110 °C) that the conventional salen complexes could not survive.[18-19]

Now that good general purpose catalysts have been developed, attention has turned toward alternate epoxide monomers such as styrene, chloropropylene, and indene oxides (Figure I-2).[29] Poly(indene carbonate) in particular, has the highest reported T_g (138 °C) for a CO_2-epoxide polycarbonate.[29-30] Renewable feedstocks in the form of limonene oxide have been tried too.[31] Increasing attention is being given toward synthesizing polycarbonate polyols as precursors for ABA-type triblock polymers; poly(propylene carbonate), 43 % CO_2 by weight, is a drop-in replacement for poly(propylene oxide) in the production of polyurethane that has been commercialized by Bayer as *polyether polycarbonate polyols*.[9] Of current interest are glycerol carbonates[32-33] and polycarbonates[34-35] ultimately derived from glycerol and CO_2. Such carbonates represent the conversion of two burdensome waste streams into useful materials.

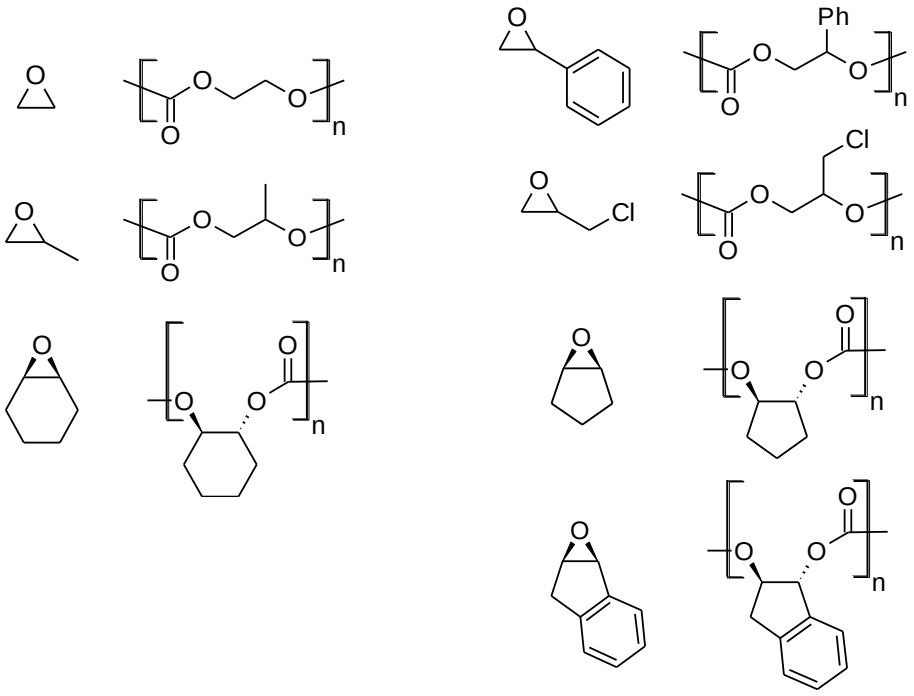

Figure I-2. Polycarbonates and their corresponding epoxide precursors. Commercialized: Poly(ethylene carbonate, poly(propylene carbonate), poly(cyclohexene carbonate); investigational: Poly(styrene carbonate), poly(chloropropylene carbonate), poly(cyclopentene oxide), and poly(indene carbonate) (top-bottom).

While much of the current mechanistic understanding of these polycarbonate-forming reactions has been derived from experimental work, the use of computational methods is increasingly popular for solving chemistry problems. The judicious use of computational chemistry can reduce the amount of experimental work to be done, leading to the use of fewer expensive reagents and the generation of less waste. Significantly, computational chemistry allows the chemist to consider elementary reactions separate from other competing reactions. In contrast, many kinetics experiments are unable to distinguish the effects of multiple pathways.

Morokuma and coworkers[36] were the first to examine the CO_2-epoxide copolymerization using computational chemistry in 2002. Much has transpired since, though no survey of these computational studies has been performed. Herein, we explore the use of quantum mechanical methods toward understanding the CO_2-epoxide copolymerization. Outside the scope of this work, reviews of computational methods applied toward utilizing CO_2,[37-38] and of the computational prediction of other polymer properties[39] are available.

Thermodynamics of polymer formation

Polymerization processes involve the agglomeration of small monomeric units, resulting in the formation of a large macromolecule, with a concomitant decrease in the system's entropy. Axiomatically, polymerization is favored at low temperature, whereas depolymerization is favored at high temperature. ΔS is normally negative, making the entropic $-T\Delta S$ component for the expression of Gibb's free energy ($\Delta G = \Delta H - T\Delta S$) positive. At relatively high temperatures, $-T\Delta S$ may be sufficiently positive that the overall reaction is no longer exergonic. The temperature at which $\Delta G = 0$ is known as the ceiling temperature, T_c, and we can define $T_c = \frac{\Delta H}{\Delta S}$.[40]

The preceding discussion assumes gaseous reactants; phase changes and solvation give rise to drastic changes in enthalpy and entropy.[41] A major exception to our axiom is the ring-opening polymerization of some large, unstrained rings: the loss of translational entropy in individual monomers is countered by the gain of rotational and vibrational entropy present in the flexible polymer chains. These polymers have floor temperatures, T_f, instead of ceiling temperatures.[41]

Conventionally, ΔH may be obtained by direct measurement of the heat evolved during a polymerization reaction. It may also be found by calorimetry: samples of polymer and monomer are burned, and the heat evolved is recorded. The difference between the two would represent the enthalpy of polymerization. ΔS may be calculated from the standard entropies of monomer and polymer. These standard entropies are themselves calculated

by $S(T) = \int_0^T \frac{C_p}{T} dt$, where C_p is the experimental heat capacity of either at constant pressure.[42]

In the case of equilibrium reactions, enthalpies and entropies can also be extrapolated by Dainton's equation.[43] In the model system reversible addition of a monomer unit, M, to a growing polymer chain, M_n*, leads to an elongated polymer, M_{n+1}*:

$$M_n^* + M \rightleftharpoons M_{n+1}^*$$

Since M_n* and M_{n+1}* are equivalent, the equilibrium constant, K, can be simplified:

$$K = \frac{[M_{n+1}^*]}{[M_n^*][M]} = \frac{1}{[M]}$$

The Gibb's free energy of reaction is the standard free energy of reaction, corrected with the reaction quotient, Q:

$$\Delta_r G = \Delta_r G° + RT \ln Q = \Delta_r H° - T\Delta_r S° + RT \ln Q$$

At equilibrium, $\Delta_r G = 0$ and $Q = K$:

$$\Delta_r H° - T\Delta_r S° + RT \ln K = 0$$

$$\Delta_r H° - T\Delta_r S° = -RT \ln K$$

Dividing throughout by T, and substituting K for 1/[M], we obtain Dainton's equation:

$$R \ln[M] = \frac{\Delta_r H°}{T} - \Delta_r S°$$

Polymerization reactions are run at different temperatures, and the equilibrium concentration of residual monomer is thereafter measured. Plotting ln [M] against 1/T provides $\Delta_r H°$ and $\Delta_r S°$.

Estimating enthalpies of polymerization

One of the oldest methods to calculate enthalpies of polymerization is to use tabulated bond dissociation energies,[44-45] be they experimental or theoretical figures. A more sophisticated approach is the Benson and Buss' group additivity method that compensates for the effects of neighboring groups.[46-48] Miller *et al.* have demonstrated both approaches for poly(ethylene) and for the ethylene-carbon dioxide copolymer.[49]

Computational chemistry can be used to calculate the enthalpies of monomer vs. oligomer directly. Enthalpies of polymerization are obtained as the enthalpy of chain extension:

$$\Delta H(\text{polymerization}) = \Delta H((n+1)\text{-mer}) - \Delta H(n\text{-mer}) - \Delta H(\text{monomer})$$

This oligomer approach requires the ends of the model polymer to be defined. Hydrogen is the conventional choice, even though hydrogen-capped oligomers are not observed in the actual polymerization processes. This process should in principle be repeated until convergence,[49-51] but intramolecular hydrogen bonding may complicate matters.

We may consider polymers to be infinitely repeating linear chains, periodic boundary conditions (PBC) having been applied. In so doing, the chain-end approximations are obviated and complications due to intramolecular bonding are avoided. Additionally, fewer computational resources are needed for modeling a small repeat unit than for a relatively large oligomer. At first glance, the enthalpy of polymerization may simply be calculated:

$$\Delta H(\text{polymerization}) = \Delta H(\text{repeat unit}) - \Delta H(\text{monomer})$$

Brothers *et al.* point out that vibrational analysis of a single repeat unit is inadequate, as vibrations in the whole polymer that are out of phase within a small repeat unit are not taken into account. As a result, supercells (containing more than one repeat unit) are used iteratively to achieve convergence.[50]

While useful fiction, a real polymer is not an oligomer, nor is it an infinitely long polymer. Even so for sterically-unencumbered poly(ethylene); linear alkanes of increasing length eventually favor hairpin structures to take advantage of favorable intramolecular van der Waals interactions.[52-54]

Benchmarking various computational methods

To the best of our knowledge, only two articles have discussed the thermodynamics of the CO_2-epoxide copolymerization. Both compared polymer vs. cyclic carbonate formation, and both groups investigated polymer formation via the oligomeric approach. In the 2011 article,[55] the authors compared the BP86, M06-L, M06, and M06-2X functionals in conjunction with electronic energies with the results of high level CCSD(T)/def-TZVPP calculations, and concluded that no one functional reproduced the high level *ab initio* results perfectly. High accuracy thermochemistry was not a stated goal. Enthalpies of copolymerization vs. cyclic carbonate formation were obtained using BP86/SV(P).

The CO_2-epoxide copolymerization

In the article that discusses the CO_2-epoxide copolymerization, polymer formation was studied via the oligomeric approach. Rieger *et al.* reported enthalpies obtained by density functional theory (BP86/SV(P)).[55] Of passing relevance is the article by Miller *et al.* that modeled the copolymerization of ethylene with carbon dioxide using the oligomeric approach, with enthalpies obtained by DFT (B3LYP/6-31G(d')).[56] The enthalpies of polycarbonate formation are compared in Table I-1.

Table I-1. Enthalpies of the reactions to produce polymers and cyclic carbonates.

	Polymer		Cyclic carbonate	
	BP86/SV(P)[55]	**Lit.**	**BP86/SV(P)[55]**	**NIST[57-58]**
Ethylene carbonate	-17.8	-20.8[a]	-15.0	-15.2
Propylene carbonate	-13.6		-14.7	-16.1
Cyclohexene carbonate[b]	-17.4		-14.5	

[a]ΔH_{poly} = -124.5 kJ/mol by calorimetry. The gas phase enthalpy of polymerization was estimated by subtracting -37.5 kJ/mol,[57-58] the enthalpy of vaporization of dimethyl carbonate (representing approximately one repeat unit). [b]To give the *cis*-cyclic carbonate.

Kinetics of chain growth

The kinetics of the CO_2-epoxide copolymerization was first studied computationally by Morokuma *et al.*[36] Computational analysis has been done for other first generation zinc catalysts, and for the second generation cobalt and chromium systems supported by salen ligands. Also of interest to workers in this field is similar work done for the ring-opening polymerization of lactide[59-61] and caprolactone.[62]

Zinc-catalyzed routes

The first computational study of the CO_2-epoxide copolymerization was reported by Morokuma *et al.* in 2002.[36] It was performed on Coates' (β-diiminate)zinc complex (Figure I-3), and the monomeric form was presumed. A two-layer ONIOM approach was used, with the low layer represented by the semi-empirical PM3 method, and the catalytic center calculated with the B3LYP functional and the LANL2DZ and LANL2DZ(d) (added polarization functions) basis sets (denoted PM3:B3LYP/LANL2DZ and PM3:B3LYP/LANL2DZ(d)).

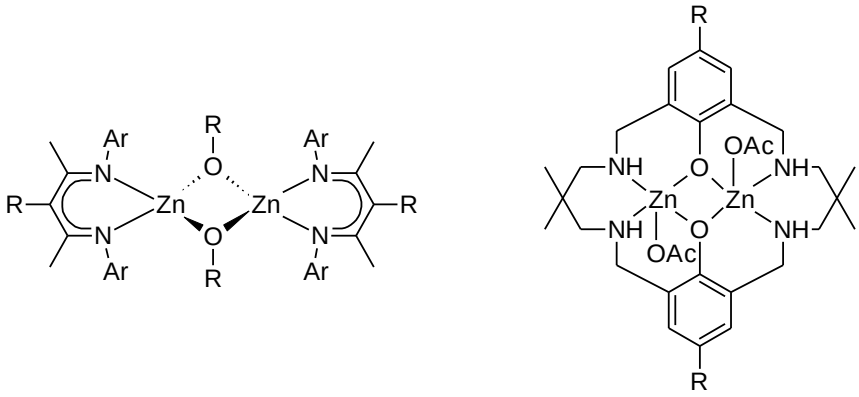

Figure I-3. General structures of the bis(β-diiminate) (left) and the Robson-type (right) dizinc catalysts.

A plausible sequence of reactions for the CO_2-epoxide copolymerization was mapped out, ethylene oxide serving as the prototypical epoxide. In this sequence, carbon dioxide weakly coordinates to the coordinatively unsaturated zinc-bound polymeric alkoxide (trigonal planar, 16 d electrons) via one of its oxygen atoms (O-Zn = 2.497 Å, binding energy = 1.7 kcal/mol) according to PM3:B3LYP/LANL2DZ, while no analogous structure was found at the PM3:B3LYP/LANL2DZ(d) level of theory. The authors found CO_2 insertion into the Zn-methoxide to be barrierless. Subsequently, epoxide coordinates to the catalytic center. The zinc-bound polymeric carbonate (represented by methyl carbonate) attacks a methylene carbon of the tethered ethylene oxide, but it is unable to approach from the back side like in an S_N2 reaction. As a result, this transformation is asynchronous, and ring-opening of the epoxide occurs before the O-C bond forms. At the transition state, the breaking epoxide O-C bond is longer than the nascent O(carbonate)-C(epoxide) bond. The rate limiting step for this reaction is the last: ring-opening ethylene oxide by the polymeric carbonate, with a very high free energy barrier of 36.4 kcal/mol.

The authors attributed cyclohexene oxide's polymerizability vs. ethylene oxide's lack thereof to relief of ring strain in the bicyclic system. In support, they showed that

hydration of cyclohexene oxide was ca. 40 kcal/mol more exoergic than the hydration of ethylene oxide. Recalculated at the CBS-4M level of theory, we find that hydration to *trans*-eq-cyclohexan-1,2-diol is exothermic by 23.0 kcal/mol, comparable to that of -22.3 to -23.9 kcal/mol for ethylene oxide. In contrast, hydration of *trans*-cyclohexene oxide to give *cis*-cyclohexan-1,2-diol is exothermic by 62.3 kcal/mol. Later studies also indicate that the enthalpies for aliphatic and alicyclic epoxides to copolymerize with carbon dioxide are similar.[55,63] Morokuma *et al.* might have considered *trans*-cyclohexene oxide instead of the *cis* isomer used for copolymerization with carbon dioxide. This point may be moot because the (BDI)zinc system has since been found to operate via a bimetallic mechanism.[23]

In the following computational report,[55] propylene and cyclohexene oxides were found to behave similarly in principle. The reason propylene oxide does not copolymerize with CO_2 is that the zinc-catalyzed carbonate-backbiting reaction successfully competes with the zinc-catalyzed enchainment reaction (epoxide ring-opening is the rate-determining step; $\Delta G^{\ddagger}$ = 23.7 and 22.6 kcal/mol, respectively). Since propylene carbonate is unable to undergo ring-opening polymerization, it serves as the thermodynamic sink of the system, and any poly(propylene carbonate) that manages to form is eventually destroyed. Cyclohexene oxide avoids this fate by having a higher free energy barrier for zinc-catalyzed carbonate backbiting than zinc-catalyzed polymer growth ($\Delta G^{\ddagger}$ = 26.4 and 18.6 kcal/mol, respectively). The authors expanded upon this work by designing a dinuclear zinc complex that solves the "entropy problem" in that at high temperatures, the monomeric zinc complexes are less likely to aggregate to provide the required catalytic activity.[64] This catalyst is flexible enough to accommodate varying Zn-Zn distances along the reaction coordinate (4.50-5.66 Å). Unusually, the rate-determining step is CO_2 insertion. Where CO_2 pressure were increased, this catalyst system's rate-determining step switches from CO_2 insertion to epoxide ring-opening. This study is noteworthy for demonstrating effects of pressure on the calculated reaction profile.

Rzepa, Williams and coworkers subsequently performed a computational-experimental investigation.[65] They chose to use the dispersion-corrected ωB97X-D functional in conjunction with the double-zeta 6-31G(d) basis set; geometries were essentially the same when a larger basis set was used. They found that the Robson-type dizinc complex (Figure I-3) favors a bowl conformation over an "S" conformation by 15.3 kcal/mol, and that only one of the acetate ligands initiates a single polymer chain. Experimental infrared spectra were compared with the predicted spectra of the zinc complexes after one CHO ring-opening reaction, and after that alkoxide complex underwent carboxylation. These spectra were in general agreement.

In this catalytic cycle, both zinc centers work cooperatively to enable CHO and CO_2 to copolymerize. The epoxide coordinates to one zinc center, and it undergoes ring-opening by the acetate ligand on the other zinc center. Two plausible scenarios exist: the acetate may attack via the zinc-coordinated oxygen atom, or it may attack through the uncoordinated carbonyl oxygen with concomitant cleavage of the zinc-oxygen bond. Unsurprisingly, the second route is more accessible than the first ($\Delta G^{\ddagger}$ = 24.3 vs. 41.9 kcal/mol). The supporting acetate bridge assists by facilitating electron flow between the two otherwise-unconnected zinc centers (Figure I-4), confirmed by appropriate changes in the acetate Zn-O bond lengths. In the next step, the zinc-bound alkoxide attacks CO_2 to generate a zwitterionic carbonate. The carbonate coordinates to the adjacent zinc center in a separate step. Eventually, the carbonate attacks another zinc-bound cyclohexene oxide ligand, preferentially by the free carbonate oxygen. In agreement with previous reports,[36,55] this step is rate-determining. The theoretical and experimental free energies were in excellent agreement too (25.7 vs. 23.5 kcal/mol at 353 K).

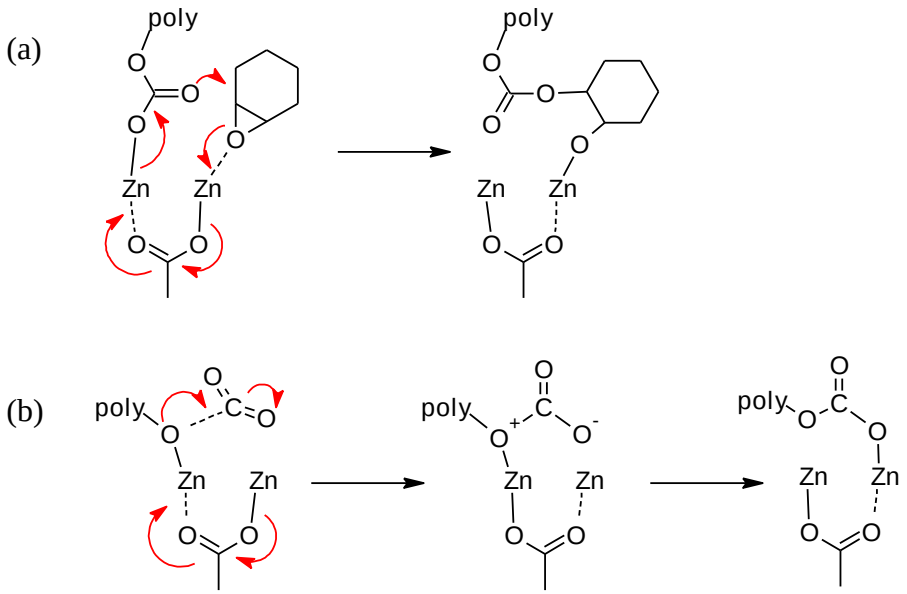

Figure I-4. The bridging acetate ligand facilitates the flow of electrons according to Rzepa, Williams, and coworkers: (a) Ring-opening of the zinc-bound cyclohexene oxide ligand via the free carbonate oxygen. (b) The zinc-bound alkoxide attacks a carbon dioxide molecule that is not pre-coordinated.

Side reactions were examined as well. Sequential epoxide ring-opening that leads to polyether defects had a very high free energy barrier ($\Delta G^{\ddagger}$ = 39.3 kcal/mol), despite being exergonic. Conversely, sequential CO_2 enchainment is endergonic and unfavored (ΔG = 22.8 kcal/mol), even though its elementary steps had modest barriers.

The defining difference between the (BDI)zinc and subsequent (salen)M(III)X (X = cocatalyst) systems is that the zinc catalyst is coordinatively unsaturated, whereas the octahedral salen complexes do not have vacant coordination sites. That is to say, the polymeric carbonate ring-opens the epoxide while both moieties are zinc-bound, whereas epoxide displaces the polymeric carbonate for at least the cobalt(III) and chromium(III) complexes, and the free polymeric carbonate ring-opens the activated epoxide ligand in an S_N2-like fashion. These details are discussed in the next section.

Liu and coworkers studied different possible pathways of $ZnEt_2$-glycerine and $ZnEt_2$-glycerine-YCl_3 catalyst systems using DFT.[66] Consistent with the literature, the rate-determining step was the ring-opening of the epoxide co-monomer. The former system was found to have lowest free energy barriers when a dizinc mechanism was considered. Epoxide ring-opening had the lowest barrier when the zinc center that activates it had the most positive NBO charge. This correlation inspired the addition of $(Cl_3CO_2)_3Y$ as a Lewis acid cocatalyst. The dizinc-yttrium complex successfully reduced the free energy barriers for epoxide ring-opening from 32.2 to 27.1 kcal/mol. Experimentally, addition of $(Cl_3CO_2)_3Y$ caused the catalyst to be thrice as active.

Besides these molecular catalysts, Luinstra and Molnar mentioned some preliminary work[67] on the heterogeneous zinc glutarate catalyst.[68] They modeled the ethylene oxide homopolymerization reaction on the zinc glutarate surface using Car–Parrinello molecular dynamics. Like the dizinc mechanisms for molecular catalysts, one zinc center activates an ethylene oxide molecule for nucleophilic attack by a polymeric alkoxide tethered to an adjacent zinc center; the propylene-CO_2 copolymerization is expected to proceed in a similar fashion.

Cobalt(III) and chromium(III)-catalyzed routes

Unlike the zinc-catalyzed routes, closed-shell singlet electronic states may not be assumed for the rest of the first transition series. Prior to an in-depth discussion on the CO_2-epoxide copolymerization, we note that the mechanism for epoxide hydrolysis has parallels with the epoxide ring-opening step of the CO_2-epoxide reaction (**Scheme I-2** and **Scheme I-3**). The nature of the hydrolysis reaction was clarified by experimental[25,69] and theoretical studies.[70-71]

In the Jacobsen article, (salen)Co(III)-bound hydroxide is the nucleophile that ring-opens the similarly coordinated epoxide. The steric bulk of the both salen ligands and the manner in which they are "stepped", controlled by the chiral cyclohexylene backbone,[72] enhance differences in reactivity between the two epoxide substrates. Differences in

electronic energy between the "matched" and "mismatched" systems were determined at the B3LYP/6-31G(d) level of theory to be 2-4 kcal/mol. Differences were more prominent (6-9 kcal/mol) at the M06-L/6-31+G(d) level that places more emphasis on weak dispersion interactions. The authors also acknowledged that the triplet (spin-unpaired) octahedral [Co]-OH complex's hydroxy ligand may be more labile (due to occupation of the anti-bonding $d(x^2-y^2)$ and $d(z^2)$ orbitals, compared with for a low-spin d_6 complex), but found that nucleophilic attack by the hydroxy ligand occurs while the ligand is still firmly bound to the cobalt center. This indicates that the hydroxy ligand's nucleophilicity while cobalt-bound determines its reactivity more than its lability.

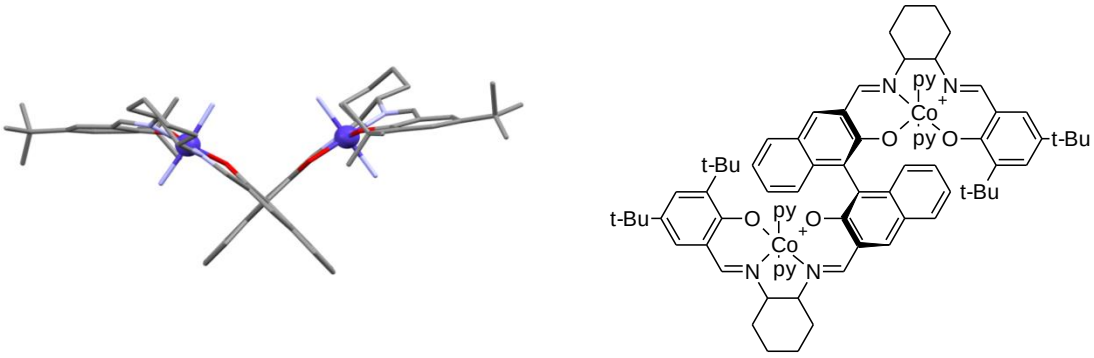

Figure I-5. Left: X-ray crystal structure of the binap-linked dicobalt catalyst,[28] showing the catalytic groove (Co-Co = 6.937 Å). Hydrogen atoms, counterions, uncoordinated pyridine molecules, and solvent not shown; pyridine ligands have been reduced to nitrogen atoms. Dark blue = cobalt; gray = carbon; red = oxygen; light blue = nitrogen. Right: A two-dimensional representation of this complex, py = pyridine.

At about the same time, Coates, Cavallo, and coworkers did a computational-experimental study of the epoxide homopolymerization using Coates' binap-linked bimetallic catalyst (Figure I-5). They found that methine attack (leading to a head-head mis-insertion) and ring-opening of R-propylene oxide by the (R,R,R,R)-dicobalt catalyst were disfavored by ca. 4 kcal/mol of free energy. The authors were able to account for

the system's good stereo- and region-selective homopolymerization (*rac*-proplyene oxide yields isotactic poly(propylene oxide) with > 99 % regioregularity). A bimetallic mechanism has also been described for the homopolymerization of propylene oxide by uranyl catalysts.[73]

Also of importance to the CO_2-epoxide copolymerization, Curet-Arana and coworkers examined plausible interactions between carbon dioxide and metal-salen complexes, and concluded that the former does not bind directly to the metal-salen complex (endothermic by ca. 50 kcal/mol).[74] This is consistent with our understanding that CO_2 insertion does not involve the metal center, based on experimental kinetics studies.[75-80]

Preliminaries aside, the first theoretical examination of the CO_2-epoxide copolymerization catalyzed by (salen)M(III) complexes was performed by Luinstra *et al.* in 2005. This older study made use of a minimal salen-like ligand for computational efficiency that was found to give results equivalent to the full salen complex. Several metal(III) complexes were examined, as were chloride, acetate, and N,N-dimethylaminopyridine cocatalysts. Luinstra *et al.* determined that when epoxides bind to square pyramidal (salen)M(III)X complexes, they are activated toward ring-opening to a great degree; $\Delta E^{\ddagger}$ = 0.5-6.9 kcal/mol (E referring to electronic energy), acetate being the nucleophile. That is to say, epoxide ring-opening has a minimal barrier for reaction.

The following CO_2 insertion reaction has significant electronic energy barriers of 10.3 kcal/mol and 23.7 kcal/mol for octahedral iron(III) and aluminum(III) acetatoethoxide complexes, whereas no such transition state could be found for chromium(III). Instead, one of the salen phenoxide ligands had to de-coordinate ($\Delta E^{\ddagger}$ = 23.9 kcal/mol) in order for the carboxylation to occur, prior to barrierless CO_2 insertion, and phenoxide re-coordination. In contrast, electronic energy barriers for the neutral (salen)M(III) acetatoethoxide complexes to undergo carboxylation were lower, at 10.8 and 9.1 kcal/mol for chromium and aluminum respectively.

Despite minimal barriers for free acetate to ring-open octahedral metal-bound ethylene oxide molecules, the only low-energy pathway for the ring-opening of the metal-bound epoxide molecule necessitated attack by another metal-bound carbonate ligand. These reactions had barriers of ca. 10 kcal/mol, regardless of the system's spin configuration. The authors acknowledge that vibrational corrections to obtain free energies may change the energy profile of these reactions. With that said, they conclude that at low CO_2 partial pressures, CO_2 insertion is rate limiting. Additionally, they note that the carbonate ligands dissociate from aluminum complexes more easily than chromium complexes (ΔG = 10.7 vs. 19.1 kcal/mol). After this dissociation, metal-free backbiting can commence, and this helps to explain why aluminum complexes are good for making cyclic carbonates.

Adhikari, Nguyen, and Baik studied the formation of cyclic carbonates (the epoxide ring-opening and carboxylation steps are common with the copolymerization reaction) using the B3LYP functional.[81] DMAP serving as the nucleophile, ring-opening [Cr]-bound propylene oxide had a free energy barrier of 23.1 kcal/mol, in contrast with Luinstra's 0.5-6.9 kcal/mol electronic energy barrier. They found that carboxylation was not rate limiting ($\Delta G^{\ddagger}$ = 16.0 kcal/mol), whereas Luinstra found that CO_2 insertion had the highest barrier ($\Delta E^{\ddagger}$ = 23.9 kcal/mol). The authors were unable to find a bimetallic pathway.

Apart from mapping the peaks and valleys in the energy profile of the copolymerization reaction, we have found an example of computational chemistry standing in for physical measurements. In 2009, Lee *et al.* noted that one of their highly-active cobalt-salen complexes behaved quite unusually. The imine nitrogens on the salen backbone that are usually expected to coordinate to the metal center was not bonded to the metal, two coordination sites having been occupied by dinitrophenolate ligands. In the absence of definitive crystallographic evidence, gas phase DFT calculations were used to support their proposed structure. The unusually coordinated complex was 34 kcal/mol lower in electronic energy to the complex with a "conventional" arrangement, plus two

dinitrophenolate ligands. The difference in electronic energy was corrected for electrostatic attraction between the free dinitrophenolate ligands and the quaternary ammonium cations on the salen ligand.[82] The use of a solvation model would have stabilized the anion better, providing more accurate differences in energy.

Kinetics of backbiting

Efforts to prepare polycarbonates have long been complicated by parallel cyclic carbonate coproduct that is entropically favored. In the generally-accepted catalytic cycle, the catalyst-bound polymeric carbonate is displaced by an epoxide unit, before being ring-opened by the displaced carbonate. Cyclic carbonate formation occurs when the free polymeric carbonate (or polymeric alkoxide, under low-CO_2 conditions) backbites upon itself to extrude one unit of cyclic carbonate, leaving behind a shortened polymer chain. The metal-bound polymeric carbonate or alkoxide are less nucleophilic, so they are less susceptible to this degradation reaction (**Scheme I-4**). Complete dissociation of the polymeric carbonate has resulted in the design of catalysts bearing tethered onium cations that trap these polymeric carbonates, preventing this deleterious side reaction. These catalysts are some of the most active yet.[18]

Scheme I-4. The principal paths by which polycarbonates degrade to cyclic carbonates.

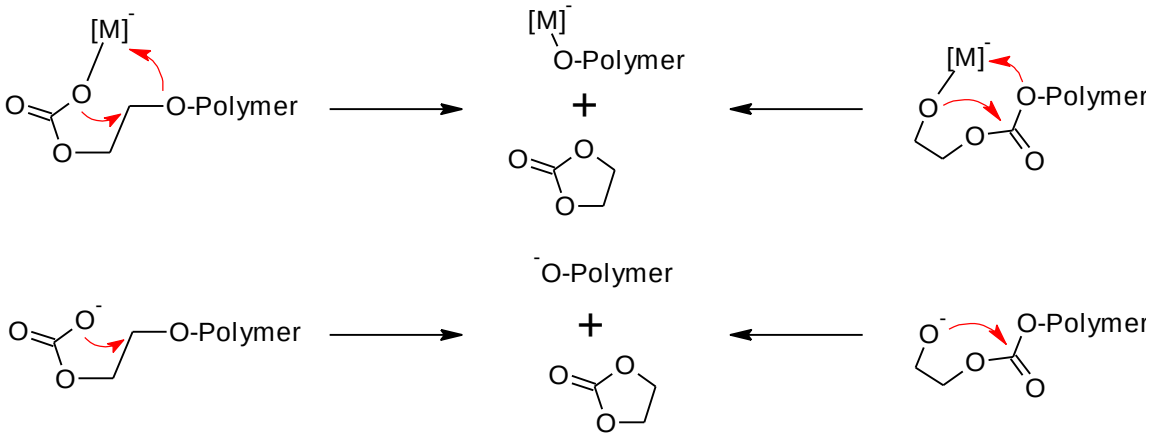

Experimentally, the kinetics of these nuisance chromium-bound degradation reactions were measured alongside the target polymerization reaction by *in situ* infrared spectroscopy,[83-84] and the metal-free degradation reactions were the focus of a dedicated investigation.[85] Luinstra, Rieger *et al.* studied the metal-bound and metal-free carbonate backbiting reactions using gas phase BP86/SV(P) geometries, supplemented by BP86/TZVP single point energies.[86] Ethylene oxide was the prototypical epoxide, and they approximated the remainder of the polymer chain with acetate. For the metal-bound degradation reactions, the chromium(III) and aluminum complexes were greatly truncated. They concluded that the metal-free carbonate backbiting reaction is the most likely degradation route, while metal-bound carbonate degradation routes are more difficult (Table I-2). The authors did not find pathways for metal-bound or metal-free alkoxide backbiting reactions, noting that a polymeric alkoxide is a poor leaving group.

Table I-2. Electronic energy barriers (kcal/mol) to carbonate backbiting per reference 86.

Polymeric carbonate bound to	**$\Delta E^{\ddagger}$**
[Cr]-OAc	22.7
[Cr]-Cl	21.5
[Cr]-DMAP	31.6
[Al]-Cl	22.2
Metal-free	8.4

Cyclic carbonate formation

For polymer chemists, cyclic carbonates are usually thought of as unwanted byproducts arising from the metal-bound or metal-free backbiting reactions.[84] However, these compounds are synthetic targets in their own right, useful as battery electrolytes and as high temperature solvents.[87-88] As one of the most exciting advancements in this field, North and coworkers demonstrated a catalytic system that converts ethylene and

propylene oxides into the cyclic carbonates using power station flue gas as the carbon dioxide source.[5]

Computational chemistry allows the uncatalyzed reaction between carbon dioxide and epoxide (that normally does not occur) to be studied, providing a point of comparison for catalyzed coupling reactions. In the uncatalyzed reaction, the epoxide oxygen attacks carbon dioxide's central carbon atom, while one of its oxygen atoms attacks the carbon atom forming the base of the epoxide. This is a concerted cycloaddition reaction: two bonds are made, while two bonds are broken, all at the same time. The barrier for this sort of reaction is extremely high: $\Delta E^{\ddagger}$ is ca. 53 and 58 kcal/mol for the reaction between propylene oxide and CO_2 (Figure I-6).[89-92]

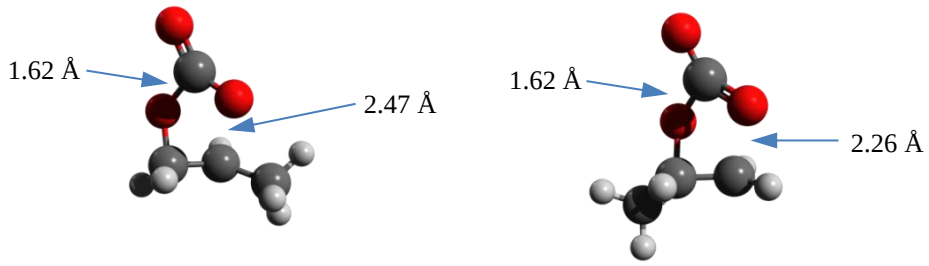

Figure I-6. Transition states for the reaction between propylene oxide and carbon dioxide (B3PW91/6-31G(d,p)). The forming O-C bond occurs at the methine position (left) and the methylene position (right).

In the more commonly discussed mechanism of cyclic carbonation formation, the epoxide is attacked by a suitable nucleophile to give an alkoxide that is usually stabilized by some sort of Lewis acid. CO_2 inserts to yield a carbonate that backbites to eliminate the initial nucleophile. This mechanism is akin to the metal-bound or metal-free carbonate backbiting reactions studied by polymer chemists. Lewis acid catalysts for this reaction that have been probed by computational chemistry include: lithium bromide,[93]

potassium iodide,[91] azolium[89] and quaternary ammonium salts.[94-95] The counterions are not mere spectators; they serve to ring-open the epoxides. The mechanisms for (salphen)Zn and (amino-tris(phenolato))aluminum complexes to catalyze the formation of cyclic carbonates are similar to that discussed in the preceding section (no CO_2 pre-coordination).[92,96]

The metal center need not merely serve as a Lewis acid. With cyanomethylcopper(I) as a catalyst, CO_2 inserts into the Cu-CH_2CN bond, serving as a reservoir of activated carbon dioxide.[90] Chen, Liu, He et *al.* looked at a cobalt-substituted phosphotungstate catalyst, where activity occurs at the cobalt(II) site.[97] Upon coordination, the epoxide is reduced by one electron (generating Co(III)). Homolysis of the epoxide O-C bond produces a carbon radical that reacts with CO_2. Reaction barriers were similar for both doublet and quartet spin states, but the radical mechanism was confirmed experimentally by loss of activity following addition of free radical scavengers. The reaction between Co(II) and CO_2 to give a metallaformate (once postulated by Paddock and Nguyen[98]) was also ruled out: CO_2 adds to the Co-O bond, generating a four-membered carbonate chelate ring that does not react further.

$Re(CO)_5Br$ is a pro-catalyst for making cyclic carbonates. Wu *et al.* studied two proposed mechanisms for cyclic carbonate formation.[99] The first invokes the oxidative addition of the epoxide O-C bond to the reduced Re(I) center. CO_2 insertion is followed by reductive elimination of the cyclic carbonate. The second mechanism involves insertion of CO_2 into the Re-Br bond. Epoxide binds, and is ring-opened by the activated CO_2 moiety. Rearrangement ensues to generate the cyclic carbonate. The first step of this second mechanism is similar to what Hazari, Kemp, et *al.* have discussed for their chemistry (CO_2 inserting into a Pd-H bond, serving as activated CO_2 for further reaction).[100] With that said, Wu *et al.* dismissed the second route as unfeasible due to the difficulty of CO_2 insertion into the Re-Br bond. This is consistent with metal-halide bonds being stronger than metal-hydride bonds, CO_2 insertion/deinsertion into the latter generally being thought of as low energy processes.

Concluding remarks

Summarizing the work done to-date, the enthalpy of the 1-mer to 2-mer reaction has been used to represent that of subsequent chain extensions. Density functional theory has not been shown to give such chemically-accurate results, but the M06 and M06-2X functionals with triple-zeta basis sets give energies that bracket those obtained by high-level CCSD(T) calculations. The BP86 and the M06-L functionals lacking Hartree-Fock exchange did not do well. The use of periodic boundary conditions should reduce the difficulty of calculation, but the ability to perform DFT frequency calculations under PBC conditions is not widely implemented at this time.

To model the large metal-containing catalytic systems for CO_2-epoxide copolymerization, compromises are necessary. Early studies made use of two-layer ONIOM models with a semi-empirical low level and a DFT high level. Others analyzed skeletal toy systems using DFT. Reflecting the better computational resources available today, recent investigations have made use of lightly-truncated or non-truncated catalyst models.

"Double-barreled" calculations utilizing geometries obtained at lower levels of theory and single point calculations at higher levels of theory have been used. DFT calculations should give qualitatively correct results, although energies obtained differently should be compared with caution. Some authors emphasize the importance of addressing non-covalent interactions to get reliable results (e.g. the dispersion-corrected ωB97X-D functional with basis sets containing diffuse functions). Per common wisdom, the use of a solvation model is helpful, and energetics are overestimated in its absence. Zinc complexes may be assumed to be low-spin singlets, but the lowest energy electronic state for other transition metal complexes should be verified.

The search for better catalysts and more useful polycarbonates continues. Pertaining to computational chemistry, several aspects of the CO_2-epoxide copolymerization have been explored: the thermodynamics of the process; the kinetics of the zinc-, cobalt-, and

chromium-catalyzed chain-extension reactions; the metal-free degradation reactions. Building upon this foundation, we would like to see more successful reports of rational catalyst design in coming years, and overall progress in the field of CO_2 utilization for polymer synthesis.

CHAPTER II

THERMODYNAMICS OF THE CARBON DIOXIDE-EPOXIDE COPOLYMERIZATION, AND KINETICS OF THE METAL-FREE DEGRADATION*

Introduction

Previous experimental studies by Darensbourg *et al.* have examined the (salen)M(III)-catalyzed copolymerization reaction from both synthetic and mechanistic viewpoints. While some specific reactions between epoxides and CO_2 have been described computationally,[55,65,89-90,99] no systematic investigations have been carried out for a variety of epoxides relevant to observed copolymerization processes. In particular, aside from one calorimetric investigation,[101] the thermodynamics of polycarbonate chain growth is not well described.

The important questions we wish to address herein with theoretical computations are: (a) the thermodynamics of the alternating copolymerization of CO_2 and epoxide (ΔH per repeat unit) for various epoxides, (b) analogous thermodynamics of cyclic carbonate formation, and (c) the kinetic barriers for the free polymer chain backbiting process involving either carbonate or alkoxide end groups. In this chapter, we report theoretical calculations of the thermodynamics of this CO_2-epoxide coupling process, and evaluate the kinetics of the depolymerization reaction to cyclic carbonates via a backbiting process.

* Adapted with permission from Darensbourg, D. J.; Yeung, A. D. *Macromolecules* **2013**, *46*, 83. Copyright 2013 American Chemical Society.

Benchmarking of computational methods

The four reactions described in (**Scheme II-1**) were modeled for a variety of cyclic and acyclic carbonates, and the calculated enthalpies were compared with gas phase data.[57-58]

Scheme II-1. Four reactions used to benchmark computationally determined enthalpies against experimental data The carbonates included in the test set were ethylene, propylene, and butylene cyclic carbonates, and dimethyl, diethyl, and diphenyl acyclic carbonates.[63]

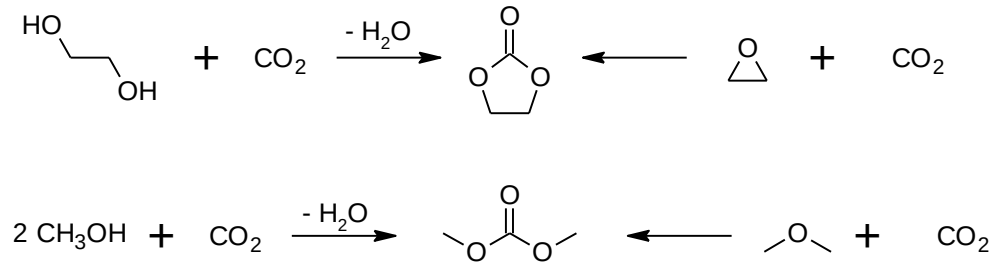

Table II-1. Calculated enthalpies – NIST-recommended enthalpies (kcal/mol) for the benchmark gas-phase reaction in **Scheme II-1**.

	MSD	**MUD**	**RMSD**
NIST error		1.9	2.4
B3LYP/6-311G(2df,p)	4.9	4.9	5.3
TPSSTPSS/6-311G(2df,p)	4.9	4.9	5.3
mPWPW91/6-311G(2df,p)	4.8	4.8	5.2
m06-2X/6-311G(2df,p)	-1.2	2.1	2.5
MP2/6-311G(3d2f,p)	3.5	3.5	3.8
CCSD/6-311G(3d2f,p)	0.7	1.6	2.0
CBS-4M	0.1	0.8	1.1
CBS-QB3	-0.3	0.7	0.8
G3MP2	1.2	1.2	1.8
G4	0.7	0.9	1.1

MSD = mean signed deviation; MUD = mean unsigned deviation, RMSD = root mean square deviation.

For this test set (Table II-1), the G4,[102] CBS-4M,[103-104] and CBS-QB3[103,105] composite methods gave the best all-round performance (ca. 1 kcal/mol deviations), while G3(MP2)[106] *occasionally* gave large deviations (3-4 kcal/mol). The good agreement found is consistent with previous work.[107] Of the DFT methods, the M06-2X functional with polarization functions had generally acceptable deviations (2-3 kcal/mol deviations). All the other functionals had significantly larger deviations of 4-7 kcal/mol.

From the benchmarking study, CBS-4M was chosen to study the thermodynamics of the polymerization reactions, while CBS-QB3 and CBS-QB3(+)[108] were chosen for studying barrier heights to polymer degradation.

Enthalpies of epoxide-carbon dioxide copolymerization

Enthalpies of polymerization were obtained via the oligomeric approach; the reactions between an n-mer with one equivalent each of carbon dioxide and epoxide to give an (n+1)-mer were modeled for up to eight repeat units using DFT, and up to four repeat units for CBS-4M, and the mean ΔH_{poly} were obtained (**Scheme II-2**). See Table II-2 below for the values determined for the copolymerization of ethylene oxide and carbon dioxide to give poly(ethylene carbonate) (poly(EC)).

The B3LYP and CBS-4M methods yielded qualitatively similar enthalpies of polymerization, and the enthalpies of successive oligomerization reactions were equally consistent. Compared to CBS-4M, the former appeared to underestimate the enthalpy of the polymerization reaction by 3-4 kcal/mol for the more elaborate polymers (poly(styrene carbonate), poly(cyclopentene carbonate), poly(indene carbonate), poly(cyclohexene carbonate), and poly(dihydronaphthalene carbonate) hereafter abbreviated as poly(SC), poly(CPC), poly(IC), poly(CHC), and poly(DhNC)). The B3LYP results remain useful because they show that the enthalpies of polymerization converge rapidly (within 3-4 iterations). The aliphatic polycarbonates gave most consistent energies because the extended-chain conformational minima adopted in the gas phase reduced any self-self interactions. The alicyclic polycarbonates tended to form

globular structures with an intra-molecular hydrogen bond between the head and the tail as illustrated in Figure II-1 for poly(cyclohexene carbonate).

Scheme II-2. The enthalpies of polymerization are determined by determining the enthalpy of successive chain-elongation steps.

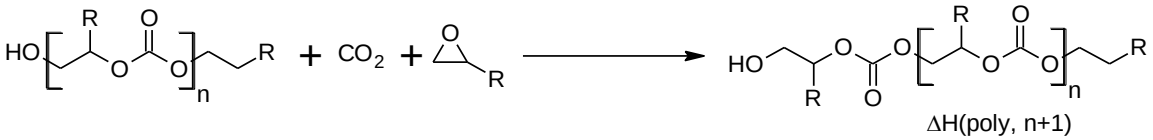

Table II-2. Successive copolymerization of ethylene oxide (EO) with carbon dioxide to give n-mers of poly(ethylene carbonate) at the CBS-4M level.

n	n-mer (hartrees)	EO (hartrees)	CO_2 (hartrees)	(n+1)-mer (hartrees)	ΔH (kcal/mol)[a]
0	-154.733	-153.565	-188.379	-496.781	-64.7
1	-496.781	-153.565	-188.379	-838.759	-21.3
2	-838.759	-153.565	-188.379	-1180.74	-21.2
3	-1180.74	-153.565	-188.379	-1522.71	-21.2
Mean (1-3)					-21.2

[a] ΔH = [H(product chain) – H(reactant chain) – H(CO_2) – H(EO)] × 627.5095 kcal/hartree.

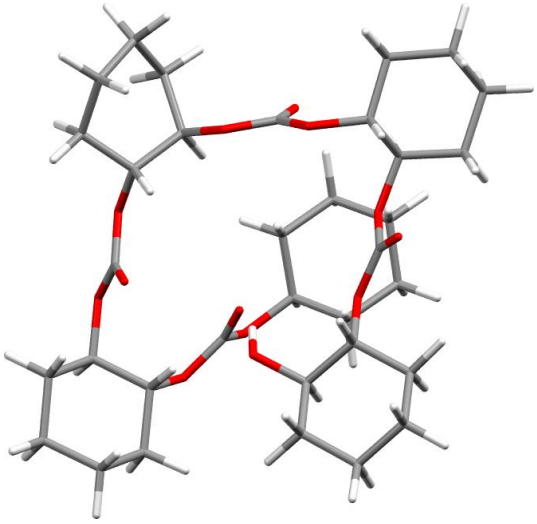

Figure II-1. Poly(cyclohexene carbonate) 4-mer adopts a globular structure, with a hydrogen bond between the terminal hydroxy group and the opposing carbonate group.

These alicyclic epoxide based polycarbonates do so because of the restricted rotation about the fused rings along the polymer strands. The globular structures are higher in enthalpy due to intermolecular steric repulsion, whereas hydrogen bonds lower their enthalpies (bond-formation being exothermic). The 2-mer is too short for intramolecular hydrogen bonding and much contortion. As a result, the reaction of the 1-mer with carbon dioxide and epoxide to give the 2-mer is used to approximate its enthalpy of polymerization, free of intra-chain effects. While several iterations are required for the enthalpies of polymerization to converge, the difference is expected to be small (< 0.5 kcal/mol), as seen for the aliphatic polycarbonates.

All the polycarbonates have essentially the same enthalpies of polymerization (21-23 kcal/mol) despite their electronic or steric properties, with the exception of poly(cyclopentene carbonate) (ΔH_{poly} = -15.8 kcal/mol). This polymer is different because its cyclopentane rings are somewhat strained (C-C-C bond angles are 102-105°), and the restricted conformations allowed cause the hydrogen substituents axial to the cyclopentane ring fused to the polymer backbone to abut the carbonate groups, leading

to steric repulsion.[63] The enthalpies for copolymer formation per repeat unit are summarized in Table II-3. Poly((R)-propylene carbonate), poly((R,S)-propylene carbonate), and head-to-head poly((R)-propylene carbonate) have essentially the same enthalpies of polymerization (DFT); when the geometry of the latter example is optimized, the methyl substituents are able to rotate out of each other's way, minimizing steric repulsion.

Table II-3. Enthalpies of the reactions to produce polymers and cyclic carbonates.

	Polymer formation			Cyclic carbonate formation		
	CBS-4M	**B3LYP/ 6-31G(d')**	**Lit.**	**CBS-4M**	**NIST**	**Lit. (DFT)**
EC	-21.2	-21.5	-20.8[55] (est.[a]) -17.8[55] (DFT)	-15.1	-15.2	-15.0[55]
PC	-21.2	-20.1	-13.6[55] (DFT)	-15.7	-16.1	-14.8[55]
R,S-PC[d]		-20.1			N.A.	
HHTT-R-PC[e]		-20.1			N.A.	
ClPC	-22.1	-19.3		-13.8		
SC	-22.8[b]	-16.9		-14.8		
CPC	-15.8[c]	-13.6		-14.5		
IC	-21.1[c]	-16.5		-18.2		
CHC	-22.6[c]	-17.0	-17.4[55] (DFT)	-16.7		-14.5[55]
1,2-DhNC	-18.3[c]			-14.0		
1,4-DhNC	-22.6[c]			-15.8		
TMC	-23.0	-20.1		-11.7		
EO	-24.3	-25.7	-24.5(4)[109] (expt.)		N.A.	
TMO	-25.1	-23.4	-19.1[110] (expt.)		N.A.	

[a]ΔH_{poly} was determined to be -124.5 kJ/mol through calorimetry. The gas phase enthalpy of polymerization was estimated by subtracting 37.5 kJ/mol,[57-58] the enthalpy of vaporization of dimethyl carbonate (redpresenting approximately one repeat unit). [b]For n = 0 to n = 3. [c]Estimated from the first oligomerization reaction. [d]Poly((R,S)-propylene carbonate). [e]Poly(head-to-head-(R)-propylene carbonate).

The copolymerization of trimethylene oxide with carbon dioxide is strongly exothermic (-23.0 kcal/mol, Table II-3), and significantly more so than cyclic carbonate formation (-11.7 kcal/mol). By Hess' law, the formation of poly(trimethylene carbonate) from trimethylene carbonate is exothermic by 11.3 kcal/mol, much more so than the endothermic ring-opening five-membered cyclic carbonates (ΔH = -1 to -8 kcal/mol). This is in agreement with previous work showing that once activation barriers are reduced by an appropriate catalyst system, near quantitative conversion of trimethylene oxide and carbon dioxide to copolymer occurs.[111] A note about trimethylene oxide: DFT and *ab initio* calculations differ on whether this compound should be planar or puckered. This problem has been discussed elsewhere,[112-114] and any errors in this regard will cancel exactly when Hess' law is applied.

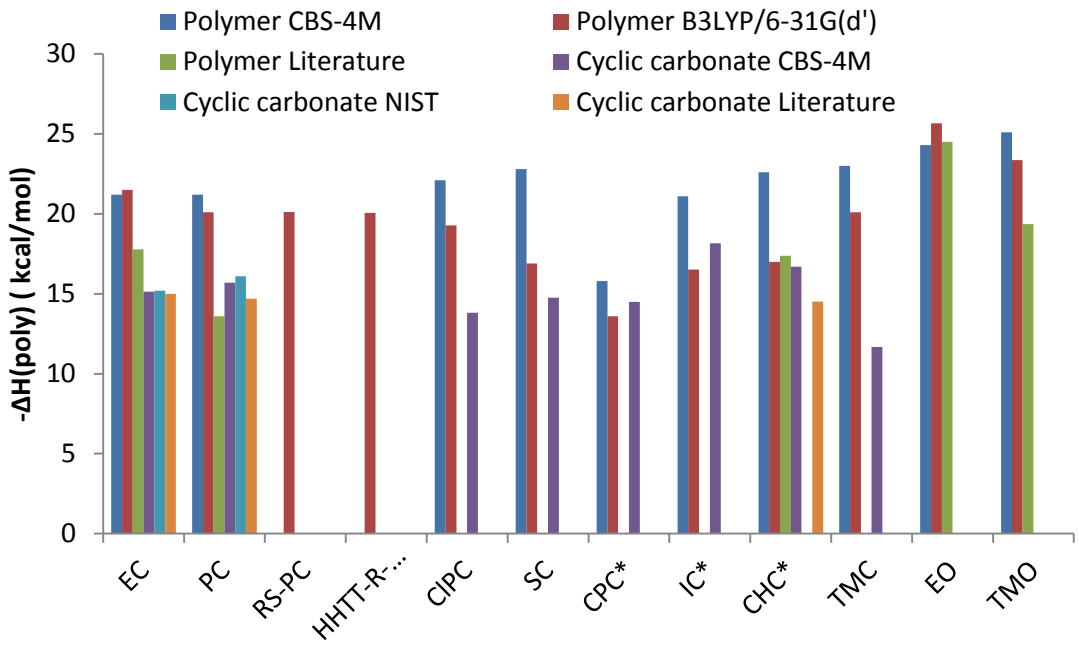

Figure II-2. Comparison of the gas phase enthalpies of chain-elongation, and cyclic carbonate formation. * Enthalpies of polymerization were approximated using the reaction between the polymer 1-mer with CO_2 and epoxide to give the corresponding 2-mer.

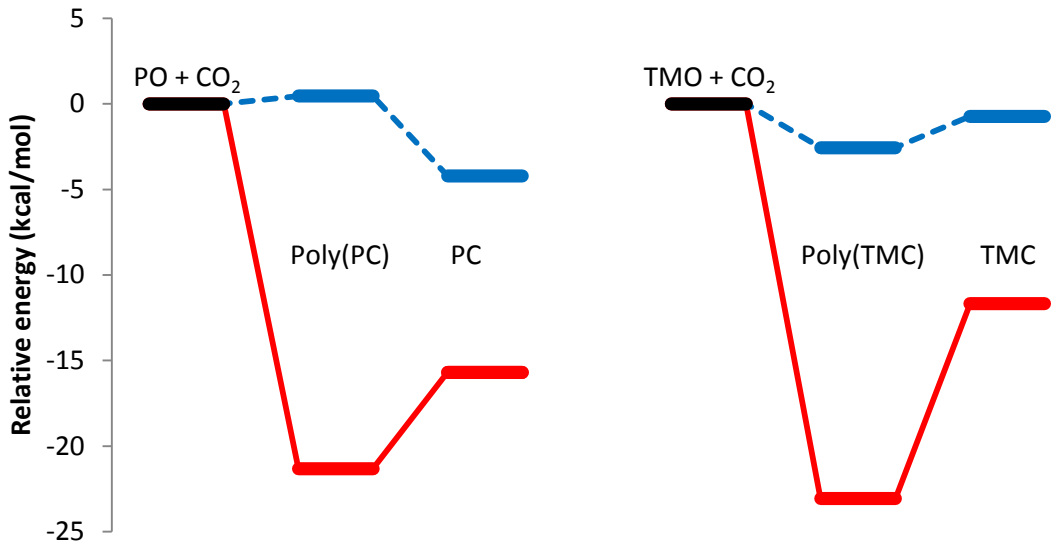

Figure II-3. Enthalpies (solid red lines) and free energies (dashed blue lines) of the reactions of propylene oxide (left) and trimethylene oxide (right) with carbon dioxide to yield polymer and cyclic carbonate (CBS-4M, gas phase). The ring-opening polymerization of TMC is exergonic, whereas the corresponding reaction for PC is endergonic.

The enchainment reactions involving one equivalent each of epoxide and carbon dioxide were more exothermic than the equivalent reactions to give the cyclic carbonate (Figure II-2); the former was more favorable by 5-8 kcal/mol for the aliphatic epoxides and cyclohexene oxide. Since the numbers of bonds broken and made are the same for enchainment and for cyclic carbonate formation, the difference represents the strain inherent in the five-membered cyclic carbonate ring compared to the extended-chain polymer, as well as any other steric or electronic effects. As a point of reference, cyclopentane is 13 kcal/mol higher in enthalpy than 1-pentene in the gas phase.[57-58] The differences in enthalpies are smaller for cyclo(pentene carbonate) and cyclo(indene carbonate) (1.3 and 2.9 kcal/mol respectively) due to the angle strain present in both polycarbonate and cyclic carbonate products. Cyclic carbonates form under copolymerization conditions because of entropy rather than enthalpy (Figure II-3). The

amount of byproduct formed is thus governed by the temperature of the reaction, and by the activation barrier for the growing polymer chain to extend vs. for it to backbite.

As previously mentioned, we revisited the copolymerization of trimethylene oxide with carbon dioxide, which is known to occur readily and at least in part by the intermediacy of the six-membered cyclic carbonate (trimethylene carbonate).[111] To our knowledge, none of the five-membered cyclic carbonates are able to undergo ring-opening polymerization while maintaining their CO_2 content. The enthalpy for ring-opening polymerization of trimethylene carbonate is -11.3 kcal/mol. This reaction is much more exothermic than the equivalent reactions for the five-membered cyclic carbonates (-1 to -8 kcal/mol).

Backbiting of metal-free polycarbonates

There are four principal paths by which carbon dioxide-epoxide copolymers can degrade: backbiting of the polymer chain by metal-bound and metal-free alkoxides, and by metal-bound or metal-free carbonates (**Scheme II-3**).[84] When copolymer is sought, degradation undesirably competes with chain growth,[83] reducing feedstock conversion and decreasing the molecular weight of the product. Previous work has indicated that the metal-bound degradation is sluggish. For example, the degradation of cyclohexene carbonate was experimentally found to have high barriers of 32 kcal/mol and 25 kcal/mol for the metal-bound carbonate[83] and alkoxides,[84] respectively.

For substituted aliphatic carbonates, backbiting via the carbonate anion can occur at two locations: the methine carbon bearing the pendant group, or the methylene carbon (Figure II-4). Steric and electronic factors strongly influence the former case, while they are weaker in the latter. Both cases must be considered because there is generally no guarantee of the regioregularity of the carbonate linkages.

Scheme II-3. The principal paths by which polycarbonates degrade to cyclic carbonates.

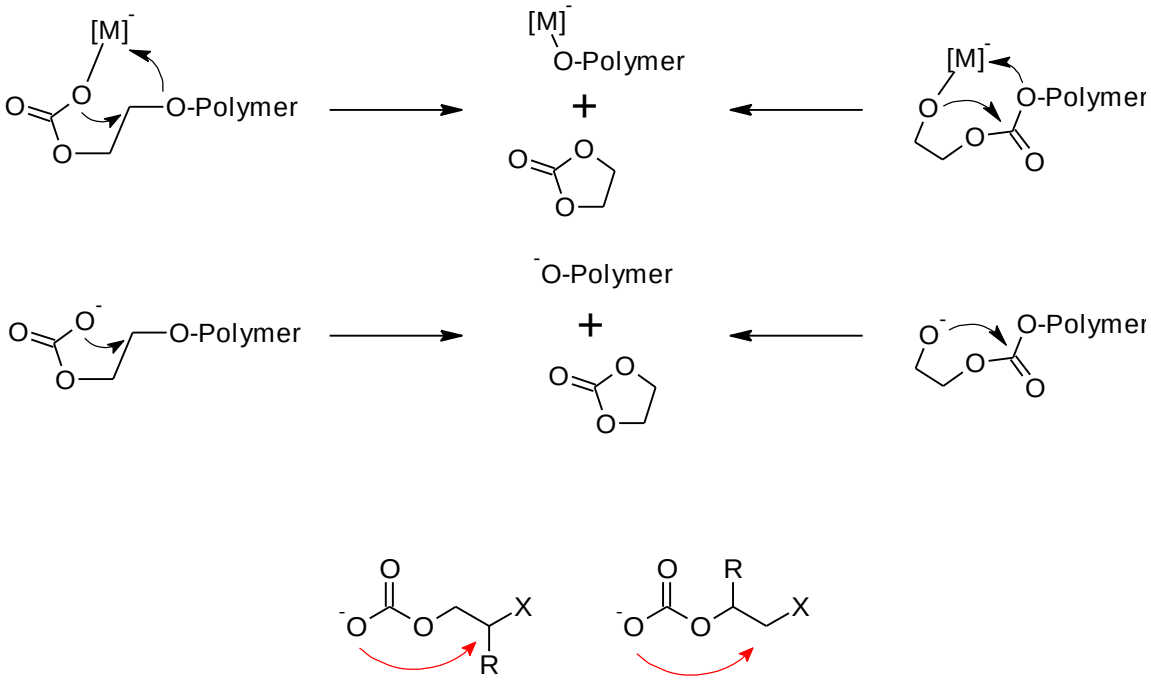

Figure II-4. The carbonate anion can attack at the methine (left) or methylene (right) positions.

In order to perform high level *ab initio* calculations, and to sidestep the steric effects of the polymer chain, the degradation reaction was first studied as a simplified model, with X = Cl instead of X = (n-1)-meric carbonate. Tetrahydrofuran was used as a prototypical solvent, to better stabilize the anionic species involved. The use of implicit solvation is also more representative of the actual solution phase reaction. In this section, free energies rather than enthalpies are more properly discussed, because the electronic energies calculated include the entropy of cavitation. With that said, the free energy barriers are consistently lower than the enthalpic barriers by approximately 1 kcal/mol (at 298 K).

Table II-4. Free energies of the species involved in carbonate backbiting.[a]

		(a) X = Chloride			(b) X = Methyl carbonate		
No.		**Open chain**	**TS**	**Cyclic carb. + X^-**	**Open chain**	**TS**	**Cyclic carb. + X^-**
1	EC-X	0	14.4	-16.0	0	20.4	-2.2
2	PC-1X	0	16.4	-16.3	0	24.0	-3.4
3	PC-2X	0	10.8	-19.2	0	18.5	-6.0
4	ClPC-1X	0	18.2	-15.5	0	25.5	-2.0
5	ClPC-2X	0	12.8	-16.7	0	19.7	-4.1
6	SC-1X	0	14.0	-14.5	0	19.5	-3.6
7	SC-2X	0	12.2	-18.2	0	20.2	-2.6
8	BDC-1X				0	21.0	-7.0
9	BDC-2X				0	19.5	-7.1
10	*cis*-CPC-X	0	13.7	-23.6	0	20.3	-5.3
11	*cis*-CHC-X	0	13.5	-21.4	0	21.1	-8.2
12	*cis*-CHC-relaxed[b]	0	8.0		0	4.7	
13	*cis*-1,2-DhNC-1X				0	17.6	-11.0
14	*cis*-1,2-DhNC-2X				0	21.1	-11.2
15	*cis*-1,4-DhNC-X				0	22.7	-7.7
16	*trans*-CHC-X	0	31.0	-12.5	0	40.5	3.1
17	EC-Br	0	15.3	-14.6			
18	EC-N_3	0	24.7	-1.8			
19	EC-PEC1	0	20.8	-4.0			
20	TMC-X	0	17.8	-12.0	0	26.1	2.9

[a]Free energies for the backbiting of an anionic 1-mer to give the cyclic carbonate and an X- anion, calculated at the CBS-QB3 level with solvation. -Cl = chloride, -Br = bromide, -N_3 = azide, -PEC1 = -$OCO_2CH_2CH_3$ (poly(ethylene carbonate) 1-mer). -1 and -2 denote attack at the methine and methylene carbons respectively. [b]Energy difference between the relaxed chair conformation and the boat conformation required for cyclohexene carbonate to backbite.

Reaction at the methylene position is easier than the analogous reaction at the methine position (Table II-4, entries 2a-7a) regardless of the electronic characteristics of the pendant groups, showing that steric factors are dominant in the backbiting mechanism. The presence of a pendant group adjacent the reaction site gives rise to a lower free energy barrier (by 2-4 kcal/mol) compared to the case with ethylene carbonate, despite

the latter compound being sterically-unhindered. The use of composite methods to determine barrier heights,[115-117] and the effects of substituents α- and β- to the carbon undergoing nucleophilic substitution[116] are in line with previous computational studies.

When X is replaced with methyl carbonate in order to better represent the next carbonate linkage on the polymer, free energy barriers are higher by 6-8 kcal/mol, and the overall reactions are much less exergonic. This is understood by chloride being a better leaving group than methyl carbonate.

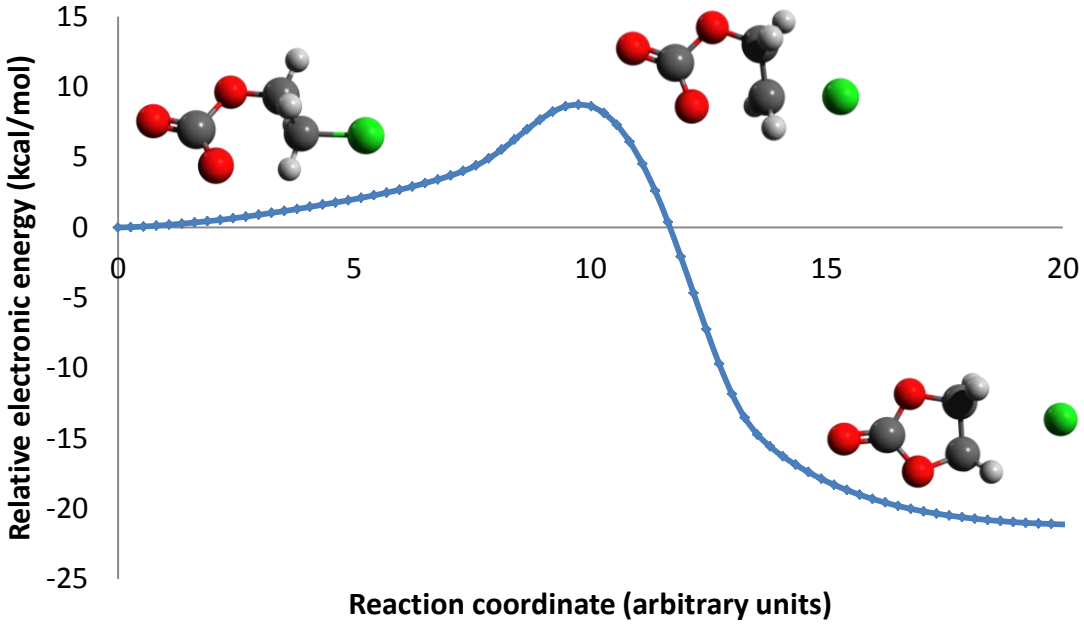

Figure II-5. Profile of the potential energy surface (B3LYP/6-311G(2d,d,p)) connecting the open-chain 1-mer to the cyclic carbonate associated with the chloride anion. In this and subsequent figures, standard CPK colors are used: gray = carbon, white = hydrogen, red = oxygen, green = chlorine.

Where the leaving group is chloride, the geometry of substitution site is trigonal bipyramidal at the transition state (see the potential energy surface in Figure II-5). The

carbon-oxygen and carbon-chlorine bond lengths are 2.1 Å and 2.2 Å respectively. Where methyl carbonate is the leaving group, both carbon-oxygen bond lengths are similar, approximately 2.0 Å. All these bond lengths are much greater than their typical lengths of 1.42 Å (C-O) and 1.77 Å (C-Cl).[118]

The efforts of the leaving group X on the free energy barriers for the process depicted in Figure II-5 when R = H was investigated and the results are summarized in Table II-4, entries 1a and 17a-19a. As seen in this table, the free energy barrier for carbonate backbiting of the anionic carbonate 1-mer to yield ethylene carbonate decreased in the order:

$$X = \text{azide} > \text{anionic 1-mer} \approx \text{methyl carbonate} > \text{chloride} \approx \text{bromide}$$

This ranking shows a good correlation between the ability of each anion to act as a leaving group, and the ease at which carbonate backbiting occurs to give the cyclic carbonate. It was also encouraging to note that carbonate anion approximates the electronics of the polycarbonate chain well. The results are also consistent with a previous computational study by Rieger and coworkers that reported an electronic energy barrier of 23 kcal/mol for X = acetate.[86] These backbiting reactions are all exergonic.

The nature of the R substituent on the epoxide precursor for the cycloaddition reaction in Figure II-3 was also investigated. Pendant groups on short chains have been observed to favor ring closure, including for cyclic carbonates.[119-120] Many rationalizations have been offered,[121] but those that involve conformational flexibility or entropic effects are not relevant to the present discussion of an elementary reaction. Structures of the open chain and the backbiting transition states of propylene, chloropropylene, and styrene carbonates show barely perturbed O-CH-CH_2 angles of 109-112°, ruling out angular compression as a major reason for the lowered activation barriers in this system (Table II-5).

Table II-5. Bond angles of species undergoing carbonate backbiting.[a]

			Open chain		Transition state	
No.		**$\Delta G^{\ddagger}$ (kcal/mol)**	**R-C-H (°)**	**O-CH-CH_2 (°)**	**R-C-H (°)**	**O-CH-CH_2 (°)**
1	EC-Cl	14.4	109.5	109.3	108.7	112.1
2	ClPC-2Cl	12.8	108.2	110.9	109.5	111.0
3	PC-2Cl	10.8	108.5	111.3	109.8	110.6
4	SC-2Cl	12.2	106.8	112.1	108.6	109.5

[a]B3LYP/6-311++G(2d,p) bond angles of the aliphatic carbonates do not show significant perturbation, suggesting a weak Thorpe-Ingold effect, if any.

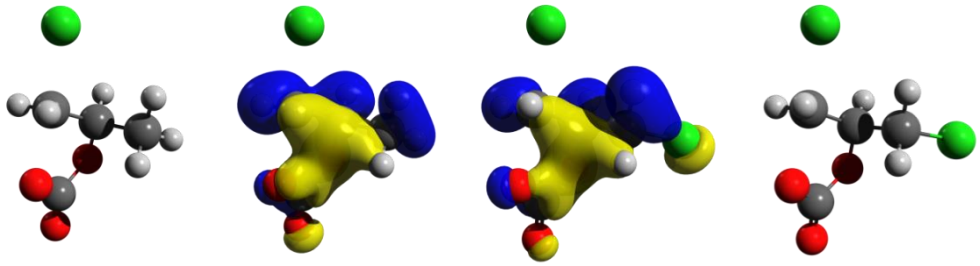

Figure II-6. HOMO-15 and HOMO-17 of PC-2Cl (left) and ClPC-2Cl (right) at their respective transition states. These two molecular orbitals indicate some interactions between the pendant group and the methylene carbon undergoing reaction.

In low-lying molecular orbitals, the electrons on the pendant groups delocalize into the p orbitals on the methylene carbons undergoing reaction (Figure II-6). This in-phase interaction is believed to contribute to the lower energy of the transition state structure.

The reactions with styrene carbonate, propylene carbonate and chloropropylene carbonate at the methine positions were examined (Table II-4, entries 2, 4, and 6). At the transition state, the phenyl substituent was better able to stabilize the partial positive charge on the methine carbon (Mulliken charge of +0.335) than the methyl (Mulliken charge of +0.445), and the chloromethyl substituents (Mulliken charge of +0.702). In the

language of valence bond theory, the superior electronic stabilization is due to the ability of the phenyl p_π electrons to delocalize with the p orbitals on the sp^2 methine carbon. This stabilization is not possible with the methyl and chloromethyl substituents; the calculated molecular orbital of the transition state structure clearly show the favorable interactions between the phenyl substituent and the methine center (Figure II-7). The free energy barrier for reaction at the methine carbon is thus lower for styrene carbonate than for propylene carbonate and chloropropylene carbonate (14.0 kcal/mol vs. 16.4 and 18.2 kcal/mol). When the carbonate attacks the methylene carbon, the lack of resonance stabilization leads to qualitatively similar free energy barriers (12.2 kcal/mol vs. 10.8 and 12.8 kcal/mol, respectively). Similar observations were made for butadiene and 1,2-dihydronaphthalene carbonates, where methine attack is stabilized by the adjacent π system (Table II-4, entries 8, 9, 13, and 14).

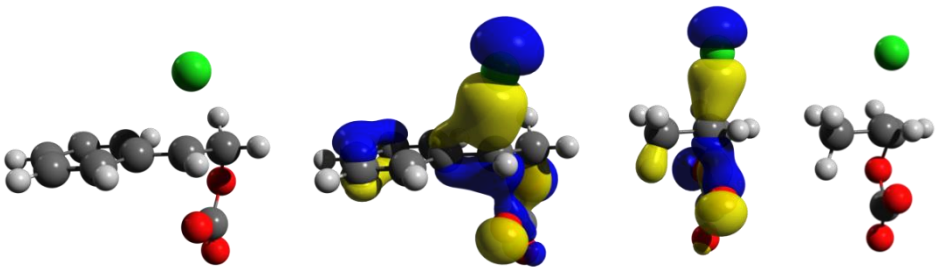

Figure II-7. HOMO-8 (left) of the styrene carbonate transition state to carbonate backbiting, and the equivalent HOMO-6 (right) for propylene carbonate. The transition state for styrene carbonate shows delocalization of the aromatic p_π electrons into the carbon p orbital. Stabilization of the transition state species reduces the activation barrier to carbonate "backbiting". The molecular orbitals for propylene carbonate show no such substituent participation.

Trends in free energy barriers discussed for X = Cl are also observed for X = methyl carbonate. Although steric bulk increases the barrier for reaction at the methine carbon, any pendant group adjacent to the carbon undergoing substitution decreases the barrier

by helping to disperse the positive charge there. Styrene carbonate reacts easily at both methine and methylene positions due to resonance stabilization of the transition state when reaction occurs at the methine position, and by aiding in dispersing the positive charge when reaction occurs at the methylene position.[116]

Relative stabilities of alicyclic carbonates

As an extension of the benchmarking section of this report, the enthalpies of cyclic carbonate formation from carbon dioxide and epoxide at the CBS-4M level are presented in Figure II-8. In the lower-energy chair conformation, *cis*-cyclohexene carbonate is more stable than *trans*-cyclohexene carbonate by 4 kcal/mol (enthalpy). Intuitively, the reverse order is expected because the *cis*-isomer bears substituents at the axial and equatorial positions, whereas the *trans*-isomer's substituents occupy only equatorial positions (Figure II-9). However, the O-CH-CH_2 angles for the *trans*- and *cis*-isomers are 108.3^o and 118.0^o, respectively. In this instance, angle strain appears to outweigh the steric repulsion suffered by axial substituents.

Cyclopentene carbonate and indene carbonate are lower in enthalpy as the *cis*- isomer than the *trans*- by 18 and 22 kcal/mol due to the extreme angle strain found at its tetrahedral bridgehead carbon (O-CH-CH_2 *trans*-: 127°, *cis*-: 111° for CPC, *trans*-: 130°, *cis*-:113° for IC; see Figure II-10).

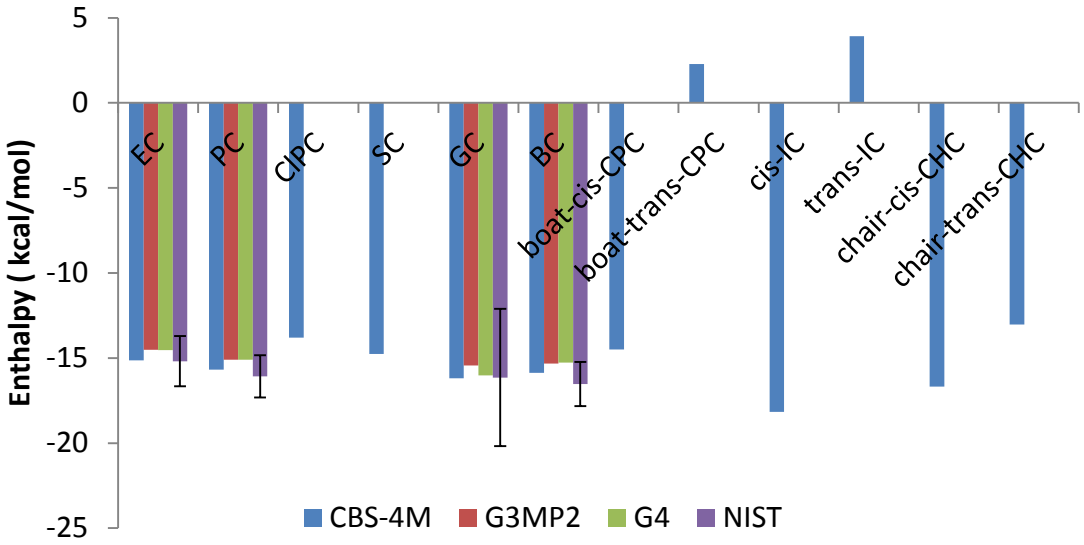

Figure II-8. The enthalpy of the reaction between carbon dioxide and an epoxide to give the corresponding cyclic carbonate(s). The uncertainty of the experimental values presented are denoted by the error bars.

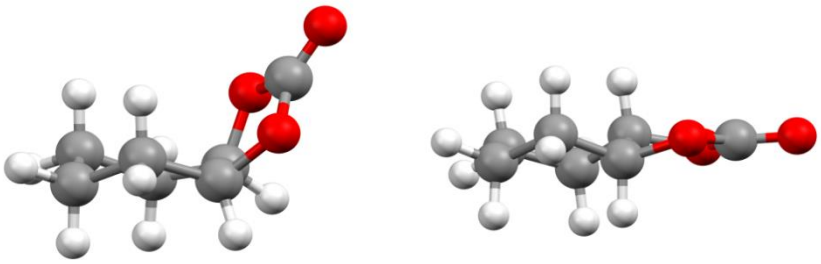

Figure II-9. The carbonate group is attached to *trans*-cyclohexene carbonate (right) at equatorial positions, whereas for the *cis*- isomer (left), it is attached at one equatorial and one apical position. However, the O-CH-CH_2 angles are 108.3° and 118.0° respectively; angle strain is more significant than steric repulsion here, and the *cis*- isomer is more stable by 4 kcal/mol (enthalpy, CBS-4M).

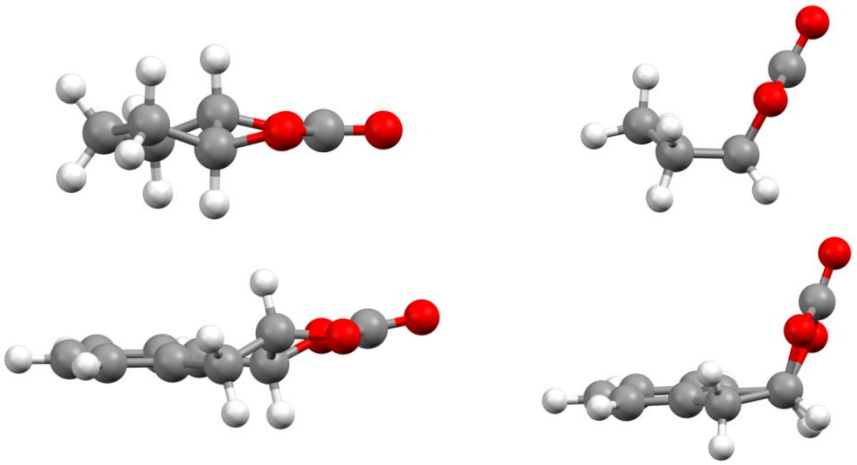

Figure II-10. *trans*- and *cis*- cyclopentene carbonate (top left and right) and indene carbonate (bottom left and right). The *cis*- isomers are more stable by 20 and 23 kcal/mol (cyclopentene carbonate and indene carbonate respectively, in electronic energy) due to the lack of appreciable angle strain (*trans*: 127°, *cis*: 111° for cyclopentene carbonate; trans: 130°, *cis*: 113° for indene carbonate). The boat-like conformation was chosen for cyclopentene carbonate because it is more stable than the chair-like conformation by 2 kcal/mol (electronic energy).

The relative stabilities of cyclohexene carbonate's conformations are important because they directly influence the enthalpy of cyclic carbonate formation via the backbiting mechanism. The backbiting mechanism can only lead to the *cis*-cyclohexene carbonate isomer (poly(*cis*-cyclohexene carbonate) is not present in the polymer). Many research groups including our own have previously reported that cyclohexene oxide readily copolymerizes with carbon dioxide to give poly(*trans*-cyclohexene carbonate) upon catalysis, and that very little cyclic carbonate is produced as an undesired by-product. In particular, when catalyzed by a (salen)chromium(III) X complexes, enchainment and cyclic carbonate formation have activation energies of 11.2 and 31.8 kcal/mol, respectively.[83]

In the present computational study (Table II-4), the free energy of activation for the carbonate of an anionic 1-mer to backbite to lose a chloride anion was 13.5 kcal/mol, but

the transition state required for this reaction had a cyclohexane backbone in a boat-like conformation (a chair-like transition state could not be found). The relaxed chair conformation is 8.0 kcal/mol lower in free energy, establishing 21.5 kcal/mol as the floor for the overall activation barrier. Degradation of this copolymer thus occurs by the polymer first undergoing an energetically demanding chair to boat conversion, before the carbonate backbiting mechanism is able to continue (Figure II-11). In the same fashion, the corresponding overall free energy barrier leading to the loss of methyl carbonate is 25.8 kcal/mol. We thus independently arrived at the same conclusion as a study by Rieger, *et al.*[55]

Where more accessible pathways such as chain growth (E_a = 11.2 kcal/mol when catalyzed by a (salen)chromium(III) X complex[83]) exist, they predominate over the degradation of poly(cyclohexene carbonate), and cyclic carbonate formation is low. Tangentially, the carbonate backbiting of a hypothetical poly(*cis*-cyclohexene carbonate) to give *trans*-cyclohexene carbonate has an extremely high barrier (Table II-4, entries 9 vs. 11), and is unlikely to proceed.

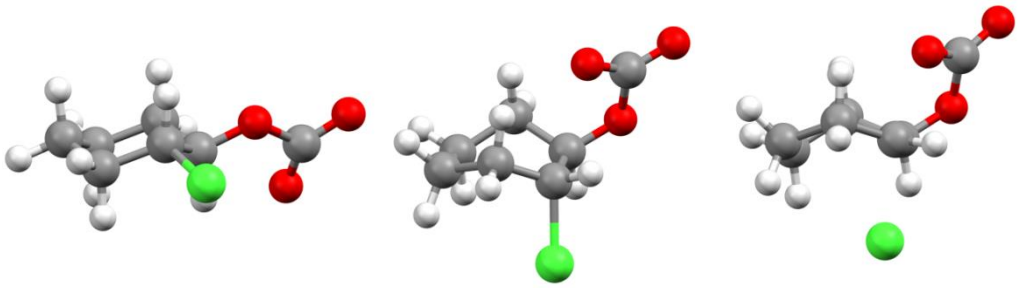

Figure II-11. Relaxed poly(cyclohexene carbonate) 1-mer (left), twist-boat conformation (ΔH = +8.6 kcal/mol), transition state to carbonate backbiting (ΔH = +9.4 kcal/mol from the twist-boat conformation).

Poly(1,4-dihydronaphthalene carbonate) is expected to be a polymer with a high T_g, without suffering from the ease of degradation by carbonate backbiting as described for styrene carbonate. Surprisingly, copolymerization of 1,4-dihydronaphthalene oxide with carbon dioxide gives rise to a significant amount of *cis*-1,4-dihydronaphthalene carbonate coproduct,[122] whereas the analogous reaction for cyclohexene oxide and CO_2 using similar catalysts only produces poly(cyclohexene carbonate).[84] The enthalpies and free energies of the reactions between cyclohexene and dihydronaphthalene oxide with CO_2 to give polycarbonate and cyclic carbonates are very similar (Table II-3), showing that the reason for cyclic carbonate formation was not thermodynamics.

The free energy barriers for carbonate backbiting were similar between both polycarbonates too (Table II-4, entries 11 and 15). The difference is that poly(1,4-dihydronaphthalene carbonate) does not relax to a lower energy conformation beyond the first energy minimum (substituents being pseudo-axial), whereas poly(cyclohexene carbonate) does. Specifically, the only other conformation available for poly(1,4-dihydronaphthalene carbonate) has the substituents in the pseudo-equatorial positions (Figure II-12), and this conformation is 0.9 kcal/mol higher in free energy. Benzannulation removes the unfavorable steric 1,3 interactions with hydrogen atoms that would normally disfavor both substituents being in axial positions.

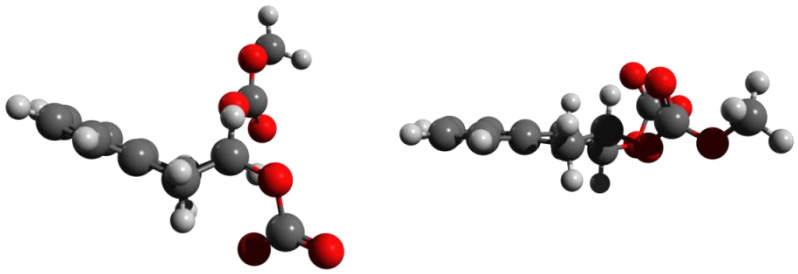

Figure II-12. The first energy minimum after the transition state for poly(1,4-dihydronaphthalene carbonate) to undergo carbonate backbiting has both substituents in the pseudo-axial positions. The only other possible conformation is for the two substituents to be in the pseudo-equatorial positions, and that conformation is 0.9 kcal/mol higher in free energy.

As a result, poly(1,4-dihydronaphthalene carbonate) has a lower barrier to carbonate backbiting than poly(cyclohexene carbonate) ($\Delta G^{\ddagger}$ = 22.7 vs. 25.8 kcal/mol). This barrier is on par with other polycarbonates known to produce cyclic carbonates. The catalysts chosen ordinarily do not produce cyclic carbonate coproduct with conventional epoxides like PO. Perhaps the bulky growing polymer chain binds poorly to the metal center due to steric hindrance, allowing it to undergo metal-free carbonate backbiting more easily.

Backbiting of metal-free alkoxides

While the carbonate backbiting degradation of polycarbonates operates under polymerization conditions (i.e. in a carbon dioxide environment), the alkoxide backbiting degradation is of greater relevance in the absence of carbon dioxide. Since the alkoxide anion is a strong base, this reaction is not expected to occur under ambient conditions since the alkoxide will be protonated by moisture in the air. Rather, polymers may be deliberately recycled to cyclic carbonates for purification and eventual reuse, e.g., as a high temperature solvent.

To the best of our knowledge, the mechanism of the base transesterification of organic carbonate esters has not been studied computationally. In this study, we drew inspiration

from the base hydrolysis of organic carbonates[123] and carboxylate esters.[124] In our proposed mechanism, the alkoxide-carbonate reactant complex eventually forms a tetrahedral intermediate with four oxygen substituents. This intermediate can eliminate either of the alkoxide ligands to revert to the starting material, or to proceed to the product (**Scheme II-4**).

Scheme II-4. Proposed mechanism for alkoxide backbiting.

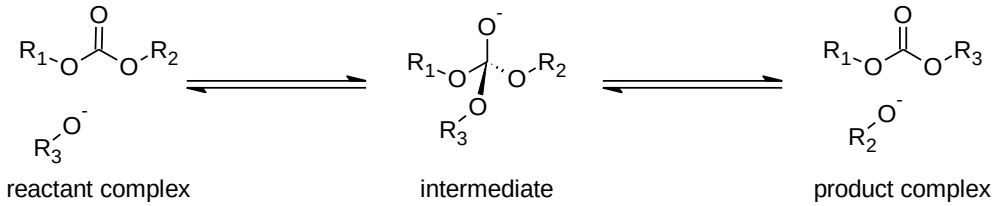

While B3LYP/6-311G(2d,d,p) pre-defined in the CBS-QB3 composite method was suitable for the carbonate backbiting study, it was inadequate for describing loosely-bound transition states involved in the alkoxide backbiting process due to the lack of diffuse functions. The CBS-QB3(+) composite method that uses B3LYP/6-311+G(2d,d,p) reference geometries was used instead,[24] and the results are summarized in Table II-6. Despite various attempts, the transition state between the tetrahedral intermediate and the open chain form of cyclohexene carbonate (where the pendant groups are *anti* to the carbonyl oxygen) could not be located.

The working model of the alkoxide backbiting process is depicted in **Scheme II-5**. The polymer chain is represented by a methoxide anion for computational economy. The alkoxide nucleophile can be on the methylene or the methine carbon of the future cyclic carbonate, and the substituent can be *syn*- or *anti*- with the carbonyl oxygen ("up" and "down") respectively.

Scheme II-5. Working model for alkoxide backbiting to form cyclic carbonate.

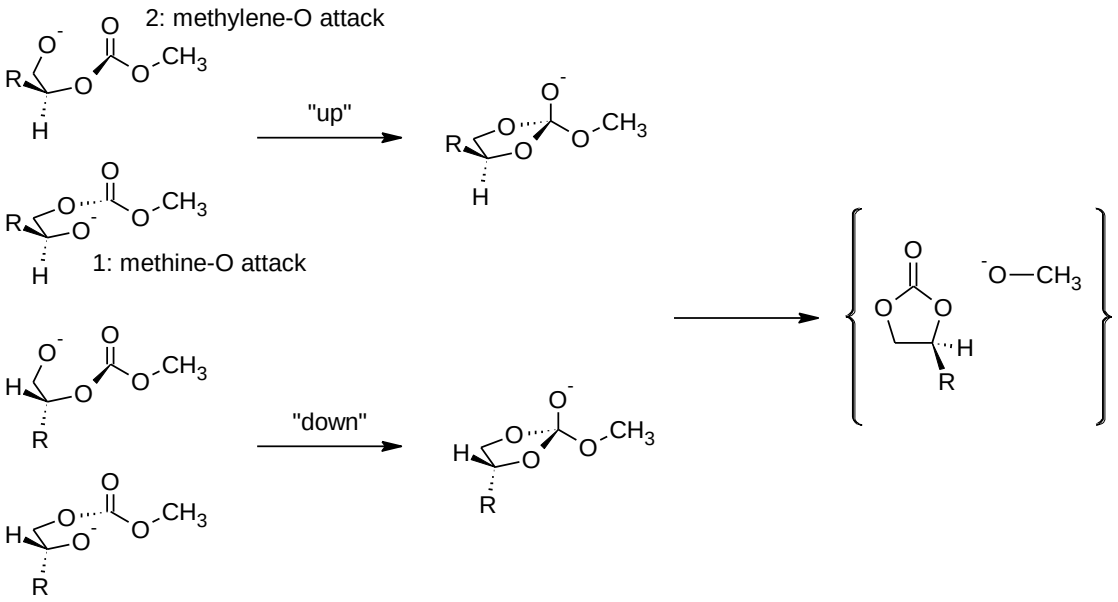

Table II-6. Free energies (kcal/mol) of the various species involved in the alkoxide backbiting reaction, relative to the tetrahedral intermediate.

	Open chain	**TS1**	**Tetrahedral intermediate**	**TS2**	**{Cyclic carbonate + methoxide}**
EC	9.4	9.5	0	11.6	8.9
PC-up-1	10.6	10.4	0	12.7	9.0
PC-up-2	10.0	10.0	0	12.7	9.0
PC-down-1	7.5	8.8	0	11.8	9.5
PC-down-2	7.6	10.1	0	11.8	9.5
ClPC-up-1	7.9	8.8	0	14.1	11.5
ClPC-up-2	9.7	10.0	0	14.1	11.5
ClPC-down-1	5.7	5.8	0	12.4	11.5
ClPC-down-2	10.3	12.1	0	12.4	11.5
SC-up-1	7.9	8.0	0	13.0	10.5
SC-up-2	9.2	9.3	0	13.0	10.5
SC-down-1	4.9	6.2	0	10.7	8.9
SC-down-2	8.0	7.5	0	10.7	8.9
BDC-down-1	4.5	6.2	0	12.5	8.4
BDC-down-2	6.4	7.2	0	12.5	8.4
cis-CHC-up	9.8	10.3	0	11.5	6.4
cis-CHC-down			0	14.8	11.6
trans-CHC	6.2	6.8	0	14.6	11.0
trans-1,4-DhNC	4.9	5.5	0	14.9	11.9
trans-1,2-DhNC-up-1	1.1	5.3	0	15.9	12.1
trans-1,2-DhNC-up-2	3.9	5.4	0	15.9	12.1
trans-1,2-DhNC-down-1	1.1	5.3	0	16.1	12.4
trans-1,2-DhNC-down-2	3.9	5.4	0	16.1	12.4
cis-CPC-up	10.2	9.6	0	12.3	8.7
cis-CPC-down	5.6	7.9	0	9.9	8.6
trans-CPC	-3.4	4.3	0	16.5	13.0

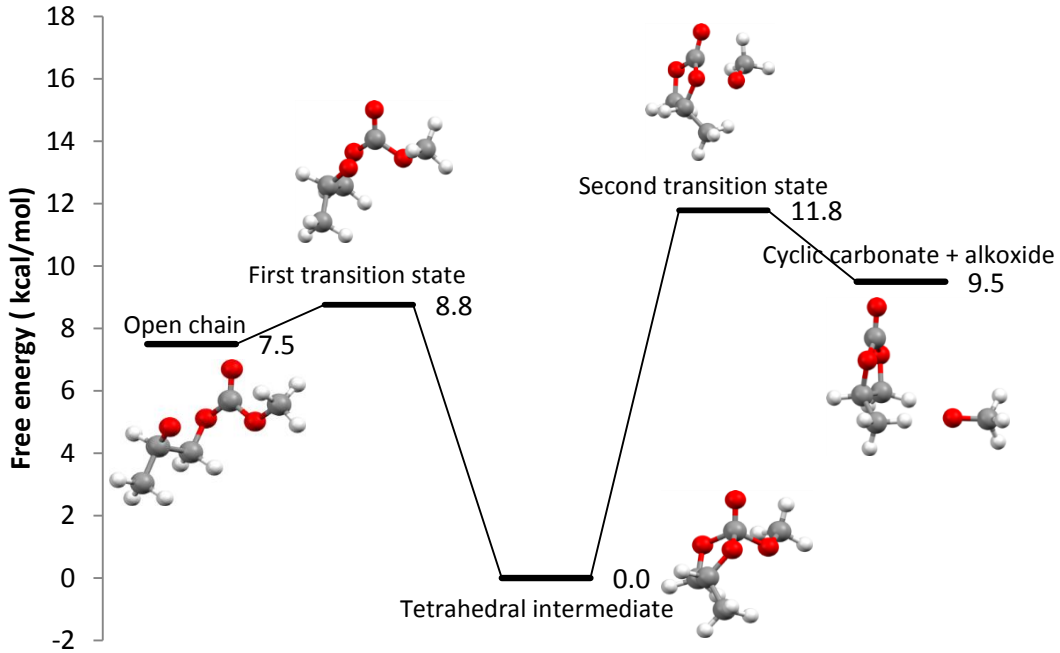

Figure II-13. Free energy diagram for alkoxide backbiting to eventually yield propylene carbonate and an alkoxide polymer chain (represented by methoxide; see entry PC-down-2 of Table II-6).

With the exception of *trans*-cyclopentene carbonate, the free energy barrier required for the polymeric alkoxide to reach the tetrahedral intermediate is very small (Table II-6 and Figure II-13). In some instances, negative free energy barriers are noted. The electronic energy barrier for these reactions are small in all cases.[63] After vibrational corrections are taken into account, some of these barriers may be inundated by the height of the first vibrational mode. Consequently, there is little to no barrier for the alkoxide to backbite to give the tetrahedral intermediate. By the same reasoning, there is a negligible energy barrier for a polymeric alkoxide to attack a cyclic carbonate unit, leading to chain growth. However, this pathway is entropically disfavored at high temperature. Furthermore, the ring-opened cyclic carbonate readily reverts to the tetrahedral

intermediate because the alkoxide anion is tethered to the new carbonate group. This "chelate effect" helps ensure that the alkoxide ring-opened product is disfavored.

Generally, the alkoxide backbiting intermediate is less stable (by 0.2-3.3 kcal/mol, free energy) when the pendant group is *anti* to the carbonyl oxygen ("down"), than when the pendant group is *syn* ("up"). The energy differences between the *syn*- and *anti*-conformers at the second transition state are small (0.1-1.5 kcal/mol). The difference in activation barriers to backbiting is attributed to the energies of the intermediate, rather than the energies of the second transition states. Poly(ethylene carbonate) has no pendant groups, and the substituents for poly(cyclopentene carbonate) and poly(cyclohexene carbonate) are required to be "up" and "down" at the same time due to their *trans* conformation.

Except for cyclopentene carbonate, loss of the shortened polymeric alkoxide from the tetrahedral intermediate is rate limiting. This free energy barrier is lower for aliphatic polycarbonates (EC, PC, SC, BDC) than for alicyclic polycarbonates (CHC, CPC, DhNC): 11-13 vs. 14-17 kcal/mol. The difficulty in alkoxide backbiting correlates well with the O-CH-CH_2 (or equivalent) angle. At the second transition state (TS2), the O-CH-CH_2 angles for the species derived from aliphatic polycarbonates only experience slight deviations from an sp^3 carbon's 109.5° (107-113°), whereas these angles are significantly deviated for the species derived from alicyclic polycarbonates (118-120°). Poly(cyclopentene carbonate) has an extremely high barrier to alkoxide backbiting (19.9 kcal/mol overall) and this is due to its high angle strain present throughout this reaction profile.[125]

Of the aliphatic polycarbonates, poly(styrene carbonate) has the lowest free energy barrier to give cyclic carbonate. Extending the ground state argument, HOMO-2 of the poly(styrene carbonate) tetrahedral intermediate shows an out-of-phase interaction between the p_π orbitals on the phenyl pendant group and the orbitals on the five-

membered cyclic carbonate ring. Such pendant group interactions are not observed for ethylene, propylene, and chloropropylene polycarbonates (Figure II-14).

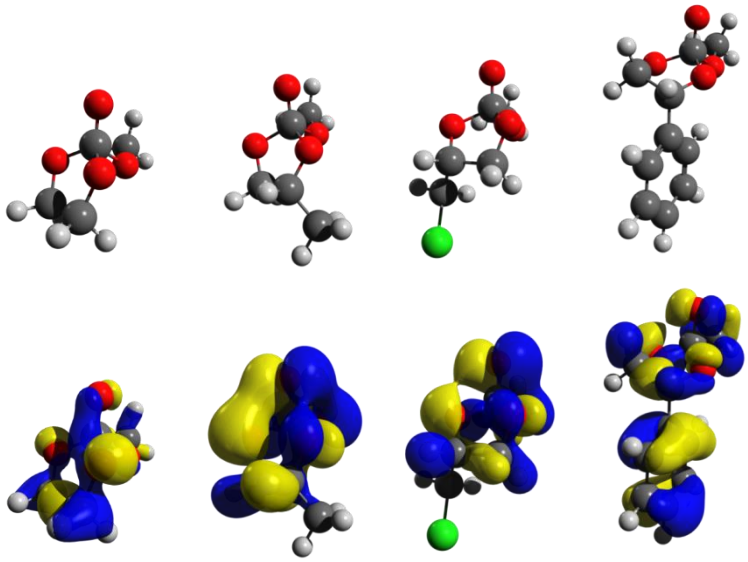

Figure II-14. From left to right: HOMO-6 of the ethylene carbonate alkoxide backbiting intermediate, and the corresponding HOMO-2s for propylene carbonate, chloropropylene carbonate, and styrene carbonate backbiting intermediates. For styrene carbonate, the out-of-phase interaction between the p_π orbitals on the pendant benzene ring and the orbitals on the base of the cyclic carbonate destabilize the intermediate, effectively lowering the barrier to eliminate styrene carbonate.

trans-Cyclopentene carbonate is anomalous because the open chain species has less angle strain than both the transition state and the tetrahedral intermediate (Figure II-15). As a result, poly(*trans*-cyclopentene carbonate) has a 7.7 kcal/mol free energy barrier for the open-chain alkoxide to backbite onto the carbonate to give the tetrahedral intermediate.

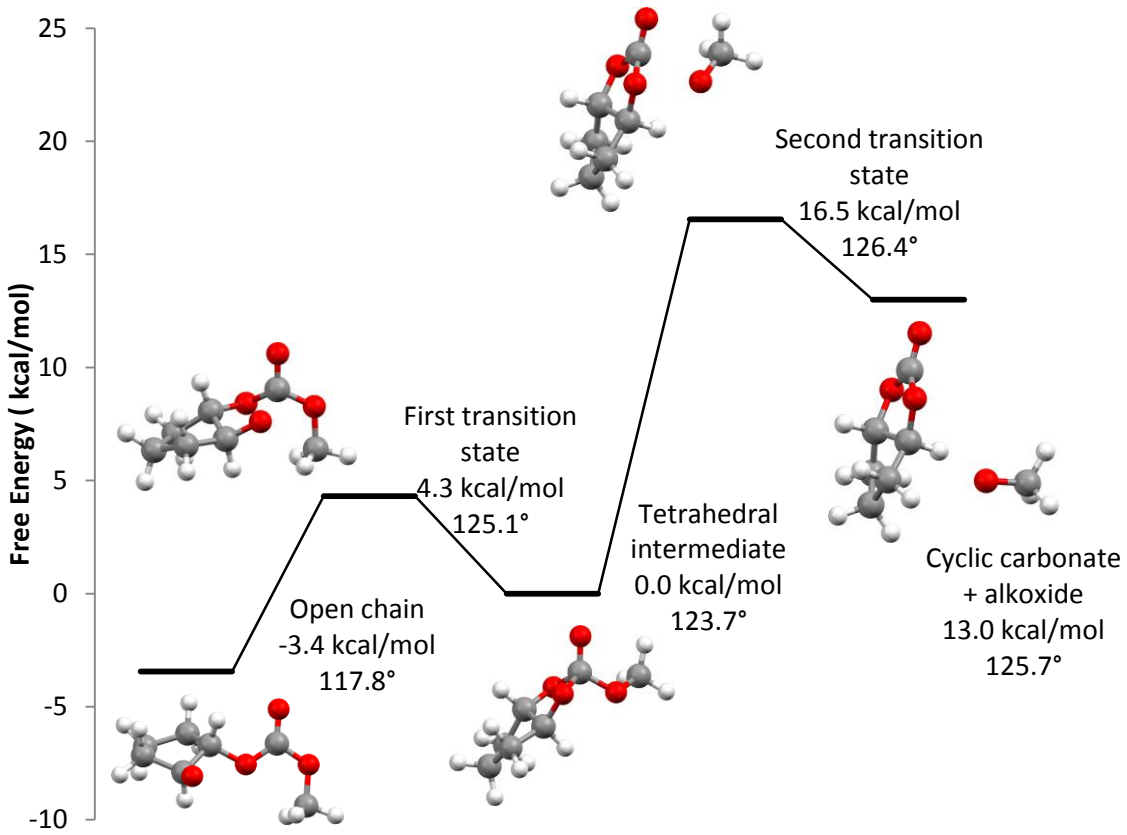

Figure II-15. Free energies and the O-CH-CH_2 bond angles for the *trans*-cyclopentene carbonate alkoxide backbiting process. This carbonate has a very high effective free energy barrier of 19.9 kcal/mol to cyclize via alkoxide backbiting compared to the other carbonates.

Comparing Table II-4 and Table II-6, the most important conclusion to be drawn is that the metal-free carbonate backbiting reactions have free energy barriers 10 kcal/mol higher than the equivalent alkoxide backbiting reactions. This alkoxide backbiting reaction has been investigated experimentally by our group as well.[85] In that study, azide was used as a base to deprotonate purified, metal-free polymers bearing hydroxy end groups, and the rates of reaction were monitored by *in situ* infrared spectroscopy (**Scheme II-6**).

Scheme II-6. The alkoxide backbiting reaction monitored examined by *in situ* infrared spectroscopy.

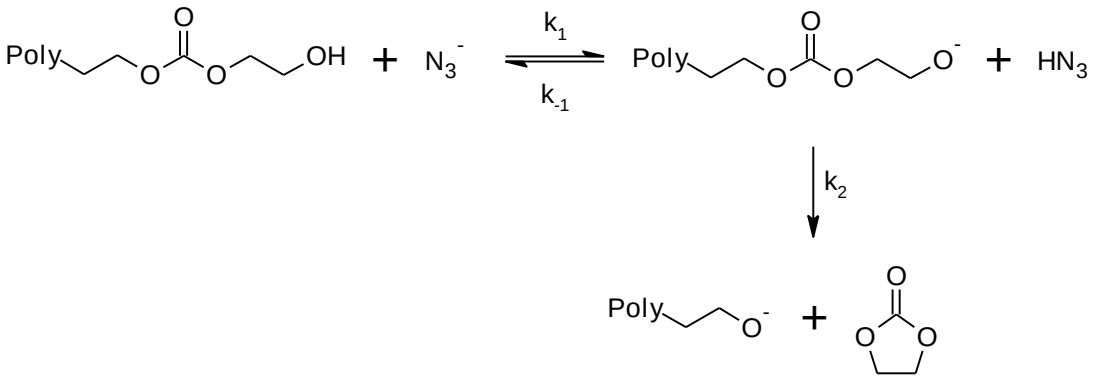

The observed rate constants take into account the equilibria between the alcohol and alkoxide forms of the polymer chains. Even so, the computationally-derived results agree qualitatively with what was previously reported: the activation barriers for alkoxide backbiting are lowest for poly(SC), and that the activation barriers for poly(PC) and poly(ClPC) are similar and higher.

Concluding remarks

The enthalpies of polymerization of several aliphatic polycarbonates and poly(cyclohexene carbonate) were found by computational methods to be essentially the same (-21 to -23 kcal/mol), and the polymerization reactions are all more exothermic than cyclic carbonate formation. On the other hand, the enthalpy of polymerization for poly(cyclopentene carbonate) formation was found to be significantly lower at -15.8 kcal/mol due to ring strain. It is apparent that cyclic carbonate formation is more entropically favored than polymer growth, since cyclic carbonate formation is the thermodynamically favored product in all cases.

Metal-free carbonate backbiting is believed to be the main pathway to cyclic carbonate co-production under polymerization conditions where there is an excess of carbon dioxide, as the metal-bound carbonates backbiting has a much higher activation barrier

than backbiting via the alkoxide chain end. The barrier is increased by steric bulk at the carbon undergoing reaction regardless of the pendant group's electron-donating or electron-withdrawing ability, except where the transition state is stabilized by p_{π}-p delocalization.

Three special cases merit reiteration: The reaction of styrene oxide and carbon dioxide gives rise to large amounts of cyclic carbonate byproduct despite the formation of the latter being less exothermic by 8.0 kcal/mol. This is due to the low activation barrier for carbonate backbiting. Conversely, preparation of poly(cyclohexene carbonate) yields little cyclic carbonate byproduct because: (i) the latter is 5.9 kcal/mol less stable (enthalpy), and (ii) the growing polymer chain must undergo an 4.7 kcal/mol chair-boat conformational change before it is able to overcome a 21.1 kcal/mol free energy barrier to backbite. Unlike poly(cyclohexene carbonate), preparation of poly(1,4-dihydronaphthalene carbonate) leads to cyclic carbonate coproduct because there is no lower-energy conformation to raise the effective free energy barrier for cyclic carbonate formation.

In the absence of a CO_2 atmosphere, the polymer chain end will be in the form of a free alkoxide anion. Metal-free alkoxide backbiting is proposed to occur via a tetrahedral intermediate. Alkoxide attack of the carbonate to give the tetrahedral intermediate is generally barrierless. The rate-determining step to alkoxide backbiting is therefore the activation barrier to the second transition state that leads to cyclic carbonate formation. The free energy barrier for this process is more favorable than the carbonate backbiting process by about 10 kcal/mol. Chain extension through alkoxide attack is not likely because the ring-closing reaction is much more favorable due to the "chelate effect".

In closing, the CBS-QB3 composite *ab initio* method was successfully used to determine the enthalpies of polymerization and cyclic carbonate formation, and the energy barriers for carbonate and alkoxide backbiting reactions. The energies determined are expected to be "chemically accurate" (± 1 kcal/mol), and we have shown this to be true for a set of

benchmark reactions. The importance of validating DFT calculated reaction enthalpies with experimental data and/or high level *ab initio* calculations cannot be overemphasized.[126]

Computational methods

All calculations were performed using the Gaussian 09 suite.[127] The *ab initio* and DFT methods chosen were used primarily with Pople-style basis sets.[128] All local minima and saddle points were confirmed by their calculated vibrational frequencies (zero and one imaginary frequencies respectively). The saddle points found were confirmed to be the correct ones by visualizing the imaginary vibrational modes with AGUI[129] and Avogadro.[130]

Where solvation was applied, tetrahydrofuran was the prototypical solvent used, and the Integral Equation Formalism Polarization Continuum Model (IEFPCM) calculation with radii and non-electrostatic terms for Truhlar and coworkers' SMD solvation model was used.[131]

Benchmarking

Geometries and frequencies of all species were calculated at the B3LYP/6-31+G(d') level. Single-point energies were obtained using other methods and basis sets, and the previously obtained thermodynamic corrections were applied. The B3LYP/6-31+G(d') structures were also used as the starting geometries for the composite methods (CBS-4M,[103-104] CBS-QB3,[103,105] G3(MP2),[106] and G4[102]). These calculated gas phase enthalpies were compared to critically-evaluated thermodynamic data published by the NIST.[57-58]

Enthalpies of polymerization

B3LYP/6-31G(d') geometries of the polycarbonate oligomers were found, and they served as starting points for the CBS-4M calculations in the gas phase.

Carbonate and alkoxide backbiting

For the carbonate backbiting calculations, gas phase B3LYP/6-311++G(2d,p) optimized geometries with single-point solvation energy corrections were used, whereas geometries were optimized at the B3LYP/6-311+G(2d,d,p) level with solvation throughout for the alkoxide backbiting calculations. Molecular orbitals were visualized at the same levels of theory. Unmodified CBS-QB3 calculations with solvation were performed for the carbonate backbiting reaction, whereas the CBS-QB3(+) model as modified by Martin and co-workers[108] with solvation was used for the alkoxide backbiting reaction. B3LYP/6-311+G(2d,d,p) reference geometries and frequencies were read-in, and the CBS-QB3 calculation proceeded directly to the third step (CCSD(T)/6-31+G(d')) using the CBS-QB3(StartMP2) keyword in Gaussian 09. The scale factor for the zero-point energies was not changed from the 0.99 pre-defined by CBS-QB3.

CHAPTER III

BASE INITIATED DEPOLYMERIZATION OF POLYCARBONATES TO EPOXIDE AND CARBON DIOXIDE CO-MONOMERS*

Introduction

Extensive mechanistic studies of the metal-catalyzed reaction between carbon dioxide and different epoxides to give polymers have been carried out.[10-20] Polymer growth is often accompanied by cyclic carbonate formation as the anionic growing polymer chain (metal-bound or metal-free) undergoes alkoxide or carbonate backbiting, leading to the loss of one repeat unit, and the formation of one equivalent of cyclic carbonate.[19,84-85] Complementary to experimental reports by ourselves and others, we have recently performed a computational study on the thermodynamics of the enchainment reaction, and the reaction barriers of both the metal-free backbiting reactions.[63]

In that article, we reported that the metal-free carbonate and alkoxide backbiting reactions had free energy barriers of 18-25 kcal/mol and 10-14 kcal/mol, respectively. In contrast, where a (salen)Cr(III) catalyst was used, the analogous metal-bound degradation reaction of poly(cyclohexene carbonate) had higher activation energies, 32 kcal/mol[83] and 25 kcal/mol[84] respectively. The theoretical results indicate that backbiting requires more energy when metal-bound, helping to explain the success of contemporary catalysts for the polymerization reaction that have tethered onium cations.[18] These onium cations prevent the growing polymer chain from dissociating fully, thus avoiding metal-free degradation.[132]

---

* Darensbourg, D. J.; Yeung, A. D.; Wei, S.-H. Green Chem. **2013**, *15*, 1578. - Reproduced by permission of The Royal Society of Chemistry. This article is also located at http://pubs.rsc.org/en/Content/ArticleLanding/2013/GC/c3gc40475g.

This chapter presents the reaction barriers of another degradation pathway that causes these polycarbonates to revert to the epoxide and carbon dioxide co-monomers. Such a depolymerization reaction is particularly attractive in the context of recycling plastic waste:[133] by returning the waste polymer to monomer indistinguishable to raw material in an energy-undemanding process, the original polymer can be recreated with no compromise as to its physical properties.

The results will be discussed in the context of the carbonate- and alkoxide-backbiting reactions that yield cyclic carbonate. These computational results will also be used to rationalize experimental observations with regard to the degradation of poly(*trans*-cyclopentene carbonate). They emphasize that poly(*trans*-cyclopentene carbonate)'s behavior sets it apart from other members of this class of polycarbonates.

Results and discussion

The motivation for the investigation undertaken herein was an interesting experimental observation.[134] That is, when treated with the sodium bis(trimethylsilyl)amide, a strong base, hydroxy-terminated poly(*trans*-cyclopentene carbonate) was degraded to a mixture of cyclopentene oxide and *cis*-cyclopentene carbonate. However, upon performing the same reaction in the presence of added carbon dioxide, only *cis*-cyclopentene carbonate was obtained (**Scheme III-1**).

Scheme III-1. Behavior of hydroxy-terminated poly(*trans*-cyclopentene carbonate) when treated with a strong base, with and without added carbon dioxide.

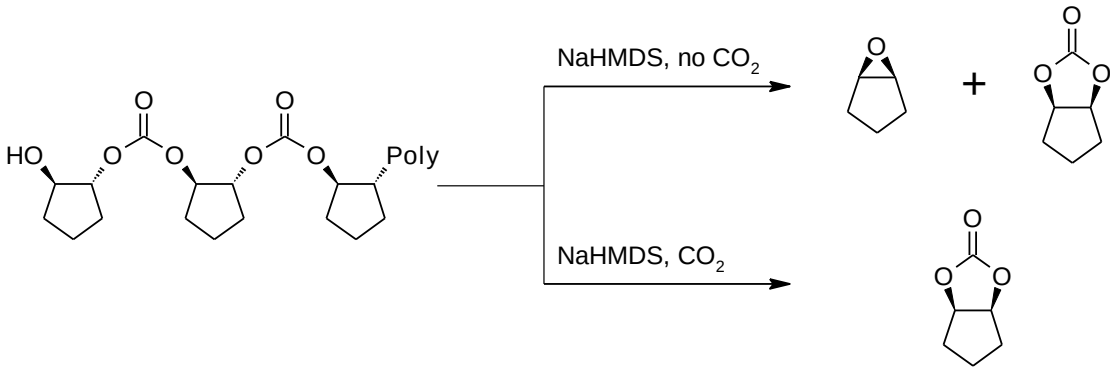

Formation of the epoxide indicated that the alkoxide had undergone an intramolecular nucleophilic substitution, displacing a carbonate-terminated polymer represented by the methyl carbonate anion (**Scheme III-2**). This reaction is akin to the formation of an epoxide by the deprotonation of a chlorohydrin.

Scheme III-2. Intramolecular nucleophilic substitution reactions leading to an epoxide. Methine attack occurs where $R_2 \neq H$ and methylene attack occurs where $R_2 = H$.

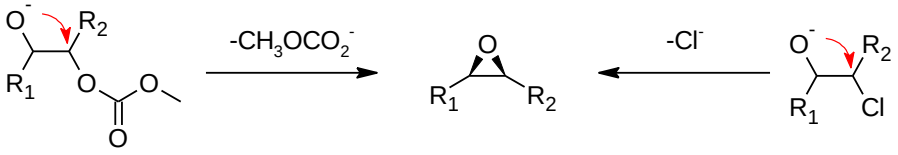

<u>Reaction barriers for the alkoxide backbiting reaction to give epoxide</u>

In this study, we considered a free alkoxide anion generated by the complete deprotonation of a hydroxy-terminated polymer, solvated by tetrahydrofuran. This approach allowed us to evaluate barriers to epoxide formation that are uncomplicated by ion pairing, and by the equilibrium that arises when the alcohol is deprotonated by a poorer base.[85]

At the transition state, the appropriate carbon-oxygen bonds are ca. 2.0 Å in length, significantly greater than the typical C-O length of 1.42 Å.[118] To yield epoxides, the alkoxide oxygen is only two bonds away from the carbon center undergoing substitution; the O-C-O angles of 148-157° are significantly distorted. For the oxetane-forming reaction, the alkoxide oxygen is three bonds away, permitting an O-C-O angle of 175° that is close to the ideal 180°.

The free energy barriers for the alkoxide backbiting reaction to yield epoxides were computed (Table III-1) in advance of experimental kinetic data. The trends previously reported for carbonate backbiting reactions to give cyclic carbonates[63] were also observed for the current system that yields epoxides, and they are consistent with S_N2-type reactions in general:[116]

1. There is a higher barrier to reaction at the methine position than at the methylene position; this is a steric effect (entries 2 and 4; see **Scheme III-2**).
2. In some cases, there is a lower barrier to reaction at the methylene position, compared with the alkoxide derived from ethylene carbonate (entries 3 and 5). For the case of carbonate backbiting, we showed that this lowering was due to favorable interactions between the pendant group and the carbon atom undergoing substitution. Such interactions are less obvious for the cases we have studied here.
3. The reactivity trends mentioned above are not observed for the alkoxides derived from styrene carbonate. The p_π electrons on the phenyl pendant group delocalize onto the empty p orbital of the carbon undergoing substitution, thereby reducing the barrier to reaction (entry 6 and Figure III-1).

Table III-1. Relative free energies (in kcal/mol) of the species involved in alkoxide backbiting to give the corresponding epoxide.[a]

No.		Open-chain alkoxide	Transition state	Epoxide + methyl carbonate
1	EC	0	14.6	-16.7
2	PC-1	0	14.9	-19.1
3	PC-2	0	12.7	-18.8
4	ClPC-1	0	17.4	-15.7
5	ClPC-2	0	13.7	-14.2
6	SC-1	0	14.5	-18.0
7	SC-2	0	15.4	-14.0
8	CPC	0	13.3	-20.6
9	CHC	0	15.6	-17.1
10	TMC	0	20.7	-19.6

[a]Open chain alkoxide derived from ethylene carbonate (EC) = $^{-}OCH_2CH_2OCO_2CH_3$. PC = propylene carbonate; ClPC = chloropropylene carbonate; SC = styrene carbonate; CPC = cyclopentene carbonate; CHC = cyclohexene carbonate; TMC = trimethylene carbonate. -1 and -2 denote alkoxide attack at the methine or methylene positions, respectively. The convention used here is consistent with that used in our last report on this topic.[63]

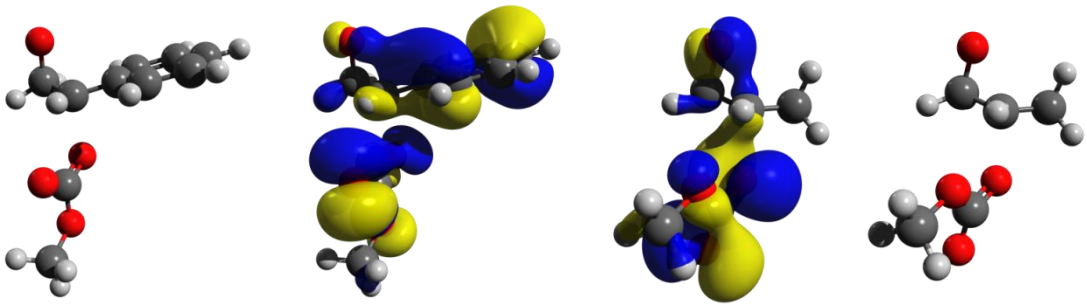

Figure III-1. HOMO-3 of the alkoxides derived from styrene carbonate (left) and propylene carbonate (right) at the transition state to epoxide formation (methine attack). The filled p_π electrons on the phenyl pendant group of delocalize into the empty p orbital on the carbon undergoing substitution, stabilizing the transition state, and lowering the barrier for reaction (left). The methyl pendant group provides no such stabilizing interaction (right).

The alkoxide derived from trimethylene carbonate (entry 10) has an unusually high free energy barrier to ring closure (20.7 kcal/mol), compared with that derived from ethylene carbonate (14.6 kcal/mol, entry 1), even though the ring strain energies for cyclobutane and cyclopropane are approximately the same (26.2 and 27.6 kcal/mol, respectively).[116] An extended discussion of this topic is beyond the scope of this chapter, but we do note that at the transition state, the substituents on two carbons are eclipsed for the alkoxide derived from trimethylene carbonate, whereas such an arrangement is absent in the alkoxide derived from ethylene carbonate. When allowed to relax, the alkoxide derived from trimethylene carbonate is able to extend and relieve such strain. From a different perspective, more conformational change is needed for trimethylene carbonate's alkoxide to attain the transition state to cyclic ether formation, compared with ethylene carbonate's. Similar attempts were made to rationalize the free energy barriers for cyclopentene and cyclohexene carbonate-derived alkoxides to form the corresponding epoxides, but no straightforward explanation was found for their differing reactivity.

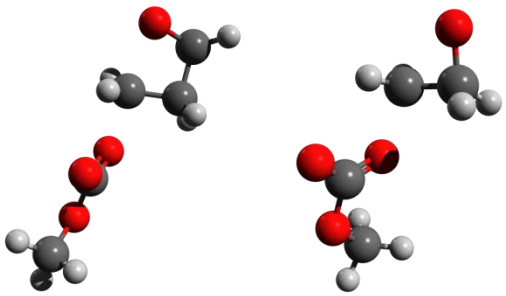

Figure III-2. At the transition state to cyclic ether formation, the substituents on the two carbons of the alkoxide derived from trimethylene carbonate are eclipsed, whereas that is not the case for the alkoxide derived from ethylene carbonate. This may help explain why the former's free energy barrier to cyclic ether formation is 6.1 kcal/mol higher.

The data in Table III-1 indicate that the epoxide-forming reactions are exergonic, which may seem surprising given the strain present in the three-membered cyclic ethers. However, the methyl carbonate leaving anion is a poor nucleophile. Consequently, it has a very high free energy barrier to cause the epoxide to undergo ring-opening. Note that the methyl carbonate anion and the epoxide are considered as separate species rather than as a product complex, so the TΔS component of free energy is overestimated by approximately 10 kcal/mol.

Alkoxide backbiting reactions to give epoxide vs. cyclic carbonate

For a given alkoxide, epoxide formation has a higher barrier than cyclic carbonate formation (Table III-2). The barrier to cyclic carbonate formation was previously found to be the energy required for the polymeric alkoxide (represented by a methoxide anion) to dissociate from the tetrahedral intermediate. Formation of the tetrahedral intermediate is barrierless, in comparison.[63] The alkoxide derived from cyclopentene carbonate is an anomaly, and it will be discussed *vide infra.*

Table III-2. Free energy barriers (in kcal/mol) for both alkoxide backbiting reactions.

No.	Parent carbonate	Epoxide formation	Cyclic carbonate formation[63]
1	EC	14.6	11.6
2	PC-1	14.9	11.8
3	PC-2	12.7	11.8
4	ClPC-1	17.4	12.4
5	ClPC-2	13.7	12.4
6	SC-1	14.5	10.7
7	SC-2	15.4	10.7
8	CPC[a]	13.3	19.9[b]
9	CHC[a]	15.6	14.6
10	TMC	20.7	15.8[c]

[a]The oxygen and the methyl carbonate substituents of the alkoxide anion are mutually *trans*, as they would appear in the polymer. The epoxide will have a *cis* configuration, whereas the cyclic carbonate formed will have a *trans* configuration. [b]Overall barrier from the open chain alkoxide, through the tetrahedral intermediate to the cyclic carbonate + methyl carbonate anion. [c]Not previously published.

Because epoxide formation has a higher barrier than cyclic carbonate formation, it follows that cyclic carbonate formation should dominate. Indeed, no trace of the corresponding epoxide was observed when propylene and styrene polycarbonates were treated with base. Furthermore, sequential epoxide formation steps generate carbon dioxide. In a closed system, an equilibrium between polymeric alkoxide (left) and carbonate (right) exists:

$$\text{Poly-O}^- + CO_2 \rightleftharpoons \text{Poly-OCO}_2^- \quad (1)$$

This equilibrium reduces the concentration of free alkoxide that is required for epoxide formation. With that said, this equilibrium cannot be used to exclude epoxide formation outright since the alkoxide derived from cyclopentene carbonate is able to form appreciable amounts of epoxide in a closed system.

It remains of great interest to depolymerize polycarbonates to recover the starting epoxides. Recycling the co-monomers allows the production of new polycarbonates no

different from virgin polymer. This is superior to current recycling efforts that blend recovered polymer with fresh material to give a product with inferior physical properties. Cyclic carbonates formation may be avoided by conducting the base-initiated degradation reaction under a mild vacuum. By removing any carbon dioxide formed, carbonate backbiting (to cyclic carbonate) can be excluded, and epoxide formation will be able to compete with cyclic carbonate formation.

Understanding poly(*trans*-cyclopentene carbonate)

At this point, we return to the poly(*trans*-cyclopentene carbonate) story that inspired this line of inquiry: Absent added carbon dioxide, poly(*trans*-cyclopentene carbonate) degrades to a mixture of cyclopentene oxide and *cis*-cyclopentene carbonate. In a carbon dioxide atmosphere, *cis*-cyclopentene carbonate is the only product.

cis-Cyclopentene carbonate has a low free energy barrier to formation (9.9 kcal/mol) via alkoxide backbiting of poly(*cis*-cyclopentene carbonate), but the polymer is of a *trans* configuration.[63] Unlike all the other open chain alkoxides, the alkoxide derived from *trans*-cyclopentene carbonate is lower in free energy than the tetrahedral intermediate leading to cyclic carbonate formation. This tetrahedral intermediate is, in turn, lower in free energy than the *trans*-cyclopentene carbonate + methoxide product complex, and this is attributed to angle strain. Rather than a 10-15 kcal/mol free energy barrier for the loss of the polymeric alkoxide (modeled as methoxide), the overall free energy barrier for cyclopentene carbonate to undergo alkoxide backbiting is 19.9 kcal/mol,[63] significantly higher than the free energy barrier for epoxide formation (13.3 kcal/mol).

The great disparity between these two free energy barriers helps explains why no *trans*-cyclopentene carbonate (the product of alkoxide backbiting) is produced (**Scheme III-3**).[134] Additionally, *trans*-fused five-membered cyclic rings are unstable relative to *cis*-fused isomers due to their strained geometries (Table III-3), and this statement is generally true.[135] Replacing oxygen with sulfur leads to less strain due to the C-S bond

(ca. 1.83 Å) being longer than C-O bonds (1.44 Å), and *trans*-cyclopentene trithiocarbonate is well known.[135-136]

Table III-3. Relative enthalpies (in kcal/mol, CBS-QB3) of the different conformations of cyclopentene carbonate and trithiocarbonate.

Conformation	Cyclopentene carbonate	Cyclopentene trithiocarbonate
cis-boat	0	0
cis-chair	2.5	0.1
trans	19.2	5.0

To explain the formation of *cis*-cyclopentene carbonate, the polymeric alkoxide is rapidly converted to carbonate in the presence of carbon dioxide (e.g. from epoxide-forming reactions).[137] The polymeric carbonate product backbites, giving rise to the *cis*-cyclopentene carbonate that is observed experimentally. Given significant amounts of carbon dioxide, negligible free alkoxide should exist. Carbonate backbiting is the only possibility, making *cis*-cyclopentene carbonate the sole product.[10-20]

Scheme III-3. The possible degradation routes available for poly(*trans*-cyclopentene carbonate). Free energy barriers are noted.

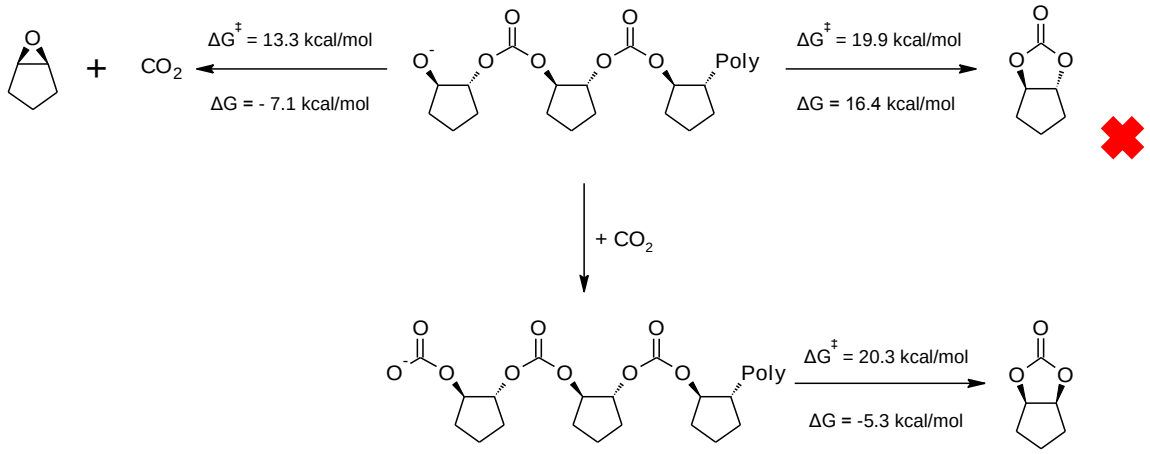

Experimental confirmation

Having understood the details behind poly(cyclopentene carbonate)'s degradation, further experimental studies were done.[134] Firstly, the hydroxy terminal groups on poly(cyclopentene carbonate) were acetylated. The resultant ester-capped polymer did not degrade under similar basic conditions, confirming that such polymers degrade via an unzipping mechanism, instead of by random scission of the polymer chains.

Addition of 0.7 MPa of CO_2 retarded the degradation reaction, and the sole product was cyclopentene carbonate (Figure III-3). This is because polymeric alkoxides are converted to polymeric carbonates (so epoxides are not formed). The slowness of the reaction was due to the carbonate backbiting having a high reaction barrier. Conversely, application of a mild vacuum greatly increased the rate of polymer degradation, and cyclopentene oxide was the dominant product.

The computational predictions were thus substantiated by experimental work, that ultimately led to an efficient method of recycling poly(cyclopentene carbonate) via the co-monomers.

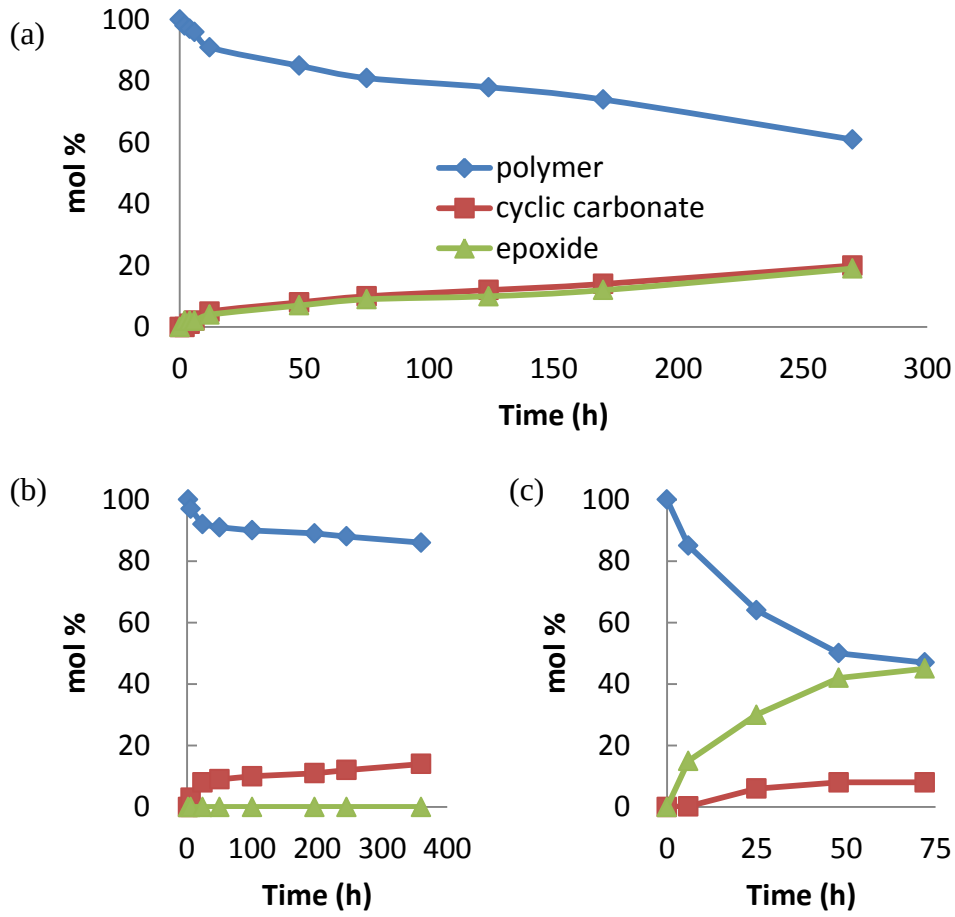

Figure III-3. Degradation of poly(cyclopentene carbonate) when treated with sodium bis(trimethylsilylamide) at 110 °C in toluene-d_8.[134] (a) Under argon; (b) under 0.7 MPa of added CO_2; (c) under a mild vacuum.

Concluding remarks

Beyond the established carbonate and alkoxide backbiting routes, an additional degradation mode for cyclic carbonates has been described, and the computational results presented have explained experimental observations well. This epoxide-forming degradation is only observed for poly(*trans*-cyclopentene carbonate) without added carbon dioxide, because its free energy barrier is lower than the free energy barrier to cyclic carbonate formation via alkoxide backbiting. In all other cases examined, cyclic carbonate is the sole product because epoxide formation has a higher barrier for reaction, and because epoxide formation gives rise to polymeric carbonates that undergo carbonate backbiting.

Nevertheless, epoxide formation reactions have small barriers, and this pathway may be competitive if carbon dioxide were continually removed. Key aspects of these predictions have been tested, and the base initiated degradation may serve as a low energy route to recycle waste polycarbonate to fresh polymer.

Computational methods

All calculations were performed using the Gaussian 09 suite.[127] Geometries were fully optimized using the B3LYP functional[138-140] and the Pople-style 6-311+G(2d,d,p) basis set.[141-143] Molecular orbitals were visualized at this level as well. The Integral Equation Formalism Polarization Continuum Model (IEFPCM) calculation with radii and non-electrostatic terms for Truhlar and coworkers' SMD solvation model[131] was used with tetrahydrofuran as the prototypical solvent throughout.

All local minima and saddle points were verified by their calculated vibrational frequencies (zero and one imaginary frequencies respectively), except for one example noted in the text. The saddle points found were confirmed to be the correct ones by visualizing the imaginary vibrational modes with AGUI[129] and Avogadro.[130] No attempts were made to locate global energy minima of the structures studied.

To be consistent with our previous work,[63] the enthalpies and free energies of the various species at their stationary points were obtained using CBS-QB3(+) calculations:[108] B3LYP/6-311+G(2d,d,p) reference geometries and frequencies were read-in, and the CBS-QB3[103,105] calculation proceeded directly to the third step (CCSD(T)/6-31+G(d')) using the CBS-QB3(StartMP2) keyword in Gaussian 09. The scale factor for the zero-point energies was not changed from the 0.99 pre-defined by CBS-QB3.

Experimental methods

Degradation of polycarbonates with base

15 mg of propylene, styrene and cyclopentene polycarbonates were charged into separate J. Young-sealed NMR tubes. 0.4 mL of a stock solution of sodium bis(trimethylsilyl)amide in toluene-d8 (11 mM) was added to each NMR tube. The solutions were heated to 110 °C for 16 hours, and the NMR spectra were recorded.

CHAPTER IV

KINETICS AND THERMODYNAMICS OF THE DECARBOXYLATION OF 1,2-GLYCEROL CARBONATE TO PRODUCE GLYCIDOL*

Introduction

Glycerol carbonates[32-33] and polycarbonates[34-35] (Figure IV-1) may potentially be synthesized from glycerol and carbon dioxide. Both starting materials are themselves inexpensive and renewable carbon sources. Glycerol is a coproduct of the transesterification of triglycerides that occurs during biodiesel manufacture,[144] and carbon dioxide is produced by various activities, such as the combustion of carbonaceous fuel for the generation of electricity.[145] Straightforward routes to glycerol carbonates and polycarbonates and practical applications for them are highly sought. Success in this endeavor will permit the conversion of two waste products into useful chemicals and materials.

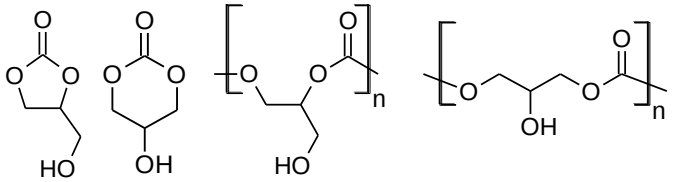

Figure IV-1. Left to right: 1,2- and 1,3-glycerol carbonate; 1,2- and 1,3- poly(glycerol carbonate).

---

* Darensbourg, D. J.; Yeung, A. D. *Green Chem.* **2014**, *16*, 247. - Reproduced by permission of The Royal Society of Chemistry. This article is also located at http://pubs.rsc.org/en/Content/ArticleLanding/2014/GC/c3gc41643g.

Although several groups have successfully prepared poly(1,3-glycerol carbonate) and related derivatives,[146-148] there have been no successful reports of the ring-opening polymerization of 1,2-glycerol carbonate. Rather, the common method of preparing these poly(1,2-glycerol carbonate) polymers is to copolymerize glycidol with carbon dioxide[34-35,149-155] using the well-developed CO_2-epoxide chemistry;[10-20] in this case, glycidol serves as a glycerol surrogate, and its free hydroxyl moiety is invariably shielded by an appropriate ether. The benzyl protecting group is a favorite, where easy and complete deprotection by hydrogenation is desired.[34-35,146,155]

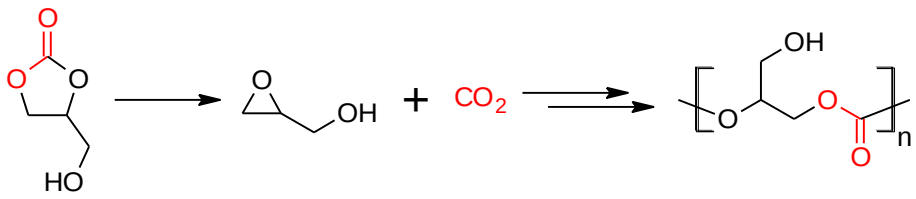

Scheme IV-1. 1,2-Glycerol carbonate is decarboxylated to glycidol. After suitable protection, it copolymerizes with CO_2, and poly(1,2-glycerol carbonate) is obtained after deprotection. In this idealized scheme, glycidol copolymerizes with CO_2 that is produced by decarboxylation.

There have been few reports of the successful conversion of 1,2-glycerol carbonate (that can be obtained ultimately from CO_2 and glycerol) to glycidol, catalyzed by acids or bases (**Scheme IV-1**).[156-164] We anticipate that this reaction, an indirect method to obtain glycidol from glycerol for eventual copolymerization with carbon dioxide, will be of increasing interest. As a result, we undertook a computational study that attempts to understand the kinetics and thermodynamics of the base- and acid-catalyzed decarboxylation reactions. Our results are presented herein.

Results and discussion

We note that as a matter of thermodynamics, decomposition of 1,2-glycerol carbonate into glycidol and carbon dioxide causes an increase in entropy. A direct result is that decarboxylation is favored at higher temperature. To illustrate, experimentalists have found elevated temperatures of ca. 200 °C to be appropriate.[156-157,159-160,163] Since one of the reaction products is a gas, the use of a vacuum to remove one of the coproducts is helpful too, similarly demonstrated.[156-157,163]

The base- and acid-catalyzed decarboxylation reactions were modeled using the composite CBS-QB3 method[103,105] designed to give "chemical accurate" energies (± 1 kcal/mol), modified per Martin *et al.* by the use of added diffuse functions in the geometry optimization step.[108] Solvation models were applied throughout the calculations. We assume that the cationic and anionic reactants are well solvated, such that ion-pairing may be neglected.

Base-catalyzed decarboxylation

The formation of a highly-strained three-membered cyclic ether is difficult, but precedence exists. When deprotonated, poly(cyclopentene carbonate) yields the corresponding epoxide via an intramolecular nucleophilic displacement reaction; an alkyl carbonate is an adequate leaving group for this reaction.[125,134] The pendant hydroxy group on glycerol has been implicated in the degradation of poly(1,2-glycerol carbonate) as well.[34]

In the transesterification of dimethyl carbonate with glycerol catalyzed by triethylamine, Ochoa-Gómez *et al.* observed too, that trace glycidol was produced.[161] We agree with their proposed mechanism (Figure IV-2(a) and **Scheme IV-2**), and studied it with the "chemically accurate" CBS-QB3(+) method.[108]

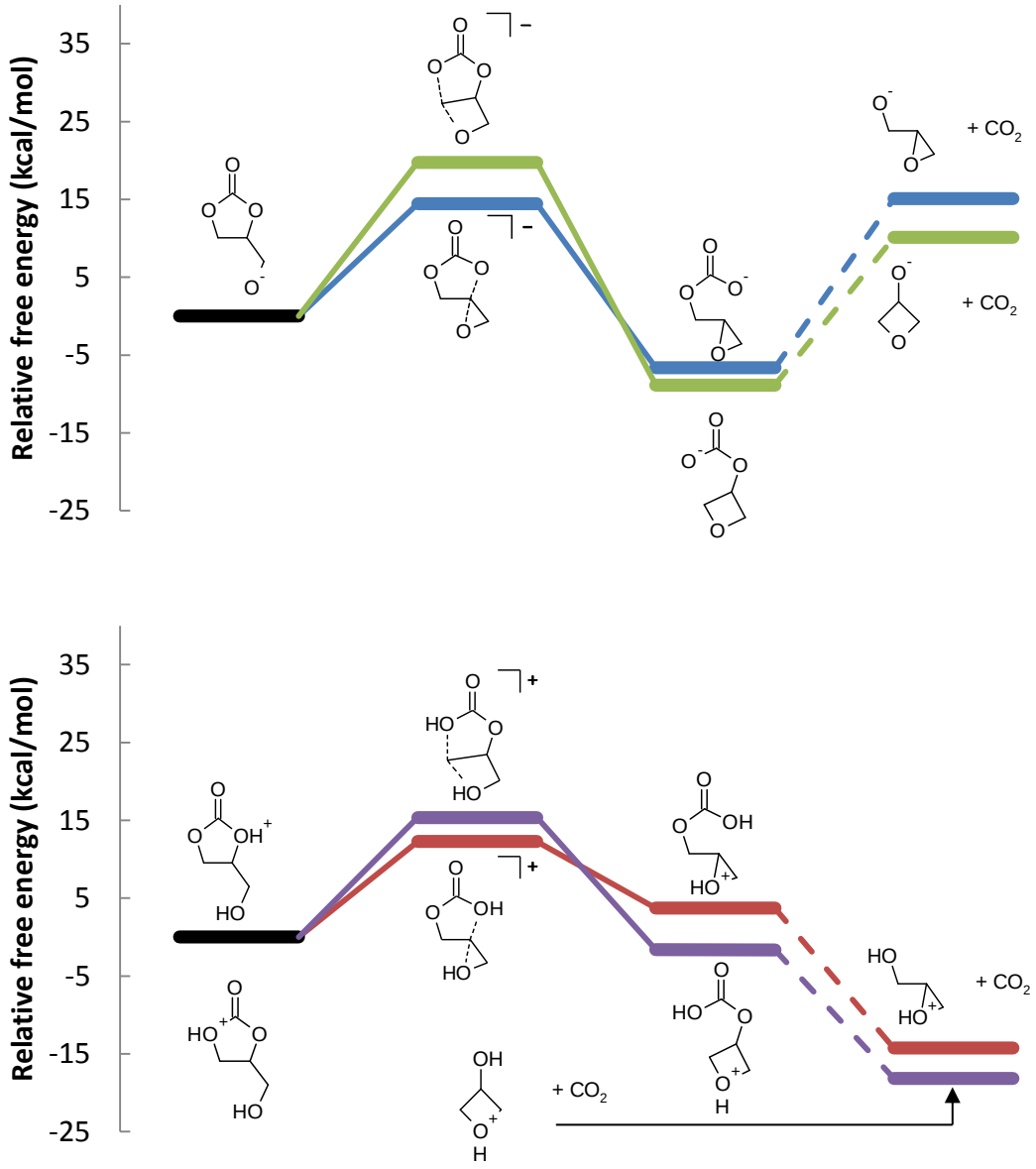

Figure IV-2. Free energy profiles for the base-catalyzed (top) and the acid-catalyzed (bottom) decarboxylation reactions (see **Scheme IV-2** and **Scheme IV-4**). The transition states are also depicted in Figure IV-3.

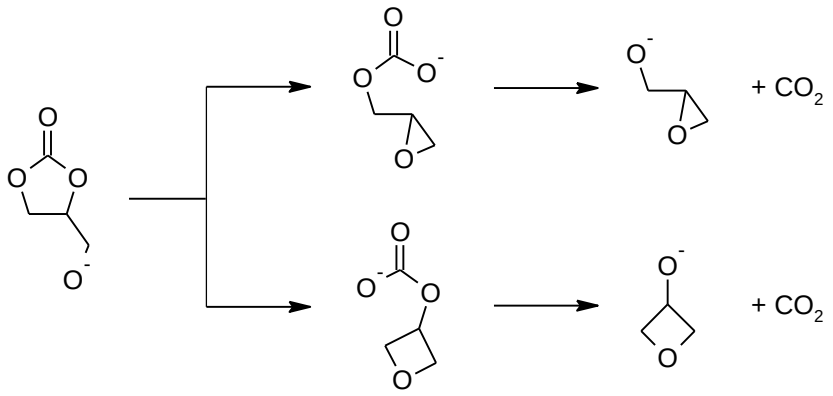

Scheme IV-2. Proposed mechanism for the base-catalyzed decarboxylation reactions leading to (a) glycidol (top) and (b) 3-hydroxyoxetane (bottom) after hydrolysis.

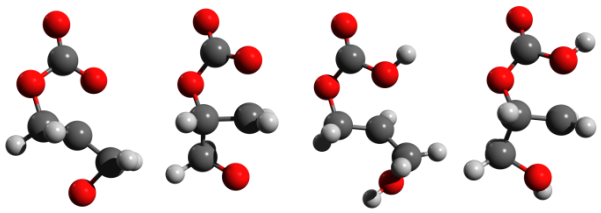

Figure IV-3. Transition states toward cyclic ether formation. Legend: red = oxygen; black = carbon; white = hydrogen. Left-right: Base-catalyzed epoxide and oxetane formation; acid-catalyzed epoxide and oxetane formation. Respective distances (Å): $O_{carbonate}$-C 1.88, 1.96, 2.10, 1.95; O_{ether}-C 1.93, 2.03, 1.99, 2.06. Frequencies of imaginary vibrational mode (cm^{-1}): 461i, 572i, 265i, 444i.

In the proposed mechanism, a strong base deprotonates 1,2-glycerol carbonate's pendant hydroxyl group (not shown), leading to a cyclic carbonate-alkoxide. An intramolecular nucleophilic substitution reaction occurs, ring-opening the five-membered cyclic carbonate, yielding a carbonate anion; the transition states are shown in Figure IV-3. The O-C bonds and O-C-O angles for this base-catalyzed example are similar to the

corresponding bonds and angles when polymeric alkoxides degrade to epoxides, and require no further comment.[125]

Parenthetically, we acknowledge an alternate mechanism, in which the chosen base acts as a nucleophile and attacks the carbonate carbon of glycerol carbonate. In an experimental study by Darensbourg and Wei,[85] poly(styrene carbonate) was found to depolymerize with a linear decrease in molecular weight, while its polydispersity index remained close to unity. Were random scission of the carbonate linkages preferred, the polymer's molecular weight would drop precipitously. When the terminal hydroxy groups were protected as acetate esters, a higher temperature and a longer reaction time was needed for the polymer to degrade via, presumably, this alternate route. Where terminal hydroxy groups are present, e.g. glycerol carbonate, the base-catalyzed intramolecular reaction route in **Scheme IV-2** should dominate.

The free energy barrier to form the epoxide-carbonate anion is 14.4 kcal/mol. Forming the oxetane-carbonate anion has a higher free energy barrier at 19.8 kcal/mol (Figure IV-2 (a)), likely due to mutually eclipsed substituents on the oxetane.[125] The reaction between an alkoxide and carbon dioxide is fast,[137] and the additional barrier is expected to be small, so it should be sufficient to only consider the thermodynamics of the process. Despite the gain of entropy, decarboxylation of the epoxide-carbonate and oxetane-carbonate are endergonic by 21.7 and 19.0 kcal/mol, respectively, at room temperature. At elevated temperatures, decarboxylation is expected to become easier due to the entropic component of ΔG.

Starting from deprotonated 1,2-glycerol carbonate, glycidol is the favored product due to the kinetics of ring closure. Despite the relatively low barrier for the first reaction, the rate limiting step is loss of CO_2. In practice, we expect the reaction to be feasible, especially at high temperatures and low pressures that favor the irreversible loss of CO_2. This is exemplified by experimental reports using a strong base (e.g. sodium triphosphate) and reduced pressure to drive the reaction.[156]

The free energy barriers for the anionic homopolymerization of glycidol was calculated too, the polymeric alkoxide being represented by a methoxide anion. Attack at the methine position has a lower free energy barrier than at the methylene position (**Scheme IV-3**, 12.2 vs. 17.0 kcal/mol, respectively). In the usual case, steric reasons cause attack at the methine position to be less favored.[63,116] The ease of the former reaction is due to the pendant hydroxy group hydrogen-bonding with the incoming methoxide nucleophile at the transition state for the reaction (Figure IV-4). For completeness, both ring-opening reactions are exergonic by -16.3 and -16.9 kcal/mol, respectively, giving the reverse reactions (depolymerization of polyglycerol to yield glycidol) high free energy barriers of 28.5 and 33.9 kcal/mol.

Scheme IV-3. Free energy barriers for the ring-opening polymerization of glycidol. Methine attack (top) has a lower free energy barrier than methylene attack (bottom) (12.2 vs. 17.0 kcal/mol), because hydrogen bonding stabilizes the former case's transition state (Figure IV-4).

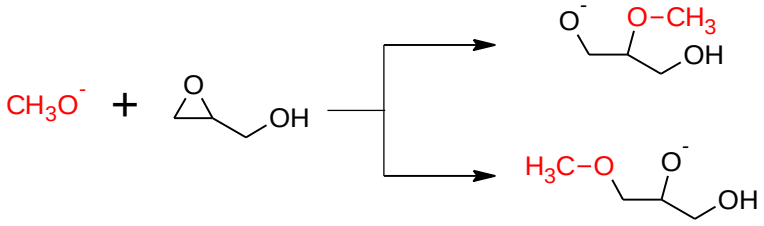

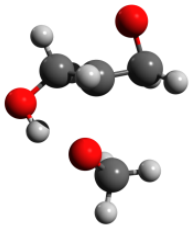

Figure IV-4. Transition state for methoxide to ring-open glycidol at the methine position. Distances (Å): CH_3O-C 2.13; $O_{epoxide}$-C 1.88; OH-OCH_3 1.58.

These results indicate that if sufficient heat is available for the decarboxylation reaction, there should be sufficient heat for the homopolymerization of glycidol due to its low free energy barrier, as has been observed.[165] This should explain why Seki *et al.* advise that 1,2-glycerol carbonate be dropped into the decarboxylation system, and that the glycidol's residence time in the reactor be reduced by continuous distillation.[159]

Acid-catalyzed decarboxylation

In 2010, Ferreira *et al.*[166] investigated the acid-catalyzed hydrolysis of epoxides using theoretical methods. Inspired by that work, the acid-catalyzed decarboxylation to give both 1,2- and 1,3-glycerol carbonates were studied. Instead of water, the incoming nucleophile is 1,2-glycerol carbonate's pendant hydroxy group. Similar to Ferreira, a naked proton was used as the prototypical acid; such a simplification may be directly applicable toward heterogeneous catalysts with hydroxyl groups on the surface. This present work may also be helpful in understanding Lewis acid-catalyzed decarboxylation reactions.[158-160,163]

Only the S_N2 mechanism is discussed; this mechanism is favored according to Ferreira. The S_N1 mechanism (spontaneous ring-opening of protonated cyclic carbonate or cyclic ether) was examined too, but we were similarly unable to locate stable geometries for the resultant primary carbocations, despite using a solvation model.[166]

The proposed mechanism (**Scheme IV-4**) is similar to the base-catalyzed reaction (**Scheme IV-2**). Protonated 1,2-glycerol carbonate undergoes nucleophilic substitution by the pendant hydroxy group, leading to a protonated cyclic ether-carbonic acid. At the transition states (Figure IV-3), the O-C distances are slightly longer than for the base-catalyzed examples, while the frequencies of the imaginary vibrational mode are lower. The O-C interactions for the protonated species are weaker than for the deprotonated species, as expected. Decarboxylation proceeds thereafter, followed by proton transfer to another 1,2-glycerol carbonate molecule.

Scheme IV-4. Proposed mechanism for the acid-catalyzed decarboxylation reactions leading to (a) glycidol (top) and (b) 3-hydroxyoxetane (bottom) after hydrolysis.

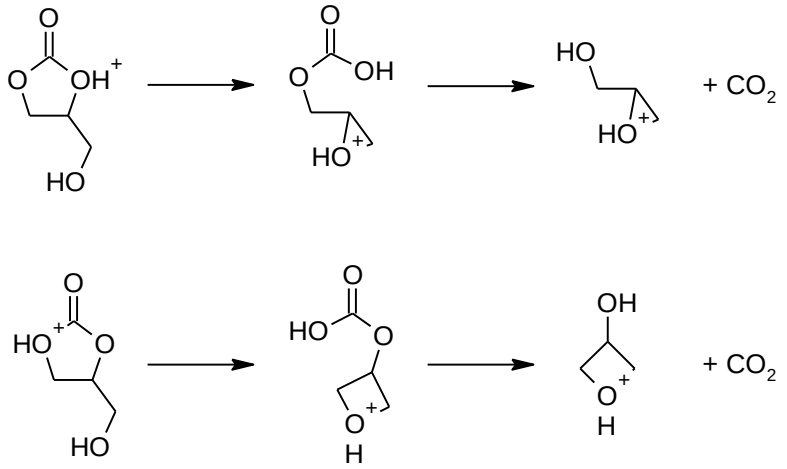

Ring closure has a relatively small free energy barrier (12.3 and 15.4 kcal/mol, leading to glycidol and 3-hydroxyoxetane, respectively). Subsequent decarboxylation of the cyclic ether-carbonic acid under acidic conditions is exergonic, paralleling the water, CO_2, and carbonic acid system.

To be clear, both protonated 1,2-glycerol carbonate molecules in **Scheme IV-4** are within 1.3 kcal/mol (free energy) of each other, so both free energy profiles in Figure IV-2(b) can be directly compared. Additionally, the protonated oxetane (b) is 6.6 kcal/mol lower in free energy than protonated epoxide (a), in agreement with our understanding of oxetanes as stronger bases than epoxides.[167]

On the surface, the calculated free energy barriers indicate that the acid-catalyzed reaction is more accessible than the base-catalyzed one; the supposition is that 1,2-glycerol carbonate is as easily protonated as it is deprotonated. The protonated epoxide-carbonic acid is 1.6 kcal/mol lower in free energy than the protonated cyclic carbonate-alcohol (Figure IV-5), suggesting that their acidities are comparable. The proton affinities of ethylene carbonate and ethylene oxide are close, at 774.2 and 814.2 kJ/mol

respectively (positive by convention).[168] In contrast, the deprotonation of alcohols to yield alkoxides is well understood. The absolute basicity of cyclic carbonates is not addressed in this chapter, though we would point out that cyclic carbonates do react with electrophiles.[169]

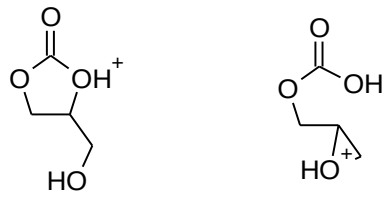

Figure IV-5. The protonated epoxide-carbonic acid (right) is 1.6 kcal/mol lower in free energy than the protonated cyclic carbonate-alcohol (left); refer to the free energy profiles in Figure IV-2(b).

To sum up, protonation aside, the free energy barriers for the acid-catalyzed decarboxylation reactions are simply attributed to that of the initial cyclic ether-formation reaction. Glycidol is preferred for both instances, consistent with how 3-hydroxyoxetane is not observed experimentally.[170-171] Since both classes have been confirmed by experiments, [157-161,163] the current analysis remains quite relevant.

Ring-opening polymerization of 1,2-glycerol carbonate

Early this year, Bañares proposed that the decarboxylation of 1,2-glycerol carbonate proceeded by its oligomerization, followed by some sort of backbiting reaction that yielded glycidol with the loss of carbon dioxide gas.[160] In the laboratory, we have not been able to have five-membered cyclic carbonates undergo ring-opening polymerization to yield the polymer, though the six-membered cyclic carbonates do so quite well.[111] Subsequent computational work rationalized this observation: the ring-opening polymerization of five-membered cyclic carbonates is endergonic, and the ring-opening polymerization of trimethylene carbonate is exergonic.[63]

We determined the enthalpies and free energies of CO_2 and the epoxide or oxetane to react to give the respective polymer vs. cyclic carbonate formation using the CBS-4M method,[37,40] similar to our previous report (Table IV-1).[63] In that report, we found that the enthalpies for the 1-mer to 2-mer reactions predicted the average of three iterations within 1 kcal/mol, so we only examined the 1-mer to 2-mer reaction in the current study.

Table IV-1. Enthalpies and free energies (kcal/mol) for polymer vs. cyclic carbonate formation.*

	Enthalpy		Free energy	
	Polymer	**Cyclic carbonate**	**Polymer**	**Cyclic carbonate**
1,2-GC	-21.3	-16.2	0.6	-4.3
1,2-MeGC	-22.1	-15.3	0.0	-3.9
1,3-GC	-22.3	-9.0	-0.5	1.7
1,3-MeGC	-20.9	-8.2	0.7	2.8

* From CO_2 and the corresponding cyclic ether. GC = glycerol carbonate; MeGC = glycerol carbonate, methyl ether.

Polymer formation is exothermic by ca. 22 kcal/mol, while formation of the five- and six-membered cyclic carbonates are exothermic by 15 and 9 kcal/mol respectively. The ring-opening polymerization of five-membered cyclic carbonates is endergonic, and that of the six-membered analogs is exergonic. Specifically, ring-opening 1,2-glycerol carbonate is endergonic by 4.9 kcal/mol, and CBS-4M free energies have successfully been used to explain why trimethylene carbonate undergoes ring-opening polymerization, where the isomeric propylene carbonate does not. Glycerol-derived oxetanes do not appear distinct from other aliphatic oxetanes,[63] and that the necessity of ether protecting groups is unrelated to the thermodynamics of the overall reaction.

The study of glycerol-derived polycarbonates and cyclic carbonates affords us with the unique opportunity to more-fairly compare the enthalpies of the 1,2- and 1,3-glycerol

polycarbonates, as well as the isomeric propylene and trimethylene carbonates (Table IV-2). From these two examples, five-membered cyclic carbonates appear lower in enthalpy than the six-membered cyclic carbonates, although the reasons for it are not obvious. We speculate that the carbonate O-C(=O)-O angles for the five-membered cyclic carbonate are closer to that of unstrained dimethyl carbonate, than for the six-membered cyclic carbonates.

Table IV-2. O-C(=O)-O angles for cyclic carbonates.

	DMC	**GC**	**PC/TMC**
1,2-Carbonate (5-membered ring)	110.0	108.8	108.8
1,3-Carbonate (6-membered ring)		116	116.6
Enthalpy difference (1,2)-(1,3), kcal/mol	N.A.	-7.3	-9.0

DMC = Dimethyl carbonate; GC = glycerol carbonate; PC = propylene carbonate; TMC = trimethylene carbonate.

Concluding remarks

Although it is not possible to prepare poly(1,2-glycerol carbonate) directly by the ring-opening polymerization,[172] it can be done indirectly, by decarboxylation of 1,2-glycerol carbonate to prepare glycidol for subsequent copolymerization with CO_2. The proposed degradation of 1,2-glycerol carbonate via oligomerization followed by backbiting appears is unfavorable according to thermodynamic arguments (ΔG = 4.9 kcal/mol for ring-opening 1,2-glycerol carbonate).

The free energy profiles of the base- and acid-catalyzed routes have been studied. The base-catalyzed reaction has a modest free energy barrier for ring formation, but decarboxylation is the rate-determining step ($\Delta G^{\ddagger} \approx 21.7$ kcal/mol); this reaction has been demonstrated for 1,2-glycerol carbonate,[156,161] and for related systems,[134] including under reduced pressure. For the base-catalyzed reaction, anionic homopolymerization of

the glycidol formed is a concern, such that continuous removal of the glycidol product by distillation is recommended.[159]

Ease of protonating 1,2-glycerol carbonate notwithstanding, the acid-catalyzed reaction has a lower free energy barrier for decarboxylation, and the rate-determining step for the acid-catalyzed reaction is ring formation ($\Delta G^{\ddagger}$ = 12.3 kcal/mol). It is unclear how easily 1,2-glycerol carbonate may be protonated, but the successful use of zeolites (that contain both Brønsted and Lewis acidic sites) to produce glycidol supports this mechanism.[159-160]

Computational methods

All calculations were performed using the Gaussian 09 suite.[127] All local minima and saddle points were verified by their calculated vibrational frequencies (zero and one imaginary frequencies respectively. The saddle points found were confirmed to be the correct ones by visualizing the imaginary vibrational modes with AGUI[129] and Avogadro.[130] No attempts were made to locate global energy minima of the structures studied.

Consistent with previous work,[63,125] free energy barriers were obtained using CBS-QB3(+) calculations:[108] B3LYP[138-140]/6-311+G(2d,d,p) [141-143] reference geometries and frequencies were read-in, and the CBS-QB3[103,105] calculation proceeded directly to the third step (CCSD(T)/6-31+G(d')) using the CBS-QB3(StartMP2) keyword in Gaussian 09. The scale factor for the zero-point energies was not changed from the 0.99 pre-defined by CBS-QB3. The Integral Equation Formalism Polarization Continuum Model (IEFPCM) calculation with radii and non-electrostatic terms for Truhlar and coworkers' SMD solvation model[131] was used with tetrahydrofuran as the prototypical solvent. Also consistent with our previous work,[63] enthalpies of polymerization were obtained by the CBS-4M method in the gas phase.[103-104]

CHAPTER V

KINETICS OF THE (SALEN)CR(III)- AND (SALEN)CO(III)-CATALYZED COPOLYMERIZATION OF EPOXIDES WITH CO_2, AND OF THE ACCOMPANYING DEGRADATION REACTIONS

Introduction

Of the three generations of catalysts for the CO_2-epoxide copolymerization, we are most interested in the second and third generation catalysts based on (salen)M(III) complexes. Our recent review indicated that the CO_2-epoxide copolymerization is not well-studied using computational chemistry.[173] In 2005, Luinstra *et al.* showed that metal-bound epoxides were greatly activated toward ring-opening by acetate ($\Delta E^{\ddagger}$ = 0.5–6.9 kcal/mol), and that carboxylation may be rate limiting; a minimal ligand was used then.[86] More recently, Adhikari, Nguyen, and Baik subsequently studied a similar reaction for a chromium salen complex, and found ring-opening [Cr]-bound epoxide by DMAP to have a significant barrier ($\Delta G^{\ddagger}$ = 23.1 kcal/mol).[81]

Several mechanistic questions remain unresolved in previous reports on this subject. Among these include: (i) the origin of the rate limiting epoxide enchainment step: epoxide binding or epoxide ring-opening; (ii) differences in reactivity between (salen)Cr(III) and (salen)Co(III) catalysts; and (iii) the reason for the lack of ether linkages in resulting copolymers. In this chapter, we present our computational studies that are designed to elucidate the origins of these experimental observations. This systematic study provides fundamental information that can lead to better-designed catalysts for this reaction.

Results and discussion

Method selection and validation

Zhao and Truhlar's pure M06-L functional (no Hartree-Fock exchange) was initially chosen to preempt problems with the multi-reference nature of these transition metal complexes.[174] This functional was successfully used by Jacobsen and coworkers to study the (salen)Co(III)-catalyzed hydrolytic kinetic resolution of epoxides.[71] Free energy barriers calculated using this functional and the BS2 basis set (defined below) were underestimated by ca. 4-6 kcal/mol compared with benchmark CBS-QB3 results (Table V-1);[63] similar observations for enthalpies have been noted in the literature.[55,173]

Table V-1. Free energy barriers (kcal/mol) for metal-free carbonate backbiting.

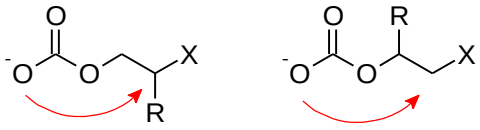

	M06-L/BS2	M06/BS2	M06/BS2+*	CBS-QB3[63]
EC	16.5	19.4	20.6	20.4
PC-1	17.8	21.9	23.5	24.0
PC-2	14.5	18.6	19.2	18.5
SC-1	16.2	19.3	20.6	19.5
SC-2	14.0	17.5	20.1	20.2
CHC	20.9	25.8	26.5	25.8
CPC	15.3	18.8	20.3	20.3

"-1" and "-2" refer to backbiting at the methine (left) and methylene (right) positions, respectively. EC = ethylene carbonate; PC = propylene carbonate; SC = styrene carbonate; CHC = cyclohexene carbonate; CPC = cyclopentene carbonate. SMD solvation, THF solvent throughout. * Mean signed deviation (from CBS-QB3): -0.3 kcal/mol; mean unsigned deviation: 0.5 kcal/mol; root mean squared deviation: 0.6 kcal/mol.

The hybrid M06 functional (containing Hartree-Fock exchange), used in conjunction with diffuse functions on heavy atoms (the BS2+ basis set, defined below), was

subsequently found to give results in excellent agreement with that obtained via CBS-QB3. SCF convergence with the chromium and cobalt complexes was straightforward, although calculations were significantly slower than the local M06-L functional used without diffuse functions (the BS2 basis set). Our experience has shown that these diffuse functions are important to describe the weakly-bound transition states relevant to carboxylation and alkoxide backbiting.[63] The M06 functional in conjunction with the BS2+ basis set was used for all metal-containing systems throughout this work, except where noted.

The original goal was to perform calculations on full models of the catalyst systems in contemporary use for these copolymerization reactions. In this way, steric effects and electronic effects would be incorporated in the analysis. However, these systems were too large to be calculated routinely, in view of the broader goal of comparing different epoxide co-monomers. Accordingly, lightly truncated (salen)M(III) complexes were used to approximate the second generation binary cobalt and chromium catalyst systems: tert-butyl appendages were removed, and the cyclohexylene backbone that enforces the salen ligand's twist and chirality[72] was replaced with an ethylene backbone. Counter-cations were omitted too. Similar to our previous work, methyl carbonate and methoxide stood in for the remainder of the growing polymer chain.[63] In the same way, the SMD solvation model, tetrahydrofuran being the prototypical solvent, was used to approximate typical reaction conditions where epoxide serves as solvent and reactant.

The chromium-containing compounds were expected to have quartet spin states (three unpaired d electrons), consistent with the literature.[81] The ring-opening reaction for hexacoordinate [Co]-bound ethylene oxide by methyl carbonate was modeled for the singlet, triplet, and quintet spin states (Table V-2) using the M06-L/BS2 method. The lowest barrier was obtained for the low-spin singlet state that was consistent with Jacobsen *et al.*'s work.[71] All hexacoordinate cobalt-containing complexes are therefore treated as singlets in this study.

Table V-2. Energy barriers (kcal/mol) for [Co]-bound ethylene oxide to undergo epoxide ring-opening by methyl carbonate.

	$\Delta H^{\ddagger}$	$\Delta G^{\ddagger}$
[^{1}Co]	7.3	8.7
[^{3}Co]	15.2	17.1
[^{5}Co]	14.3	14.0

Thermodynamics of ligand binding

For the catalyst to turn over, the polymeric carbonate intermediate must be displaced by an epoxide substrate molecule (Figure V-1). This reaction should proceed through a dissociative mechanism since the metal-salen complex is coordinatively saturated. This equilibrium affects the overall rate of the copolymerization reaction, because it affects the fraction of the metal catalyst that has a bound epoxide able to be ring-opened by a polymeric alkoxide.

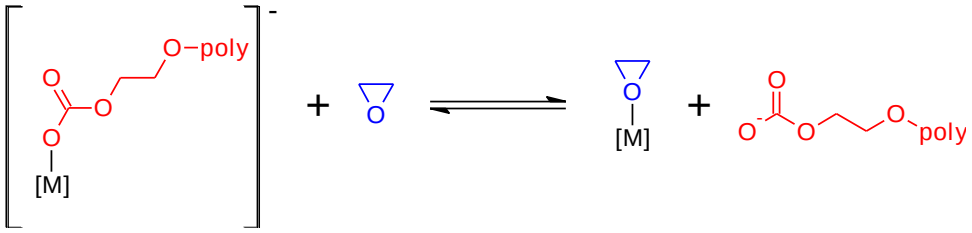

Figure V-1. The equilibrium between metal-bound polymeric carbonate and free epoxide, with metal-bound epoxide and free carbonate.

Where only one epoxide is present, this equilibrium cannot be disentangled from the activation parameters of the overall reaction. Through crossover experiments that provided the catalyst two possible epoxide substrates, the epoxides' basicities were

indeed found to affect the rates of polymer growth.[167] That study approximated the epoxides' basicities toward the (salen)Co(III) catalyst with their basicities toward protons (i.e. pK_bs). The metal-ligand bond dissociation energies for epoxide, alkoxide, and carbonate ligands were calculated to quantify their separate influences on the overall copolymerization reaction (see Figure V-2 and Table V-1). The thermodynamics of these reactions suffice since these bond dissociation reactions are usually thought to have low barriers.

The pentacoordinate (salen)M(III) fragments were taken to have quartet and singlet electronic states for chromium and cobalt, just as they would be as hexacoordinate complexes. The pentacoordinate species is lower in energy as the triplet, rather than the singlet electronic state (ΔH = 13.4, ΔG = 15.3 kcal/mol), consistent with the literature.[71,175] We do not wish to speculate on the details of the spin crossover event, so we have chosen not to change the spin state for the pentacoordinate product complex resulting from ligand dissociation.

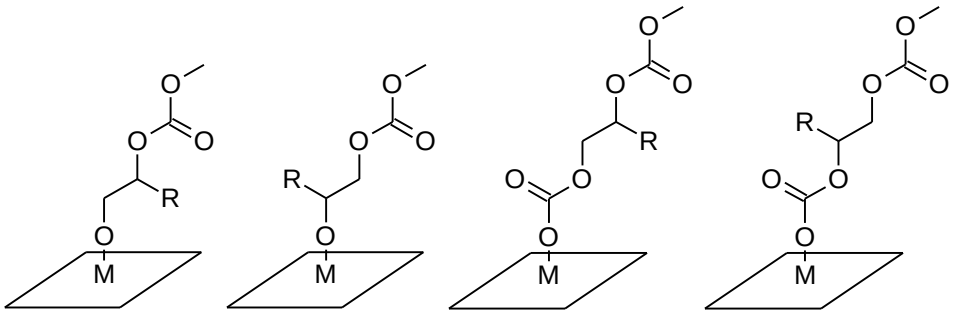

Figure V-2. Left to right: [M]-XC-1alk, [M]-XC-2alk; [M]-XC-1carb, [M]-XC-2carb.

Table V-3. Enthalpies and free energies (kcal/mol) for ligands (L) to dissociate from $(salen)^4Cr(III)ClL$ and $(salen)^1Co(III)ClL$ to give pentacoordinate square pyramidal $(salen)^4CrCl$ and $(salen)^1Co(III)Cl$ complexes, respectively.

	Enthalpy		Free energy	
Ligand (L)	**[Cr]**	**[Co]**	**[Cr]**	**[Co]**
EO	16.7	16.3	4.2	4.1
R-PO	17.8	17.2	5.5	4.6
S-PO	16.1	14.9	3.3	1.9
R-SO	17.7	17.2	5.4	4.5
S-SO	18.7	17.6	4.9	4.9
CHO	19.6	19.1	6.3	6.2
CPO	17.3	16.5	5.4	4.1
TMO	19.7	19.1	6.8	6.3
Tetrahydrofuran	19.7	17.3	28.0	25.8
Chloride	19.8	18.8	11.4	10.5
methoxide	48.3	46.2	36.7	34.1
methyl carbonate	24.8	20.5	12.7	8.4
EC-alk	45.7	42.6	29.9	28.6
PC-1alk	44.2	40.1	31.3	26.7
PC-2alk	45.7	43.4	32.1	29.4
SC-1alk	43.5	39.7	28.3	23.9
SC-2alk	46.6	43.9	32.6	29.8
CHC-alk	46.6	45.0	32.4	30.3
CPC-alk	48.1	47.9	34.6	33.9
EC-carb	24.2	22.5	10.4	9.3
PC-1carb	24.5	21.3	12.9	7.7
PC-2carb	24.2	20.3	10.1	6.4
SC-1carb	27.6	24.3	12.9	9.0
SC-2carb	22.5	19.2	7.9	4.0
CHC-carb	26.9	23.3	13.0	9.0
CPC-carb	24.8	19.0	11.8	5.7
EC	12.6	10.8	0.0	-1.8
PC	12.9	10.8	0.7	-2.3
SC	13.8	11.2	0.8	-1.8
CHC	13.7	10.1	1.1	-2.1
CPC	11.6	9.2	-0.9	-3.7

The strength of the metals' bonds with epoxides, alkoxides, carbonates, and cyclic carbonates are 16-19 kcal/mol, 39-48 kcal/mol, 19-27 kcal/mol, and 10-12 kcal/mol respectively. This ordering is easy to rationalize on the basis of the strength of these ligands as Lewis bases: alkoxide >> carbonate > epoxide > cyclic carbonate. Epoxides bind about as strongly as chloride, and any induction period in the copolymerization reaction may well be attributable to the time required for chloride to be displaced by an incoming epoxide substrate molecule. Once it ring-opens the epoxide, the chloride anion can no longer compete with epoxide for ligand binding, having been incorporated into the polymer end group.

Ring-opening converts the moderately binding epoxide ligand to a strongly binding alkoxide ligand. Carboxylation converts the alkoxide into a more weakly binding carbonate ligand. Substitution by epoxide is unfavorable by a significant amount: 2 to 9 kcal/mol in enthalpy, and -0.5 to 7 kcal/mol in free energy. Consequently, we are obliged to take the thermodynamics of the last step into account when calculating the kinetics of the overall ring-opening polymerization reaction.

Concern has been raised that cyclic carbonate byproducts may competitively bind to the polymerization catalyst, poisoning it.[22,176] The cyclic carbonates bind 4-6 kcal/mol more strongly (enthalpy) than the corresponding epoxides. Under polymerization conditions where a large excess of epoxide is present, any cyclic carbonate formed is not anticipated to poison these two polymerization catalysts. On the other hand, tetrahydrofuran does bind 2-3 kcal/mol more strongly (enthalpy) than epoxides do, and its presence may be objectionable.

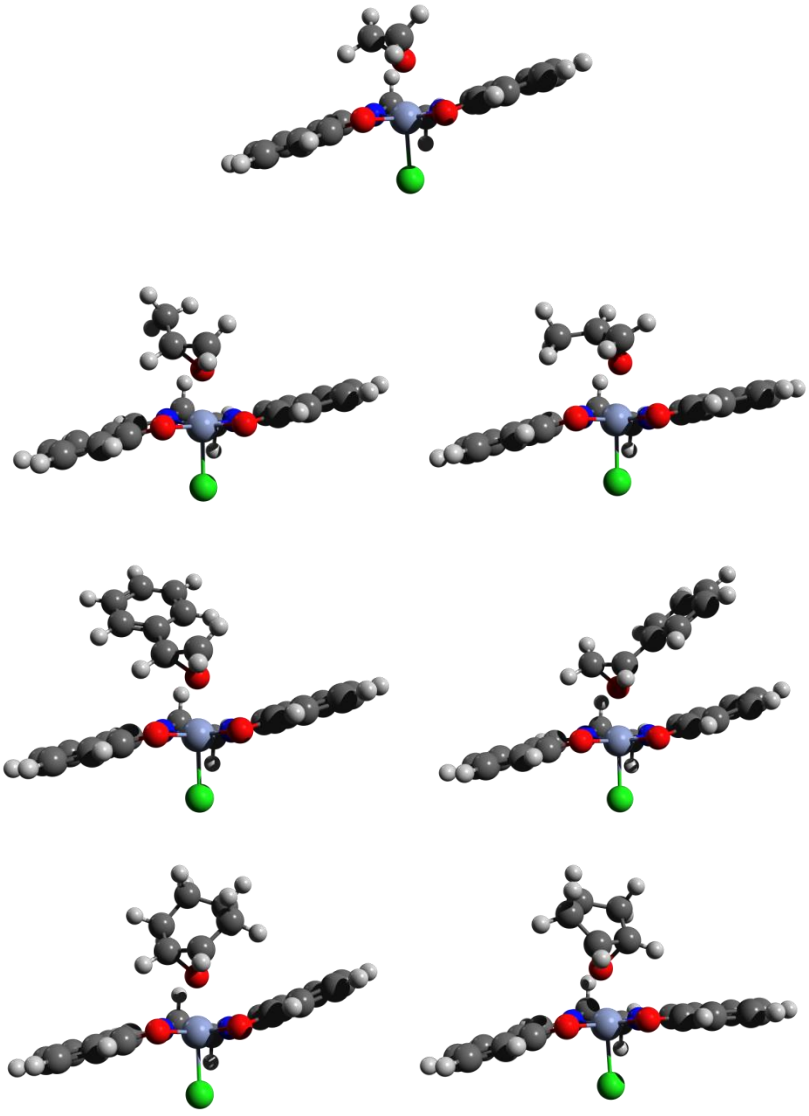

Figure V-3. Optimized structures of [Cr]-epoxide. 1st row: ethylene oxide; 2nd row: R- and S-propylene oxide; 3rd row: R- and S-styrene oxide; 4th row: , cyclohexene, and cyclopentene oxides. CPK coloring is used: C = gray, H = white, N = blue, O = red, Cl = green; Cr = light blue, Co (in other figures) = pink.

To obtain accurate values for Table V-3, a limited attempt to find the lowest energy conformations of (salen)MCl-epoxide complexes was made by rotating the bound epoxide about central Cl-M-O axis, in a relaxed potential energy surface scan, at the economical semi-empirical PM6 level of theory. Energy minima were found with the O-M-O-C dihedral angle (Figure V-4) being approximately 45°, regardless of the chirality of the epoxide ligand, consistent with the literature.[71] The R-epoxides' substituents are oriented normal to the salen plane, whereas those of the S-epoxides are suspended over the flat salen ligand (Figure V-3). tert-Butyl groups had been omitted for computational convenience. Even so, the epoxide substituents avoid that region, presumably because of repulsion from the phenol oxygen atoms. Cyclohexene and cyclopentene oxides are similarly oriented, though they have dihedrals of ca. 30° respectively. The alicyclic epoxides' rings are oriented normal to the salen plane.

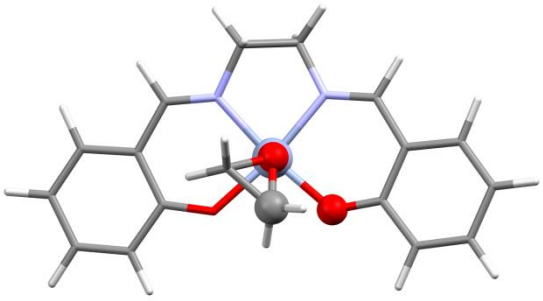

Figure V-4. [Cr]-EO, viewed along the O-Cr-Cl axis. The O-Cr-O-C dihedral angle discussed in the text is highlighted as balls.

Jacobsen *et al.* reported that R-propylene oxide preferentially binds to the (S,S-salen)Co(OH_2) fragment by 0.5 kcal/mol,[71] whereas we find the reverse: it binds less strongly by 1.7 and 2.3 kcal/mol for [Cr] and [Co], respectively. Curiously, the order of binding is reversed for styrene oxide: the R,R-like complex binds the S-epoxide more strongly by 1.0 and 0.4 kcal/mol respectively. This reversal is fully explained by

favorable π-stacking between the phenyl ring with the aromatic salen ligand; the distances between the centers of both benzene rings are 4.116 and 4.233 Å for [Cr] and [Co], respectively. Such an interaction likely explains why S-styrene oxide is oriented opposite all the other epoxides. Overall, we find that π-stacking is worth ca. 2.7 kcal/mol for both [Cr] and [Co] that is consistent with the energetic benefit obtained by benzene π-stacking.[177] Many contemporary density functionals (including M06 used here) are now suitable for studying these non-covalent interactions.[178]

The difference between our results and Jacobsen *et al.*'s might be due to the cyclohexylene backbone enforcing the salen ligand's stepped conformation better[72] than our ligand which has a more flexible ethylene backbone. In any case, these small differences in binding energy are not significant enough to favor one chiral product over the other. In the hydrolytic kinetic resolution, ring-opening the expected epoxide is favored by 6-9 kcal/mol of electronic energy; this improved discrimination is achieved by the hydrolytic reaction's bimetallic mechanism.[71]

In Table V-3, the various ligands generally bind more strongly to [Cr] than to [Co]. Epoxide binding is ca. 1 kcal/mol more exothermic for [Cr] than [Co], 2-4 kcal/mol more exothermic for alkoxides, and ca. 3 kcal/mol more exothermic for carbonates; trends in free energy are similar. The impact of these differences are discussed in detail, *vide infra*.

Complexes of the form [M]-XC-2alk (Figure V-2) have the R pendant group pointing away from the rest of the complex, whereas those R groups of [M]-XC-1alk lie parallel with the salen plane. This observation explains the former complexes having enthalpies of binding that are greater by 2-3 kcal/mol. These substituents do not significantly perturb the electronic environment about the alkoxide oxygen bound to the atom: M-O distances remain relatively constant at 1.92 and 1.90 Å for [Cr] and [Co], respectively. The carbonate ligands' pendent groups are five and four bonds removed from the metal center for the 1-carb and 2-carb complexes, respectively. They exert little influence on

the conformation of the complexes as a result. An exception exists for [Cr]-SC-2carb and [Co]-SC-2carb: the phenyl rings on these complexes exhibit displaced T-shaped π-stacking with the aromatic salen ligand (Figure V-5); the distances between each pair of benzene centroids are 5.012 and 5.097 Å, compared with 4.96 Å for the corresponding distance for the benzene T-shaped dimer obtained via microwave spectroscopy.[179] These interactions cause the phenyl substituents to be aligned in this manner.

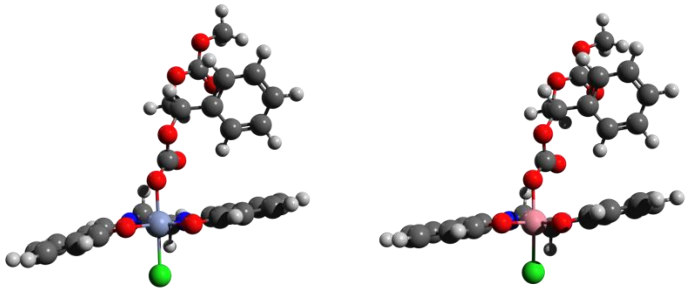

Figure V-5. [Cr]-SC-2carb (left) and [Co]-SC-2carb, showing the displaced T-shaped π-stacking between the phenyl ligand and the aromatic salen ligand

Epoxide ring-opening

In the propagation reaction, metal-bound epoxide undergoes nucleophilic attack by a polymeric carbonate (**Scheme V-1**). The chromium or cobalt Lewis acid draws electron density from the epoxide oxygen atom, weakening its C-O bond, and making it easier to break. This ring-opening step was modeled, methyl carbonate serving as the incoming nucleophile. For aliphatic epoxides, the R-isomer was used throughout this study. After all, Jacobsen has shown that the minor differences in binding to the salen complex between the R- and S-isomers were insufficient to cause stereoselectivity.[71]

Selected geometric parameters for the metal-bound and metal-free epoxide ring-opening reactions are presented in Table V-4. C-O(epoxide) and C-O(carbonate) distances were approximately 2.0 Å for the metal-free case. When the epoxide oxygen was coordinated

to a Lewis acid (Figure V-6), the C-O(epoxide) distance decreased to ca. 1.8 Å, while the C-O(carbonate) distance increased slightly to 2.1 Å. Metal-epoxide distances were approximately 2.0 Å as well. Reflecting Co(III)'s greater Lewis acidity compared with Cr(III), the M-O distances for Co were 0.05 Å shorter. The epoxide oxygen is less Lewis basic, thus the associated C-O(epoxide) distance is 0.05 Å longer for the [Co]-bound epoxide. In turn, the C-O(carbonate) distance is slightly elongated by 0.05 Å to compensate for the slightly weaker C-O(epoxide) interactions.

Scheme V-1. Ring-opening of a metal-bound epoxide by a polymeric carbonate nucleophile.

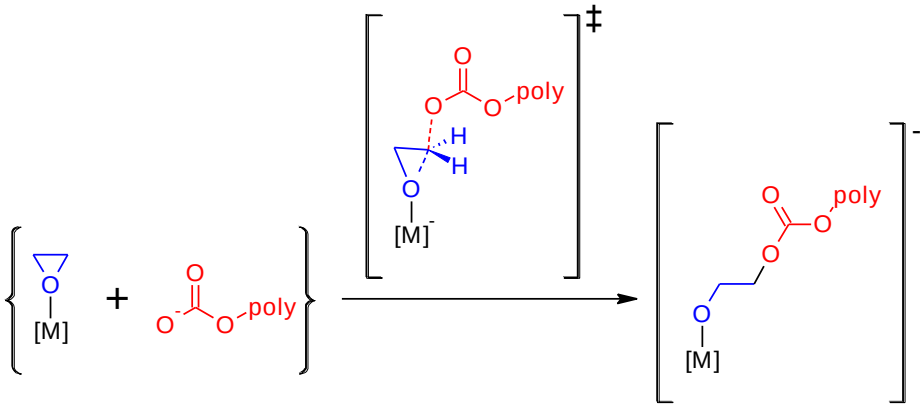

Table V-4. C-O(epoxide), C-O(carbonate) and M-O distances (Å) at the transition states for epoxide ring-opening by methyl carbonate.

	[Cr]-bound			[Co]-bound			Metal-free*	
	C-O(ep)	**C-O(carb)**	**Cr-O**	**C-O(ep)**	**C-O(carb)**	**Co-O**	**C-O(ep)**	**C-O(carb)**
EO	1.787	2.097	2.007	1.799	2.083	1.947	1.932	1.954
PO-1	1.835	2.179	1.993	1.849	2.169	1.942	1.982	2.009
PO-2	1.793	2.090	2.002	1.804	2.074	1.942	1.937	1.945
SO-1	1.862	2.210	1.981	1.776	2.013	2.089	2.014	1.985
SO-2	1.776	2.009	2.013	1.778	2.076	1.944	1.916	1.952
CHO	1.859	2.165	1.979	1.864	2.149	1.924	2.007	1.982
CPO	1.873	2.171	1.983	1.880	2.195	1.933	2.000	1.983

Ep = epoxide; carb = carbonate.

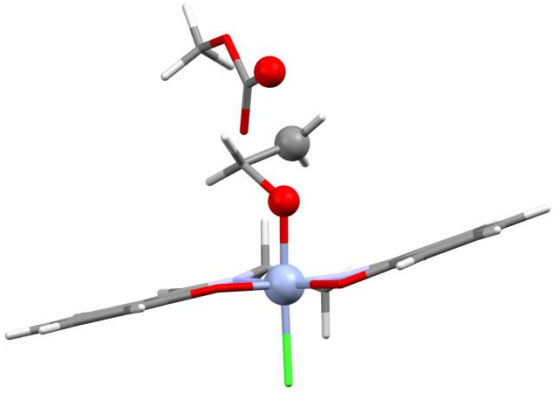

Figure V-6. Transition state of [Cr]-EO being ring-opened by methyl carbonate. Cr-O = 2.007 Å; O(epoxide)-C = 1.787 Å; C-O(carbonate) = 2.097 Å.

The activation parameters for the elementary epoxide ring-opening reaction are presented in Table V-5. The uncatalyzed epoxide ring-opening reaction has enthalpy and free energy barriers of 18-23 kcal/mol and 23-29 kcal/mol respectively. Coordination to [Cr] and [Co] causes the epoxide to be significantly activated, and the [Cr]- and [Co]-catalyzed reactions have enthalpy barriers of 10-15 and 11-13 kcal/mol. The free energy barriers are almost equal to the enthalpy barriers due to the very small entropy of activation, consistent with a unimolecular reaction. Stable reactant complexes (of metal-

bound epoxide + methyl carbonate) are observed for both metal-bound systems, but not so for the metal-free reaction. The only energy minima that we could find entailed the epoxide and the methyl carbonate nucleophile residing in distinct solvation cavities.

Nucleophilic attack at the methine position, where metal-bound or metal-free, generally has a higher enthalpy barrier than methylene attack for propylene oxide due to steric reasons, consistent with previous work (Table V-5).[63,116] The trends for the corresponding free energy barrier do not agree as well for the metal-bound ring-opening reactions, probably due to entropy.

Methine attack for metal-free styrene oxide is strongly stabilized compared with methylene attack due to delocalization of phenyl p_π electrons into the empty p orbital of the sp^2 carbon undergoing substitution for both cases (Figure V-7), consistent with previous work.[63] Such interactions were not observed for the metal-activated examples. It appears that methine attack for [Cr]- and [Co]-activated styrene oxide is favored because the phenyl ring experiences a staggered π-stacking interaction with the salen ring. In support, the distances between the centers of both benzene rings for the [Cr]- and [Co]-catalyzed complexes at the transition states for epoxide ring-opening are 4.351 and 4.195 Å (Figure V-8). For comparison, the corresponding distance for the benzene sandwich dimer, calculated at the MP2/aug-cc-pVTZ level, is 3.7 Å.[177]

Table V-5. Activation barriers (kcal/mol) for metal-free and metal-bound epoxides to undergo ring-opening by methyl carbonate.

	$\Delta H^{\ddagger}$			$\Delta G^{\ddagger}$		
	Metal-free	**[Cr]-bound**	**[Co]-bound**	**Metal-free**	**[Cr]-bound**	**[Co]-bound**
EO	20.8	11.4	12.0	25.0	12.3	12.7
PO-1	24.0	12.3	12.8	25.1	12.3	13.3
PO-2	22.4	11.9	12.0	24.0	13.4	13.2
SO-1	21.2	10.5	11.9	25.1	10.4	11.4
SO-2	19.1	12.7	13.0	23.6	12.9	13.2
CHO	23.0	10.3	11.0	25.3	12.1	13.2
CPO	23.0	14.3	11.8	26.5	15.9	13.1

"-1" and "-2" refer to the methyl carbonate nucleophile attacking at the epoxide methine and methylene positions, respectively.

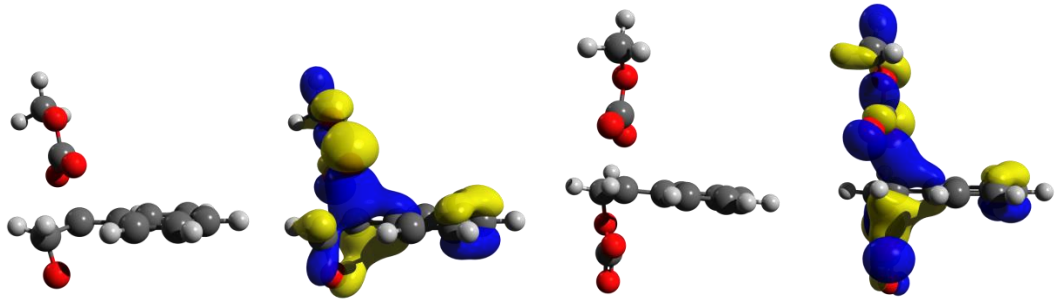

Figure V-7. The 0.03 isosurfaces of HOMO-7 for styrene oxide ring-opening (left), and HOMO-9 for styrene carbonate backbiting (right).

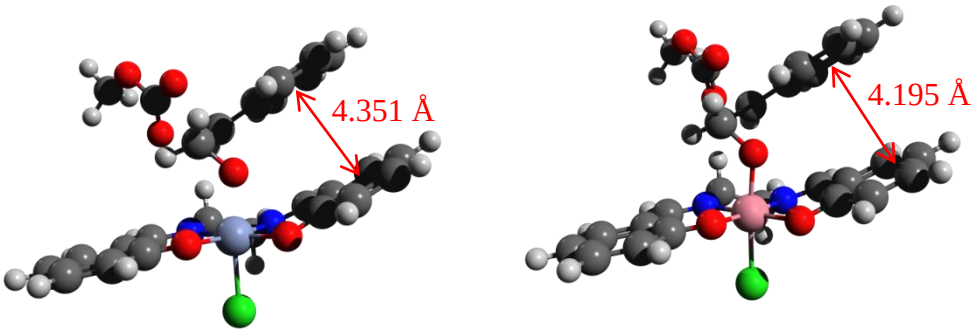

Figure V-8. Transition states for [Cr]- (left) and [Co]-catalyzed (right) ring-opening of styrene oxide at the methine position.

The most recent report on this topic was made by Adhikari, Nguyen, and Baik. Using a similarly truncated salen ligand, they found that [Cr]-bound propylene oxide needed to overcome a 23.1 kcal/mol free energy barrier in order to undergo ring-opening, as opposed to 12.3 kcal/mol in this study. Aside from minor differences arising from the authors using a different computational method, the higher free energy barrier they calculated are attributable to the much poorer Lewis basicity of the N,N-dimethylaminopyridine nucleophile they had chosen. Another study by Luinstra *et al.* has reported a negligible electronic barrier of 0.5 kcal/mol for [Cr]-bound ethylene oxide undergoing ring-opening by acetate, calculated using the BP86 density functional.[86] Their results are similar to some of the initial results we obtained when we treated the reactants as separate species, rather than as an associated complex. In other words, {[Cr]-epoxide + methyl carbonate} is significantly more stable than [Cr]-epoxide + methyl carbonate, and the former treatment would better describe the kinetics of the bimolecular reaction. An additional factor could be that the non-hybrid BP86 functional underestimates reaction barriers, similar to what we had observed for the M06-L functional (Table V-1). The poor performance of pure functionals in describing reaction barriers for S_N2-type reactions has been noted.[180]

In the preceding section, displacement of the metal-bound carbonate by an epoxide molecule (Figure V-1) for copolymerization to continue was determined to be appreciably endothermic and endergonic. The barriers for the elementary ring-opening reactions determined above should therefore be corrected with the thermodynamics of this exchange reaction (Table V-6). This correction includes the thermodynamics of forming the reactant complex, {[M]-epoxide + methyl carbonate}.

Table V-6. Overall barriers for epoxide ring-opening.

	$\Delta H^{\ddagger}$		$\Delta G^{\ddagger}$	
	[Cr]-bound	**[Co]-bound**	**[Cr]-bound**	**[Co]-bound**
EO	15.0	13.1	26.8	25.1
PO-1	14.3	12.9	25.4	24.8
PO-2	14.0	12.1	26.4	24.7
SO-1	12.1	10.3	24.6	23.8
SO-2	14.3	11.4	27.1	25.7
CHO	10.8	9.1	24.2	22.7
CPO	13.9	9.2	26.6	22.7

We should point out the major simplifying assumption in our above analysis. The concentration of epoxide is typically 500-1000 times that of the growing polymer chain at the beginning of the reaction (corresponding to the monomer to initiator ratio), responsible for a correction of 3.7 to 4.1 kcal/mol. Modest applied pressures of CO_2 ensure appreciable concentrations of dissolved carbon dioxide. Subsequently, its concentration in solution does not directly influence the kinetics of the overall reaction, since the carboxylation step is not rate limiting, *vide infra*. Subtracting this quantity, the overall free energy barriers are now a more realistic 18.6 to 23.0 kcal/mol. Since such corrections are constant and somewhat arbitrary, they do not change the arguments made in this chapter, and are ignored hereafter.

Having accounted for the exchange reaction, the differences between the Cr- and Co-catalyzed ring-opening reactions are now more obvious: the chromium-catalyzed reaction has a higher enthalpy and free energy barrier than cobalt-catalyzed reaction. This difference is due to enthalpies of activation for the Co-catalyzed reactions being consistently 1-3 kcal/mol lower. Experimentally, chromium catalysts perform best at high temperature (70-110 °C), whereas cobalt catalysts do well under milder conditions (0-40 °C).[15]

Cyclopentene oxide is distinguished by being easily ring-opened when Co-catalyzed, whereas it is hard to do so when Cr-catalyzed (overall $\Delta G^{\ddagger}$ = 22.7 vs. 26.6 kcal/mol). Experimentally, the second generation (salen)CrCl/$PPNN_3$ catalyst/cocatalyst system only produced cyclic carbonate. While the third generation bifunctional chromium catalyst (designed to preclude cyclic carbonate formation) was able to produce *some* poly(cyclopentene carbonate), the equivalent cobalt catalyst did so much more rapidly (TOF = 2.2 vs. 56.5 h^{-1}).[181]

A careful examination was made of the geometries of [Cr]- and [Co]-bound complexes: at the transition state for epoxide ring-opening, and as epoxide- and polymeric carbonate-coordinated complexes. The structures were generally similar in conformation, and relevant bond distances and angles were not out of the ordinary. The carbonate anion of poly(cyclopentene carbonate) is bound 6.1 kcal/mol (free energy) more strongly to [Cr] than to [Co]. In comparison, [Cr]-bound carbonates are bound more strongly by ca. 4 kcal/mol. [Cr]-bound cyclopentene oxide has a 2.5 kcal/mol higher free energy barrier for the elementary ring-opening step than for the [Co]-bound analogs, whereas they are usually slightly lower by ca. 0.5 kcal/mol. These small differences in energies do not have obvious singular causes. It is heartening to note that the computational results are able to accurately take into account these subtle effects, the accumulation of which, is what is responsible for the difference between [Cr]- and [Co]-catalyzed copolymerization of cyclopentene oxide with CO_2, borne out by experiments.

We wish to acknowledge parallel efforts by Nozaki *et al.* They make use of the free energy change of the exchange reaction (between metal-bound carbonate and free epoxide) to efficiently estimate the ease at which an epoxide can copolymerize with CO_2.[175] In our current work, we calculated the actual overall barriers for epoxide ring-opening, taking the exchange reaction into account.

Carboxylation of metal-bound alkoxide

Calculations were performed to determine the barriers for carboxylation of metal-bound ring-opened epoxides for the (salen)Cr(III) and (salen)Co(III) systems, and the transition states for these carboxylation reactions were found. In this sequence of reactions (**Scheme V-2**), the metal-bound alkoxide attacks a molecule of carbon dioxide that is not coordinated to the metal center.

The first energy minimum encountered thereafter has the newly formed polymeric carbonate coordinated to the chromium center through the same oxygen atom, as before the reaction. The carbonate ligand may be directly displaced by an epoxide molecule, or the complex may rearrange to give the thermodynamic chromium-carbonate complex of the "normal" configuration ("relaxed carbonate"). Calculations were performed for selected [Cr]- and [Co]-bound alkoxides (Table V-7 and Table V-8). The overall free energy barrier for the reaction was found to be approximately 6-8 kcal/mol. As a point of reference, the corresponding barrier for carboxylation of [Cr]-bound DMAP-opened propylene oxide was determined to be 16.0 kcal/mol (albeit utilizing different computational parameters).[81]

Scheme V-2. Sequence of reactions involved in the carboxylation of metal-bound alkoxides.

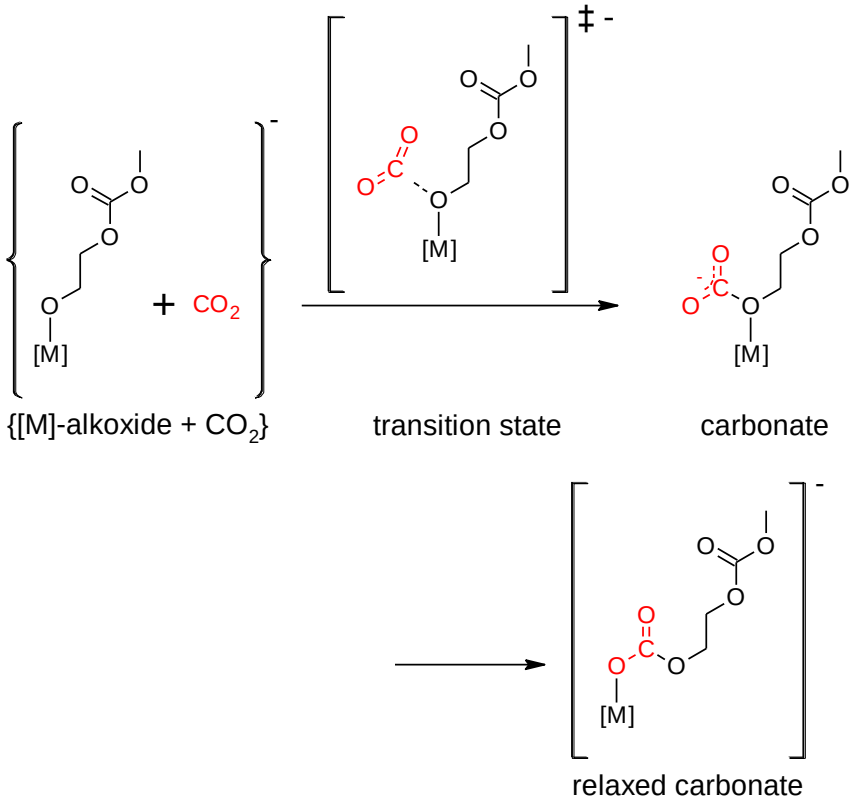

Table V-7. Relative enthalpies (kcal/mol) of the species involved in the carboxylation of metal-bound alkoxides. The parent epoxides are noted; "-1XO" and "-2XO" refers to carboxylation of the methine and methylene oxygen atoms, respectively.

	{[M]-alkoxide + CO_2}	**TS**	**Carbonate**	**Relaxed carbonate**
[Cr]-EO	0	5.7	4.8	-1.4
[Cr]-1PO	0	6.3	6.1	-1.6
[Cr]-2PO	0	6.7	5.4	-0.2
[Co]-EO	0	5.8	4.9	-1.6
[Co]-1PO	0	5.8	5.5	-0.7
[Co]-2PO	0	5.4	5.2	1.1

Table V-8. Relative free energies (kcal/mol) of the species involved in the carboxylation of ring-opened metal-bound alkoxides. The naming convention is consistent with that of the preceding table.

	{[M]-alkoxide + CO_2}	TS	Carbonate	Relaxed carbonate
[Cr]-EO	0	6.8	5.5	-0.5
[Cr]-1PO	0	8.4	7.3	-2.4
[Cr]-2PO	0	8.5	8.7	0.4
[Co]-EO	0	8.5	5.8	-0.2
[Co]-1PO	0	7.3	8.0	-0.3
[Co]-2PO	0	7.5	7.4	2.1

These reactions generally appear thermoneutral, but that is because formation of the {[M]-alkoxide + CO_2} reactant complex is exothermic by 6-8 kcal/mol. It must be stressed that no Lewis acid-base interactions between the CO_2 reactant with the metal centers are observed (M-O(CO_2) ≈ 4.3 Å; C=O ≈ 1.16 Å; O=C=O ≈ 180°). Relative free energy tracks enthalpy well too, since the overall reaction occurs in a single solvent cavity with a strongly associated CO_2 reactant molecule.

Figure V-9 shows the transition state for ring-opened ethylene oxide to undergo carboxylation. The carbon dioxide molecule undergoing nucleophilic attack does not interact with this chromium center, despite either oxygen atom being more basic than free CO_2 (-1.05 and -1.03, vs. -0.70 atomic polar tensor charges[182]). This might be due to the chromium center being coordinatively saturated (18 electrons; octahedral molecular geometry). Such interactions would create a strained four-membered ring. At the transition state, the alkoxide-CO_2 distance is 1.822 Å, longer than an ordinary C-O bond; the CO_2 molecule is slightly bent at 147°, and its C=O bonds are elongated at 1.194 Å, compared with 1.161 Å (free CO_2). As a point of reference, the CO_2 fragment in the {[Cr]-CO_2} reactant complex is loosely associated with the rest of the complex. The alkoxide-CO_2 distance is 2.700 Å, its C=O bonds are barely elongated (1.162 and

1.163 Å), and the fragment is only slightly bent at 173°. This lack of interaction during carboxylation is not general: the Zn-O(CO_2) distances at equivalent transition states for the (salphen)Zn(II) system are 2.76 and 2.85 Å,[92] whereas the Al-O(CO_2) distances are 2.10 and 2.33 Å for (aminotris(phenolate))Al(III) systems.[96] the difference here is zinc(II) and aluminum(III)'s greater Lewis acidity, compared with chromium(III) or cobalt(III). The latter complexes are coordinatively saturated as well.

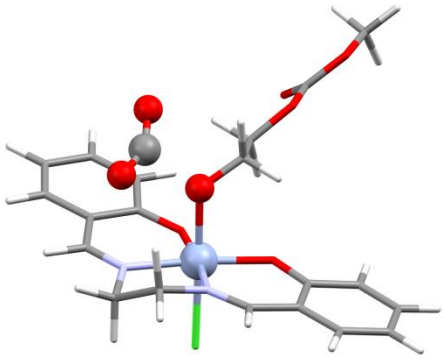

Figure V-9. Transition state for [Cr]-bound ring-opened ethylene oxide to undergo carboxylation to give the corresponding [Cr]-bound carbonate. O(alkoxide)-C(CO_2) = 1.822 Å; C=O = 1.194 Å (both); O=C=O = 147°.

For the selected examples, the free energy barrier for carboxylation (6-8 kcal/mol) is much smaller than the corresponding barrier for the preceding epoxide ring-opening reaction that starts with a metal-bound carbonate (22-27 kcal/mol for both [Cr] and [Co]). We believe it is generalizable that alkoxide carboxylation is the fast step of the copolymerization reaction, and calculations were not performed on the other alkoxides.

The energy profiles of the catalytic enchainment reaction are presented for two examples in Figure V-10 and Figure V-11. It is important to note that this profile is complete, in the sense that we start with a metal-bound carbonate, and end with a metal-bound polymeric carbonate extended by one repeat unit. Along the way, the metal-bound carbonate undergoes ligand exchange with epoxide, followed by formation of a reactant

complex that is downhill in enthalpy, but uphill in free energy. Ring-opening of the metal-activated epoxide occurs, followed by carboxylation to give the metal-bound polymeric carbonate.

These energy profiles clearly show that the rate-determining step is ligand exchange followed by epoxide ring-opening, whereas the barrier for carboxylation of the resultant alkoxide is small. The overall enthalpy of reaction is exothermic by 22.2 and 24.8 kcal/mol, consistent with the gas phase enthalpy of reaction (-21.2 kcal/mol).[63]

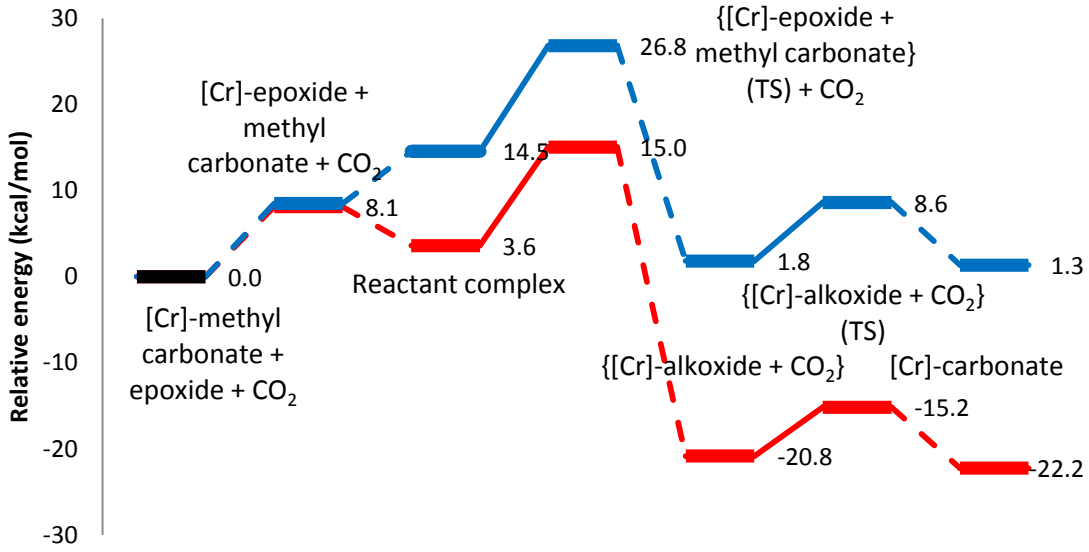

Figure V-10. Energy profiles for the conversion of [Cr]-methyl carbonate + ethylene oxide + CO_2 to the corresponding chain-extended [Cr]-polycarbonate complex. Red line: enthalpy, blue line: free energy.

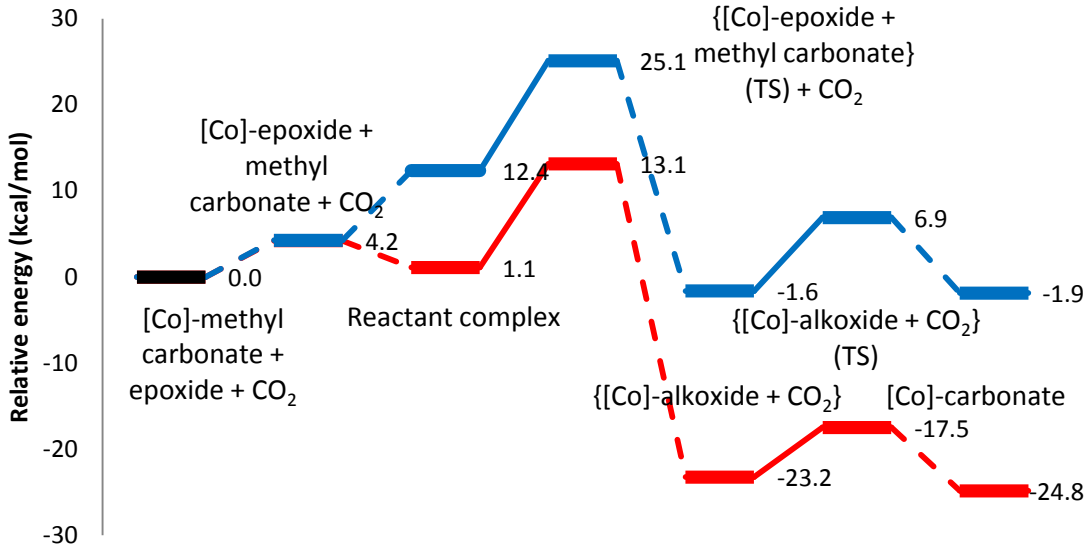

Figure V-11. Energy profiles for the conversion of [Co]-methyl carbonate + ethylene oxide + CO_2 to the corresponding chain-extended [Co]-polycarbonate complex. Red line: enthalpy, blue line: free energy.

Metal-bound carbonate backbiting

The metal-bound carbonate is expected to backbite via the free C=O oxygen atom (**Scheme V-3**). Being coordinated to a Lewis acid, the metal-bound oxygen is much less nucleophilic. Buried in the core of the salen complex, it is also more sterically hindered than the C=O oxygen atom. Other work indicates the C=O oxygen is favored as the nucleophile by 4 kcal/mol (electronic energy).[81] Having carbonyl character, the oxygen atom is less nucleophilic than if it were a free anion involved in the metal-free reaction.

Carbonate backbiting leads to a metal-bound cyclic carbonate, and a shortened polymeric carbonate. The cyclic carbonate may be displaced thereafter by an epoxide molecule or a polymeric alkoxide, enabling further copolymerization. It may also be displaced by a polymeric carbonate, to undergo more carbonate backbiting.

Scheme V-3. Pathway for metal-bound carbonate backbiting.

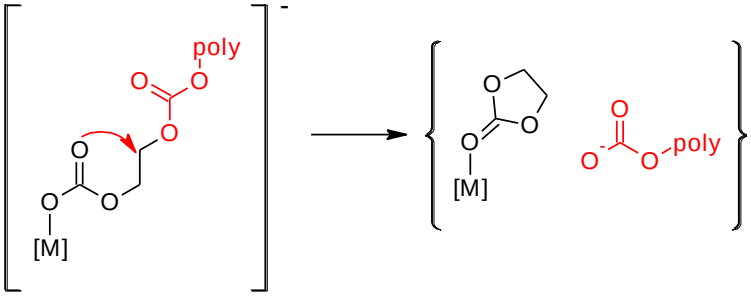

For the aliphatic polycarbonates, carbonate backbiting is easier when metal-free than when metal-bound by 3-9 kcal/mol of free energy (Table V-9). This degradation reaction is harder when the polymeric carbonate is cobalt-bound than when it is chromium-bound, consistent with the observation that cobalt catalysts produce less cyclic carbonate coproduct than chromium catalysts.

Methine attack is harder than methylene attack in general when metal-bound and metal-free due to steric repulsion.[63,116] Styrene carbonate has a lower free energy barrier for metal-free methine attack than methylene attack due to the pendant phenyl group being able to donate electrons into the electron-deficient site of substitution.[63] This stabilizing effect was not observed when metal-bound.

The calculated free energy barriers for metal-bound carbonate backbiting agree well with experimentally determined activation energies:[83] 25.8 and 23.7 kcal/mol vs. 24.0 kcal/mol for propylene carbonate, and 30.5 kcal/mol vs. 31.8 kcal/mol for cyclohexene carbonate. Since the carbonate and alkoxide backbiting reactions is unimolecular, corrections for reactant concentration that were discussed for the enchainment reactions are not applicable.

Table V-9. Free energies of activation (kcal/mol) for carbonate backbiting.

	Metal-free	**[Cr]-bound**	**[Co]-bound**
EC	20.6	26.3	29.6
PC-1	23.5	25.8 (E_a = 24.0[83])	26.7
PC-2	19.2	23.7 (E_a = 24.0[83])	24.6
SC-1	20.6	26.8	25.4
SC-2	20.1	23.4	23.0
CHC	26.5*	30.5 (E_a = 31.8[83])	31.2
CPC	20.3	25.6	19.8

* From the relaxed-chair conformation.

Metal-bound alkoxide backbiting

Relying on insight from the metal-free mechanism,[63] the metal-bound alkoxide backbiting reaction is expected to occur via the metal-bound polymeric alkoxide attacking the adjacent carbonyl group to yield a tetrahedral intermediate coordinated to the metal via the original alkoxide oxygen (**Scheme V-4**). An intramolecular rearrangement occurs to give another tetrahedral alkoxide that coordinates to the metal through the less sterically hindered carbonyl oxygen atom. Dissociation of the shortened polymeric alkoxide yields a metal-bound cyclic carbonate.

Scheme V-4. Pathway for metal-bound alkoxide backbiting: The metal-bound polymeric alkoxide backbites upon itself, leading to a metal-bound cyclic carbonate.

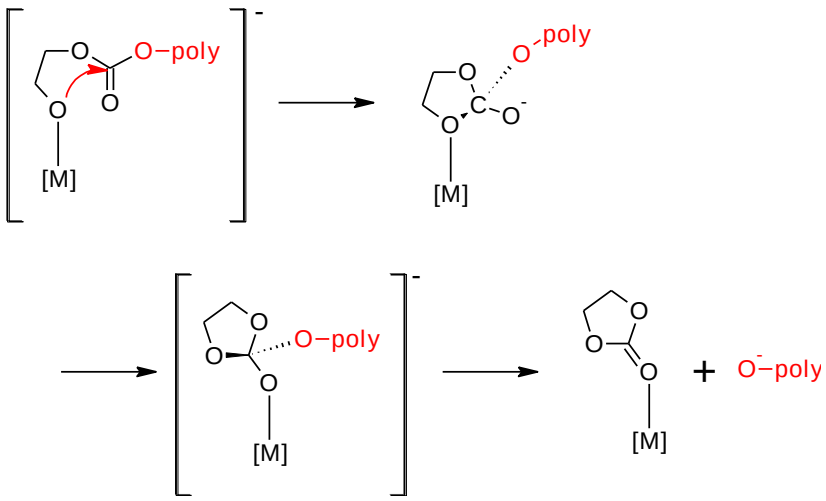

While the activation barriers for metal-free alkoxide backbiting have been extensively quantified, we were unable to locate transition states for the corresponding metal-bound degradation reactions, despite numerous attempts. The metal-bound alkoxides are significantly less nucleophilic than the free alkoxides, and so interact more weakly with the carbonate carbon that is being attacked; finding structures involving such weak interactions is difficult. In any case, under polymerization conditions, the presence of CO_2 rapidly carboxylates available alkoxides, *vide supra*. As a result, this degradation route is unlikely to be significant.

Nevertheless, the study of the metal-free alkoxide backbiting reactions revealed that for all cases except for cyclopentene carbonate formation, the rate limiting step for alkoxide backbiting is the elementary reaction involving the polymeric alkoxide departing from the tetrahedral intermediate. Furthermore, this reaction is nearly barrierless.[63] It would therefore be reasonable to estimate the barrier for metal-alkoxide backbiting from the thermodynamics of this dissociation reaction, and this data is presented in Table V-10.

Table V-10. Free energies (kcal/mol) of activation for metal-bound alkoxide backbiting.

	Metal-free[63]*	**[Cr]-bound**	**[Co]-bound**
EC	11.6	23.3	20.3
PC	11.8	20.6	19.1
SC	10.7	23.6	22.0
CHC	14.6	23.9 (E_a = 25.1)[84]	22.8
CPC	19.9	25.1	24.5

* The actual barrier from CBS-QB3(+) calculations, as opposed to estimated barriers for the metal-bound systems.

Like the case for metal-bound carbonate backbiting, the calculated free energy barriers are consistent with experimental activation energies for [Cr]-bound cyclohexene carbonate formation.[84] The data obtained indicates that despite the approximation made, the metal-free reaction has half the free energy barrier of the metal-bound systems. We can confidently say that under polymerization conditions, where CO_2 and the metal catalyst is present, alkoxide backbiting to give cyclic carbonates, or *trans*-cyclic carbonates for alicyclic epoxides, occurs only via the metal-free route.

Epoxide homopolymerization

The reaction for methoxide to ring-open [Cr]- and [Co]-bound ethylene oxide (**Scheme V-5**) was modeled, as were the subsequent carboxylation reactions. The relative energies are tabulated in Table V-11 and Table V-12. Being a superior nucleophile, methoxide ring-opens the metal-bound epoxide more easily than methyl carbonate does: the free energy barriers are 6-7 kcal/mol vs. 10-15 kcal/mol (Table V-5).

The epoxide ring-opening reaction is much more exothermic than where methyl carbonate was the nucleophile: -47 to -48 kcal/mol vs. -17 to -18 kcal/mol. The ring strain relieved should be identical. The nucleophile is two carbons removed from the metal center, making nucleophile-metal interactions irrelevant. The 30 kcal/mol discrepancy can only be attributed to: (1) the stronger O-C bond formed between

methoxide and ethylene oxide, compared with the weaker one formed by methyl carbonate; (2) the poorer stabilization of the negative charge on the methoxide reactant, compared with methyl carbonate. In support, (1) the new O(nucleophile)-C(ethylene oxide) bond is ca. 1.41 Å long where methoxide was the nucleophile, and 1.44 Å where methyl carbonate was the nucleophile; (2) the atomic polar tensor (APT) charges on O(nucleophile) was -1.41 for methoxide, and -1.17 for methyl carbonate.

Scheme V-5. Ring-opening of a metal-bound epoxide by an alkoxide, followed by carboxylation.

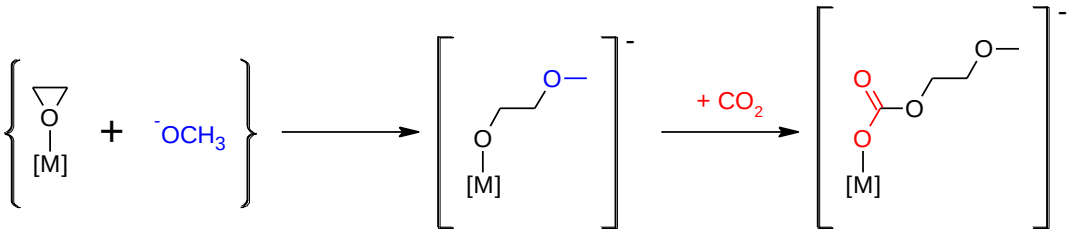

Table V-11. Enthalpy (kcal/mol) of ring-opening ethylene oxide with methoxide, followed by carboxylation.

	{[M]-EO + methoxide}	TS	[M]-alkoxide	[M]-carbonate
[Cr]	0	6.7	-48.2	-58.7
[Co]	0	6.9	-47.2	-57.4

Table V-12. Free energy (kcal/mol) of ring-opening ethylene oxide with methoxide, followed by carboxylation.

	{[M]-EO + methoxide}	TS	[M]-alkoxide	[M]-carbonate
[Cr]	0	6.5	-47.9	-47.3
[Co]	0	7.1	-46.7	-46.4

Carboxylation of the metal-bound alkoxide is exothermic by ca. 10 kcal/mol. This energy difference is negated by the TΔS component where free energy considered, although under significant pressures of CO_2, carboxylation should be exergonic.

Thus, the metal-bound alkoxide has two possible pathways for further reaction: it can undergo carboxylation, eventually leading to a polycarbonate. It can also ring-open another metal-bound epoxide. Both processes have similar activation parameters: $\Delta H^{\ddagger}$ and $\Delta G^{\ddagger}$ are ca. 6 kcal/mol.

Yet, homopolymerization can only proceed through the alkoxide being displaced by an epoxide, followed by epoxide ring-opening by the displaced alkoxide. This dissociated alkoxide is expected to spontaneously undergo carboxylation as well.[137] A smaller factor could be that in the presence of a significant partial pressure of CO_2, the reactants for carboxylation will have a higher chemical potential. The propensity for homopolymerization will be unchanged, and carboxylation is favored as a result.

This reasoning brings our theoretical results in line with the experimental observations of [Cr]- and [Co]-catalyzed copolymerization reactions generating few polyether defects.[15] Early zinc(II) catalysts[17] are reputed to generate a higher fraction of polyether defects. This could be because zinc's stronger Lewis acidity causes the metal-bound alkoxide to be much less nucleophilic toward an external CO_2 molecule. As a result, sequential epoxide ring-opening may have a lower energy barrier than carboxylation. While zinc's Lewis acidity should cause both polymeric carbonate and alkoxide to bind

more strongly, the relative differences may decrease. Polymeric carbonates may no longer have an advantage in ease of dissociation, explaining zinc catalysts' reduced selectivity for polycarbonate.

Ligand effects

The salen system used experimentally required too much computational resources for routine calculation due to its size. To understand the effects of adjusting the salen ligand's steric and electronic effects, calculations were performed on a few models. Electron-donating and electron-withdrawing methyl and fluoride substituents were installed in the ortho and para positions of the salen ligands (Figure V-12). To account for steric effects, tert-butyl groups were used at the same positions, and the ethylene backbone was substituted by bulkier cyclohexylene. Cyclohexene oxide appears prone to steric effects, so its enthalpy of binding was calculated for the latter scenario.

Enthalpies and free energies of ligand binding were obtained by M06/BS2+ single point calculations using M06-L/BS2 geometries and vibrational corrections; this data was tabulated in Table V-13. For the complexes with undecorated salen ligands, enthalpies of ligand binding obtained this way exhibit remarkable agreement with M06/BS2+ enthalpies, giving us confidence in the results of the double-barreled calculations.

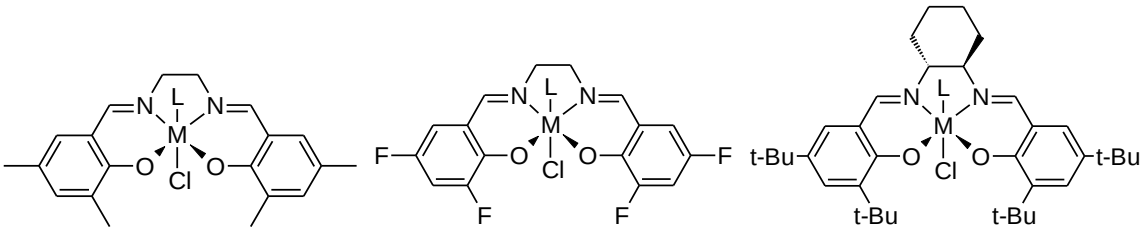

Figure V-12. (salen)MCl Systems used to determine the ligands steric and electronic effects that are denoted hereafter, [MeM], [FM], and [t-BuM].

Table V-13. Enthalpies and free energies (kcal/mol) for ligands (L) to dissociate from [M]-L complexes bearing substituted salen ligands, and the corresponding M-L distances (Å).

	Enthalpy		Free energy		M-L	
[M]-L	**[Cr]**	**[Co]**	**[Cr]**	**[Co]**	**[Cr]**	**[Co]**
[M]-EO	16.6, *16.7*	16.0, *16.3*	6.0, *4.2*	1.4, *4.1*	2.149	2.064
[M]-CHO	19.5, *19.6*	18.8, *19.1*	8.8, *6.3*	4.1, *6.2*	2.122	2.039
[M]-methoxide	48.8, *48.3*	46.8, *46.2*	38.6, *36.7*	33.1, *34.1*	1.914	1.912
[M]-methyl carbonate	25.1, *24.8*	20.7, *20.5*	14.5, *12.7*	6.8, *8.4*	1.990	1.956
[MeM]-EO	16.1	15.6	2.7	3.1	2.152	2.071
[MeM]-methoxide	46.9	45.7	34.0	33.3	1.916	1.913
[MeM]-methyl carbonate	24.1	19.4	10.6	5.6	1.993	1.960
[FM]-EO	17.4	17.0	5.1	4.3	2.144	2.065
[FM]-methoxide	52.0	50.4	39.9	38.8	1.911	1.910
[FM]-methyl carbonate	27.6	23.8	14.7	11.2	1.987	1.953
[tBuM]-EO	17.3	17.0	4.7	2.9	2.157	2.070
[tBuM]-CHO	20.8	20.7	7.6	6.8	2.136	2.040
[tBuM]-methoxide	47.5	46.6	34.8	33.5	1.919	1.912
[tBuM]-methylcarbonate	26.3	22.4	12.8	7.2	2.007	1.973

M06/BS2+//M06-L/BS2 energies. Energies calculated at the M06/BS2+ level are presented in *italics* for comparison.

We expect that electron-donating methyl and tert-butyl substituents increase the electron density at the metal center, weakening the metal's interactions with the *trans* ligand. Accordingly, the bond dissociation enthalpies for ligands coordinated to [MeM] complexes are higher by ca. 1 kcal/mol. Conversely, electron-withdrawing fluorine substituents strengthen the metal-ligand bond by ca. 2 kcal/mol of enthalpy. The calculated [M]-L lengths confirm this observation: [MeM]-L lengths are ca. 0.003 Å longer, whereas [FM]-L lengths are ca. 0.003 Å shorter.

Unfortunately, this reasoning fails when applied toward the [tBuM] systems that have a cyclohexylene rather than an ethylene salen backbone. The [tBuM] systems are expected

to be more electron-rich than the unadorned salen complexes, yet the ligands are bound more strongly by ca. 1 kcal/mol. Inexplicably, the corresponding M-L distances are longer by ca. 0.008 Å, which would usually reflect a weaker M-L bond. An attempt was made to analyze these systems using atomic polar tensor charges, but no reasonable conclusions could be drawn. It is crucial to accurately model, and more importantly, understand the effects of ligand modification, since such knowledge opens the door to rational catalyst design.

Summary and concluding remarks

The hybrid M06 functional in conjunction with the BS2+ basis set accurately reproduces benchmark CBS-QB3 free energy barriers for reactions relevant to the CO_2-epoxide copolymerization reaction. Computed barriers for metal-bound carbonate and alkoxide backbiting reactions compare well with experimentally determined activation energies, emphasizing the validity of the chosen method. For large systems, M06/BS2+ energies calculated at M06-L/BS2 geometries gives reasonable results for equilibrium geometries, whereas the latter calculations are not as accurate on their own.

The enthalpies for epoxides, polymeric alkoxides and carbonates, and cyclic carbonates to dissociate from [Cr] and [Co] were found to be 16-19 kcal/mol, 39-48 kcal/mol, 19-27 kcal/mol, and 10-12 kcal/mol respectively. These numbers are in agreement with the ligands' relative Lewis basicity.

The elementary metal-catalyzed epoxide ring-opening reactions have free energy barriers of 10-15 kcal/mol. Subsequent carboxylation is a low-energy process: $\Delta G^{\ddagger} \approx$ 6 kcal/mol, and the metal catalyst does not activate CO_2. Displacing the metal-bound polymeric carbonate by an epoxide to yield the prerequisite metal-bound epoxide is significantly endergonic, and this exchange reaction should be taken into account. Thus corrected, epoxide ring-opening is rate limiting, and it has overall free energy barriers of 22-27 kcal/mol.

The [Cr]-catalyzed reactions' free energy barriers are 0.5-3 kcal/mol higher than the [Co]-catalyzed reactions, and this difference originates in enthalpy, not entropy. This finding is consistent with how [Cr]-catalyzed copolymerization generally require higher temperatures than for [Co]-catalyzed reactions. Cyclopentene oxide is different, in that its copolymerization with CO_2 has a very high free energy barrier of 22.4 kcal/mol when [Cr]-catalyzed, and 14.7 kcal/mol when [Co]-catalyzed. This rationalizes the experimental difficulty in preparing poly(cyclopentene carbonate) with chromium catalysts.

Metal-bound polymeric carbonates and alkoxides have a low tendency to degrade to the cyclic carbonate through backbiting reactions due to the terminal nucleophile's reduced basicity. These reactions' free energy barriers are 23-31 and 20-25 kcal/mol respectively, much higher than the barriers for polymer growth. The metal-free degradation reactions have much lower free energy barriers of 18-24 and 12-14 kcal/mol respectively, in comparison.

The reaction to ring-open a [Cr]- or [Co]-bound epoxide with an alkoxide has a low free energy barrier of ca. 6 kcal/mol. Epoxide homopolymerization requires displacement of the strongly-bound polymeric alkoxide by an epoxide that binds much more weakly. Additionally, the polymeric alkoxide is easily carboxylated. Thus, [Cr] and [Co] catalysts succeed in avoiding polyether defects.

The kinetic data presented in this chapter agrees quantitatively with experimental results. They also qualitatively rationalize other experimental observations (e.g. product distributions). This foundational work sets the stage for further investigations with regard to the effects of ligand modification on the kinetics of the copolymerization reaction. The near-term goal will be to quantify the effects of electron-donating and electron-withdrawing methyl and fluorine substituents on the kinetics of the process, since the thermodynamics of ligands binding to such salen complexes have been calculated. It is important to gain a deeper understanding of these substituent effects for

future catalyst development. The effect of other modifications, such as Williams' phosphasalen complexes[183] that have iminophosphoranes in place of imines, can also be evaluated.

Another area of interest is to examine new ligand architectures, such as the tetramethylazaannulene motif.[184] Such complexes are being investigated for its greater effectiveness toward copolymerizing large epoxides like 1,4-dihydronaphthalene oxide to give novel polycarbonates, whereas the second and third generation salen complexes coproduce much cyclic carbonate. The ultimate goal is to utilize computational chemistry to evaluate proposed catalyst systems, real or imagined, toward this sort of transformation. The savings in terms of labor, materials, and energy are consistent with the principles of green chemistry, and are anticipated to accelerate the pace of research in this (or any other) field.

Computational methods

All calculations were performed using the Gaussian 09 suite.[127] The orientations of epoxides coordinated to metal complexes were determined by relaxed potential energy scans using the spin-unrestricted semi-empirical PM6 method,[185] followed by full optimizations. Spin-unrestricted density functional theory was used for subsequent work involving chromium or cobalt complexes.

Enthalpies and free energies quoted in this work are obtained using Zhao and Truhlar's M06 hybrid functional[178] in conjunction with the BS2+ basis set, and Truhlar and coworkers' SMD solvation model,[131] except where noted. Gaussian's "ultrafine" integration grid was used for the M06 family of functionals. For basis set BS2, the cobalt and chromium atoms were described by Stuttgart/Dresden effective core potentials and basis sets (SDD).[186] The all-electron 6-31G(d',p') of Petersson and coworkers were used for remaining atoms.[141-142] Basis set BS2+ was similar to BS2, except that diffuse functions were added (i.e. 6-31+G(d',p') instead of 6-31G(d',p')). Selected calculations

were performed using the pure M06-L[187] functional. Where noted, benchmark free energy barriers were obtained using the CBS-QB3[103,105] composite method.

Stationary points and saddle points were confirmed by their calculated vibrational frequencies (zero and one imaginary frequencies, respectively). Input files were prepared using AGUI.[129] AGUI, Avogadro,[130] Molden,[188] and Mercury[189] were used for visualization.

CHAPTER VI

KINETIC AND THERMODYNAMIC INVESTIGATIONS OF CO_2 INSERTION REACTIONS IN M-H AND M-C BONDS, AND STEPS TOWARD THE DIRECT SYNTHESIS OF CARBOXYLIC ACIDS*

Introduction

The insertion reactions of CO_2 into metal-hydrogen and metal-carbon σ bonds at different metal centers are well-studied processes[190-200] that produce metal formates and carboxylates respectively (**Scheme VI-1**). The former process proceeds via a H-CO_2 interaction leading to cleavage of the M–H bond with concomitant formation of a metal-bound formate ligand. That is, in general, no prior coordination of CO_2 to the metal center is required. A similar conclusion was reached for insertion of CO_2 into metal-carbon σ bonds. In early studies, Darensbourg *et al.* has performed extensive mechanistic comparisons between these two insertion reactions utilizing group 6 metal carbonyl anionic derivatives, e.g., $M(CO)_5R^-$, where R = H, alkyl or aryl.[75-80] The results of these investigations can be summarized as follows:

1. Formate formation is highly reversible, whereas carboxylate formation is irreversible.
2. CO_2 insertion into M–H bonds is much faster than insertion into the corresponding M–C σ bonds.
3. The rate of CO_2 insertion increases with the nucleophilicity of the M–H and M–C moieties, e.g., M–CH_3 >> M–Ph.

* Adapted with permission from Darensbourg, D. J.; Kyran, S. J.; Yeung, A. D.; Bengali, A. A. *Eur. J. Inorg. Chem.* **2013**, 4024. Copyright 2013, Wiley-VCH.

4. The CO_2 insertion process occurs at coordinatively saturated metal centers, i.e., prior coordination of CO_2 at the metal center is not required.
5. CO_2 insertion into M–C σ bonds occurs with retention of configuration about the α carbon center.

Scheme VI-1. CO_2 insertion into metal-hydride and metal-carbon bonds to give metal formates and carboxylates.

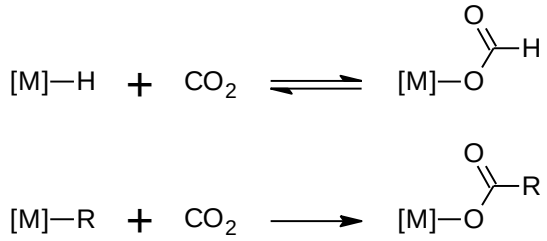

Although CO_2 inserts into *isolated* metal-hydrogen bonds more quickly than into metal-carbon σ bonds, and that decarboxylation readily occurs in the formate derivatives, it has only recently been established that thermodynamics favor formation of carbon-carbon bonds. Field and coworkers have shown the reaction sequence illustrated in **Scheme VI-2** to be operative for the $Ru(dmpe)_2(CH_3)H$ complex.[201]

Scheme VI-2. Reaction of $Ru(dmpe)_2(CH_3)H$ (1) with CO_2 to give the formate and acetate complexes (2 and 3 respectively).

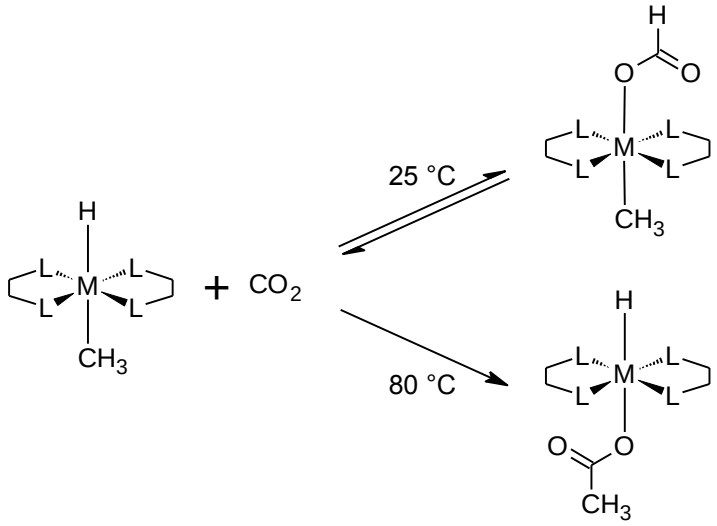

Specifically, CO_2 inserts into the ruthenium-hydride bond to afford the formate complex as the kinetic product, whereas it inserts into the ruthenium-carbon bond to give acetate as the thermodynamic product. The reaction pathway of the rearrangement presumably involves decarboxylation of the formate complex followed by insertion of CO_2 into the Ru-CH_3 bond. Further insertion of CO_2 to provide an acetate-formate ruthenium derivative was not observed.[201]

This observation is useful toward the direct functionalization of hydrocarbons, since reductive elimination would afford the more desirable carboxylic acid, as opposed to the alkyl formate alternative. Such a transformation represents a potential route for the valorization of carbon dioxide.[202] Nevertheless, because the reaction between methane and carbon dioxide to give acetic acid is not spontaneous, it is necessary to couple this reaction to an exothermic reaction to drive it forward. This is analogous to the pathway employed by Jessop and Noyori for the production of formic acid from carbon dioxide and dihydrogen.[203]

Here, the thermodynamics and kinetics of these carboxylation reactions are examined by computational methods. The effects of changing the ligands and the metal are examined, and steps toward the direct synthesis of carboxylic acids are made.

Results and discussion

The enthalpies of the reaction of various ruthenium and iron complexes with carbon dioxide to yield carboxylate complexes (**Scheme VI-3**) were calculated. Using the B3LYP/BS1 geometry (basis sets are defined section on computational methods), single-point energy calculations were performed using a variety of pure and hybrid functionals (B3LYP, BP86, TPSS, M06) using the BS2 basis set (Figure VI-1). The enthalpies of reaction were qualitatively the same between different functionals, giving us confidence in the results. There was no experimental thermodynamic data for comparison, so the B3LYP functional was chosen for subsequent work. Basis set effects were also examined, and BS2 was chosen because it gave results identical to that obtained with larger basis sets (Figure VI-2).

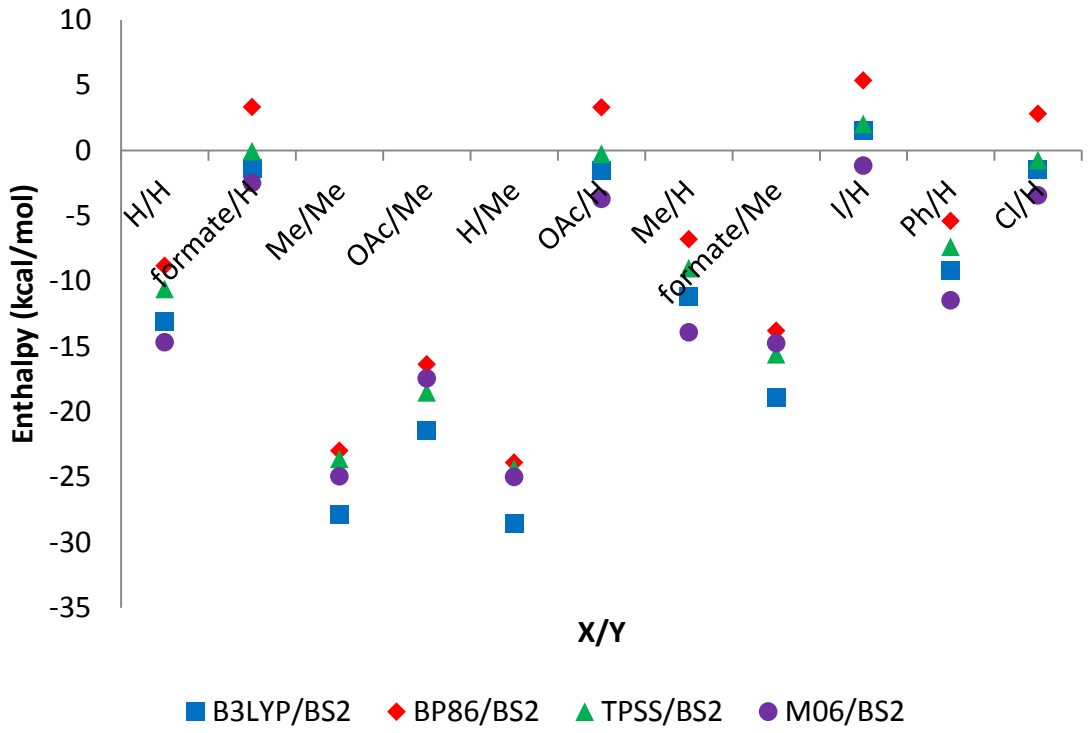

Figure VI-1. Enthalpies for the carboxylation of $Ru(dmpe)_2XY$ complexes, calculated using different functionals. While the absolute enthalpies of reaction differ between different functionals, the trends are in good agreement.

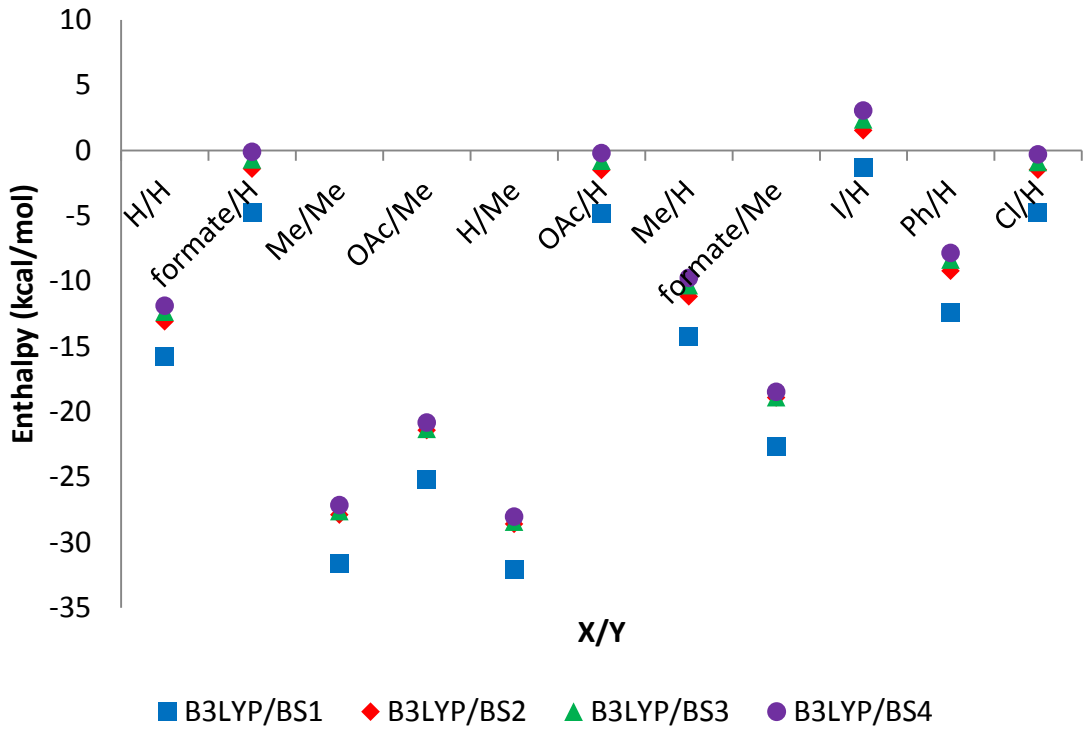

Figure VI-2. Enthalpies for the carboxylation of $Ru(dmpe)_2XY$ complexes, calculated using the B3LYP functional with different basis sets. The calculated enthalpies using triple-zeta basis sets (BS2-BS4), were in excellent agreement with each other. The SDD basis set was used for ruthenium and iodine atoms. All other atoms used the following basis sets: BS3, 6-311G(2d,p); BS4, 6-311G(2df,2pd).

In the working model for this reaction, CO_2 insertion converts the strongly σ-donating methyl or hydride ligand into a more weakly donating carboxylate ligand, thereby reducing the electron-density at the metal center. As a result, the carboxylation reaction is more favored when the electron density at the metal center is greater.

The reaction depicted in **Scheme VI-3** has been somewhat simplified, i.e., complexes of the form L_2RuXCO_2Y have two possible conformations (Figure VI-3). Where Y = H, the geometries having both oxygen atoms point toward the metal center (ii) are lower in

energy than the geometries with only one oxygen atom pointing toward the metal center (i). The difference in enthalpy for these formate complexes is non-trivial, approximately 8-9 kcal/mol (Table VI-1). Indeed, the structure in (ii) is generally observed in the solid-state by X-ray crystallography.

Scheme VI-3. The carboxylation reactions studied computationally.

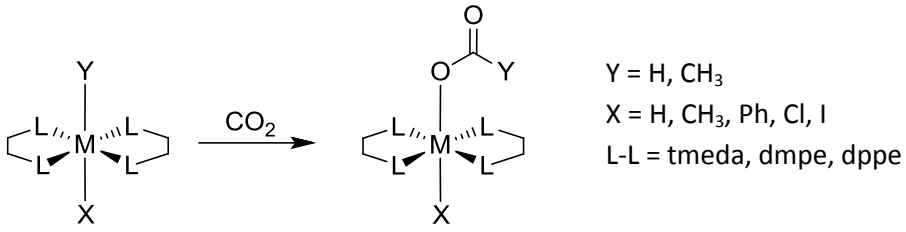

Table VI-1. Relative energies of conformation (ii) vs. conformation (i) for complexes of the form $Ru(dmpe)_2X(formate)$.

X	ΔH, (ii)-(i) (kcal/mol)
H	-9.2
Me	-8.9
Ph	-8.3
Formate	-7.9
Acetate	-7.5
Cl	-8.6
I	-8.3

The lower energy for complexes of conformation (ii) is probably due to a favorable electrostatic interaction between the carbonyl oxygen with the metal. Acetate complexes appear not to adopt conformation (i) due to steric repulsion. As a simple rotation about the C-O bond transforms one conformer to the other, the additional barrier is expected to

be low. Conformation (i) remains significant because it is the immediate product when carbon dioxide inserts into a ruthenium-hydride bond, *vide infra*.

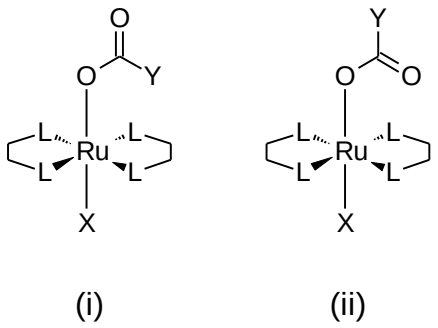

Figure VI-3. The two possible conformations of L_2RuXCO_2Y complexes. The conformation labels (i) and (ii) are used hereafter.

As noted earlier, Field and coworkers reported that *trans*-$Ru(dmpe)_2Me_2$ undergoes two sequential CO_2 insertion reactions to give the diacetate complex. In comparison, *trans*-$Ru(dmpe)_2MeH$ inserts CO_2 into the Ru-H bond to give the formate complex as the kinetic product. The methyl formate complex yields the acetate hydride upon heating, but the latter does not insert a second equivalent of carbon dioxide.[201] Our computational results explain those observations: the two sequential carboxylation reactions of *trans*-$Ru(dmpe)_2Me_2$ are strongly exothermic (-28 and -21 kcal/mol, see Figure VI-4). Both possible reactions between *trans*-$Ru(dmpe)_2MeH$ and CO_2 are exothermic. Addition of another equivalent of carbon dioxide to convert the acetate hydride complex to acetate formate complex (i) is endothermic, and the overall reaction to give acetate formate complex (ii) is barely exothermic. The loss of entropy encountered upon CO_2 insertion also helps make this reaction quite unfeasible.

This carboxylation of the hydride acetate complex is disfavored because the acetate ligand is a poor electron donor. With the electron-withdrawing chloride X ligand, the carboxylation is similarly unfavorable. Overall, no double insertion product is observed, presumably because the activation barrier from *trans*-$Ru(dmpe)_2Me$(formate) complex

to yield the dicarboxylate product is higher than the overall barrier for it to transform into the *trans*-Ru(dmpe)$_2$(OAc)H that does not react further.

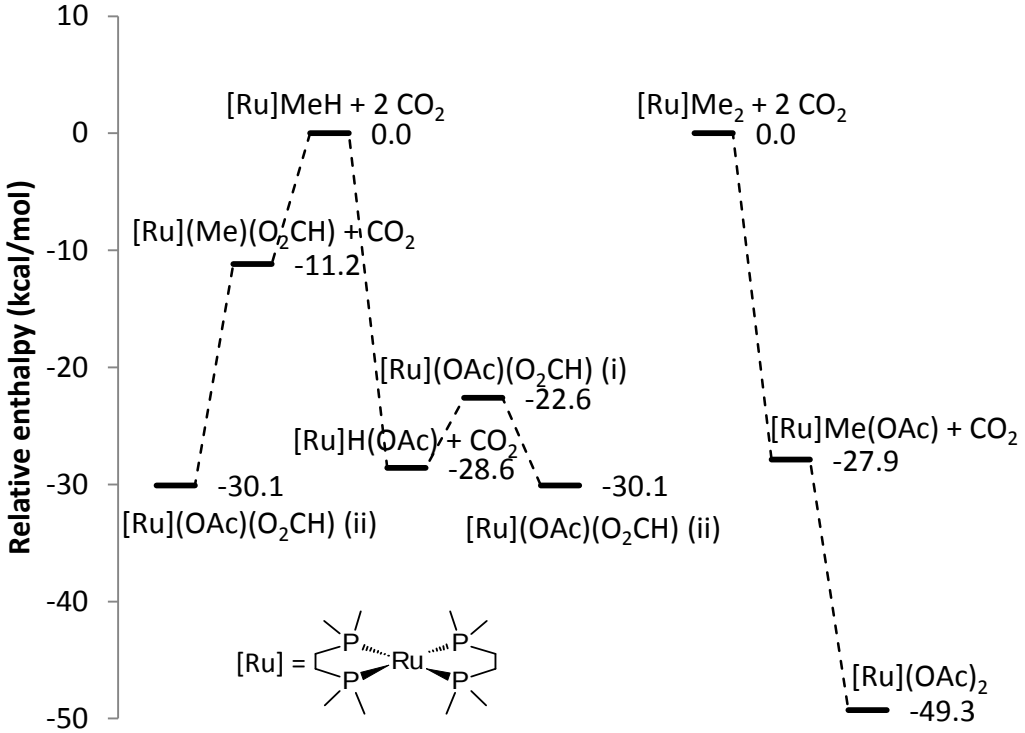

Figure VI-4. Relative enthalpies for the reactions between Ru(dmpe)$_2$ complexes with carbon dioxide; the corresponding free energy diagram is qualitatively the same.

Effect of the X ligand

The effect of several X ligands were examined for the Ru(dmpe)$_2$XY system. Electron-donating X-ligands were found to favor CO_2 insertion; the enthalpy of CO_2 insertion decreases as follows (Figure VI-5): X = H ≈ CH_3 > Ph >> acetate ≈ formate ≈ Cl > I. Incidentally, acetate formation is generally more exothermic than formate formation by approximately 17 kcal/mol.

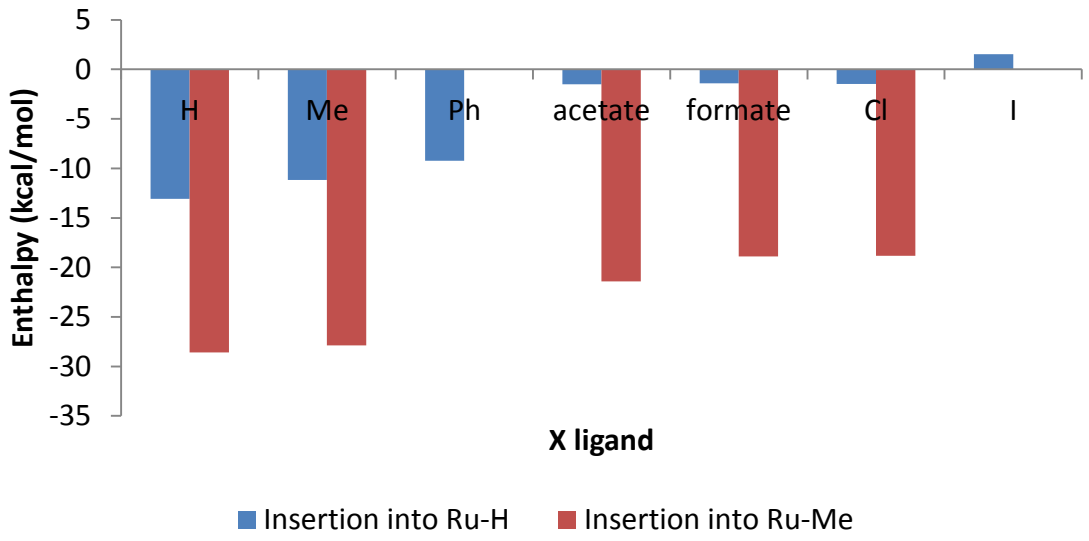

Figure VI-5. Enthalpies of CO_2 insertion into the Ru-Y bond for compounds of the form, $Ru(dmpe)_2XY$.

In benzene, the activation parameters for the first CO_2 insertion for $Ru(dmpe)_2Me_2$ were determined via *in situ* infrared and nuclear magnetic resonance spectroscopy as follows: $\Delta H^{\ddagger}$ = 12.7 ± 0.6 kcal/mol, $\Delta S^{\ddagger}$ = –31.9 ± 2.0 e.u. The second carboxylation reaction proceeds much more slowly.[204] The gas phase barriers for CO_2 insertion were also determined computationally for three complexes of the form $Ru(dmpe)_2XH$ using the B3LYP functional and the BS2++ basis set. The calculated enthalpies listed in Table VI-2 indicate that the electron donating ability of the X ligands *trans* to the hydride ligand undergoing CO_2 insertion influences both the enthalpy of the reaction, as well as its activation barrier. It is important to note that decarboxylation of these formate complexes require that they adopt the less stable conformation (i) (Figure VI-6). Accordingly, the overall barriers to decarboxylation are 7.5 – 9.2 kcal/mol higher than they appear here, *vide supra*. Unfortunately, efforts to locate the analogous transition states yielding acetate complexes were fruitless, so the free energy barriers presented in this section cannot be directly compared to the experiment.

Table VI-2. Enthalpies of species involved in CO_2 insertion reactions, transition state relative to reactant plus CO_2 (energies in kcal/mol). (B3LYP/BS2++, gas phase).

X	$Ru(dmpe)_2XH + CO_2$	Transition state	$Ru(dmpe)_2X$(formate) (i)
H	0	7.3	-5.1
Cl	0	27.9	6.4
Me	0	10.2	-3.3

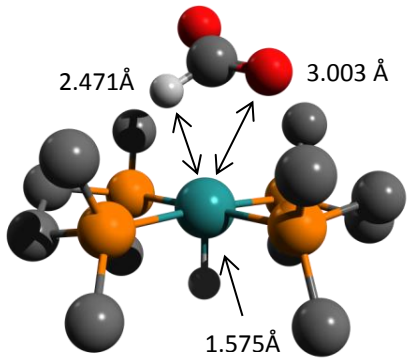

Figure VI-6. The transition state for $Ru(dmpe)_2H_2$ leading to carboxylation. The immediate product of this elementary reaction is the formate complex of conformation (i). Hydrogen atoms on the dmpe ligands have been omitted for clarity.

At the transition state for $Ru(dmpe)_2H_2$ to undergo carboxylation, the Ru-H and Ru-O distances (2.471 Å and 3.003 Å , respectively) are significantly elongated compared to the dihydride starting material, and the formate product (1.694 Å and 2.276 Å, respectively). At the transition state, the supporting Ru-H bond is shortened (1.575 Å), compensating for the central ruthenium atom's weaker interactions with the developing formate ligand. As a point of comparison, the sum of the covalent radii are 1.77 and 2.12 Å for Ru-H and Ru-O respectively.[205]

Supporting ligand effects

With dmpe supporting ligands, formate formation is favored for X = CH_3 and poorly so for X = Cl (Figure VI-7). Both reactions were slightly more favored where a chelating dicarbene was used (1,1'-dimethyl-3,3'-methylenediimidazoline-2,2'-diylidene), whereas when dppe was used, both reactions were now endothermic. In contrast, both reactions were strongly favored when tmeda was used.

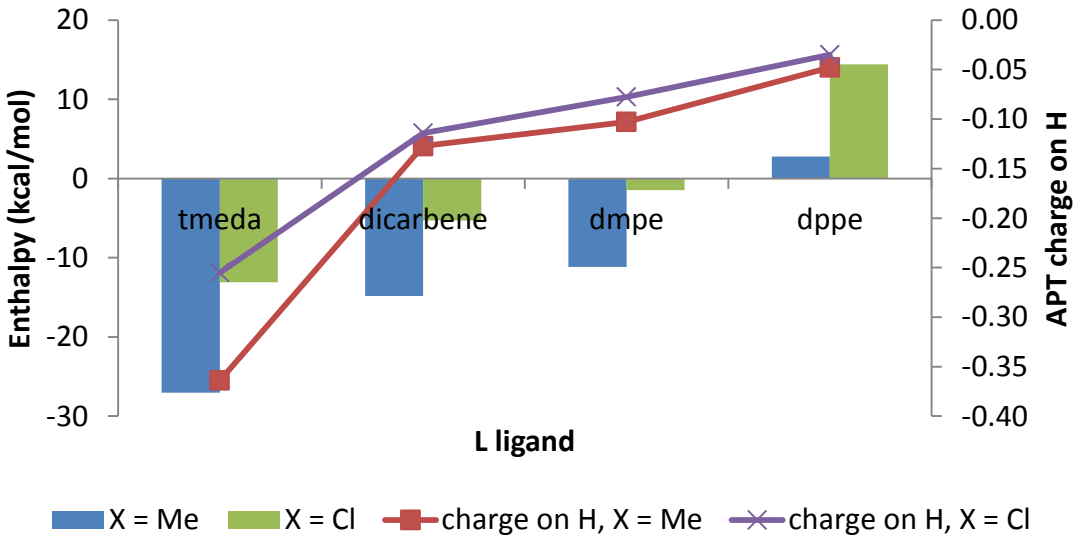

Figure VI-7. Enthalpies of CO_2 insertion into the Ru-Y bond for complexes of the form RuL_2XY.

The amount of negative charge on H, represented by its atomic polar tensor (APT) atomic charge[182] (Figure VI-7), is a function of how π-acidic the L ligands are. Strongly π-acidic L ligands like dppe cause the hydride ligand (that undergoes CO_2 insertion) to be less hydridic, whereas poorly π-acidic L ligands like tmeda cause the hydride ligand to be more so. As the hydride ligand becomes more negatively charged, CO_2 insertion into the Ru-H bond becomes more exothermic and favored.

Ruthenium vs. iron

The iron complexes were calculated to react with carbon dioxide more exothermically than the ruthenium analogs do. Notably, carboxylation of trans-Fe(dmpe)$_2$(OAc)H is exothermic by 14.4 kcal/mol vs. 1.5 kcal/mol for *trans*-Ru(dmpe)$_2$(OAc)H (Table VI-3, entry 6). Insertion of carbon dioxide into the Fe-H bond is exothermic by approximately16 kcal/mol, whereas insertion into the Fe-CH_3 bond is consistently exothermic by approximately 31 kcal/mol.

Table VI-3. Enthalpies of CO_2 insertion into the M-Y bond for complexes of the form, M(dmpe)$_2$XY.

No.	X/Y	M = Fe	M = Ru
1	H/H	-18.0	-13.1
2	formate/H	-14.6	-1.4
3	Me/Me	-32.7	-27.9
4	OAc/Me	-32.0	-21.4
5	H/Me	-31.9	-28.6
6	OAc/H	-14.4	-1.5
7	Me/H	-16.8	-11.2
8	formate/Me	-29.5	-18.9

The computational results indicate that the carboxylation of the iron formate hydride complex is favorable whereas the same for ruthenium is unfavorable, and that the sequential carboxylation reactions for the iron and ruthenium dimethyl complexes are favorable. These findings are in excellent agreement with published experimental work,[182,201,206-207] lending weight to our predictions.

Iron complexes react more exothermically than the ruthenium complexes due to its greater electron density. In fact, a leveling effect is observed for iron, in that its high electron density swamps the contribution of the X ligands. Regardless of the X ligand,

acetate and formate production are consistently exothermic by 32 and 8 kcal/mol, respectively, though the carboxylation of *trans*-Ru(dmpe)$_2$(formate)H deviates somewhat (Table VI-2, entry 2). To further illustrate, ruthenium is able to discriminate between a strongly donating hydride or methyl ligands from a more poorly donating carboxylate ligands, whereas iron is unable to do so.

Toward the direct synthesis of carboxylic acid

Having gained fundamental knowledge of the kinetic and thermodynamic factors that affect the *trans*-Ru(dmpe) system's propensity toward CO_2 incorporation, we wanted to move toward designing a catalyst that is able to convert hydrocarbons and carbon dioxide to carboxylic acids. Specifically, we wanted to assess the thermodynamics of the complete catalytic cycle (**Scheme VI-4**), because merely optimizing the carboxylation step without consideration of the preceding oxidative addition step, or the following reductive elimination step, would not result in a feasible catalytic reaction. This approach weeds out catalyst systems with unfavorable thermodynamics, and effort can be more profitably applied toward understanding mechanistic details of more feasible catalytic systems.

Scheme VI-4. General catalytic cycle for the metal-catalyzed carboxylation of hydrocarbons to yield carboxylic acids.

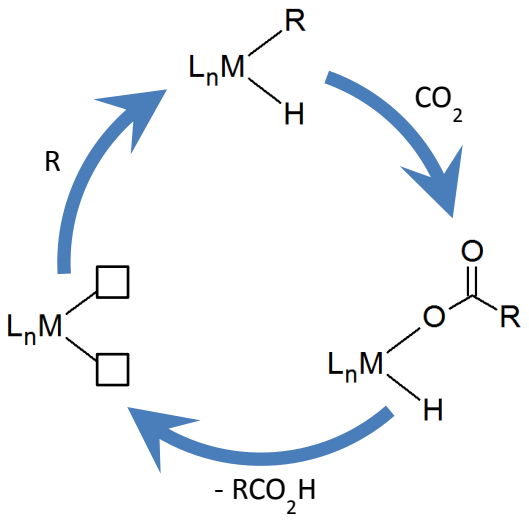

The diphosphine ligand system was retained for this work. A three-carbon backbone for these diphosphines (dmpp and dppp) was used because they are expected to provide a putative catalyst with more flexibility than the previous dmpe system. A *cis* geometry was assumed since it allows for oxidative addition of the hydrocarbon, and for reductive elimination of the carboxylic acid product. As a result, the supporting ligand is both *cis* and *trans* to the substrate ligands. The substrates examined were dihydrogen, methane, and benzene. Hydrogen is a distinct substrate for this class of reaction, while the latter two substrates represent aliphatic and aromatic hydrocarbons. The enthalpies of each step in the catalytic cycle are tabulated in Table VI-4. Care was taken to treat the carboxylic acid products as hydrogen-bonded dimers. The overall enthalpies of reaction were found to be constant for a given substrate, in accordance with Hess' law.

Table VI-4. Enthalpies (kcal/mol) of each step in the metal-catalyzed carboxylation of XH: oxidative addition (O.A.), carboxylation, and reductive elimination (R.E.).

cis-[M]	XH	O.A.	Carboxylation	R.E.	Overall
$Ru(dmpp)_2$	H_2	-38.8	-2.3	39.3	-1.7
	CH_4	-9.9	-19.7	34.6	5.0
	C_6H_6	-14.9	-21.4	35.7	-0.7
$Ru(dppp)_2$	H_2	-30.8	15.5	13.6	-1.7
	CH_4	10.7	-13.7	8.1	5.0
	C_6H_6	13.2	-23.0	9.1	-0.7
$Fe(dmpp)_2$	H_2	-29.7	-14.5	42.4	-1.7
	CH_4	-4.8	-26.3	36.2	5.0
	C_6H_6	-9.7	-28.8	37.8	-0.7
$Fe(dppp)_2$	H_2	-36.0	8.5	25.7	-1.7
	CH_4	8.2	-23.2	20.1	5.0
	C_6H_6	10.8	-32.6	21.2	-0.7

Oxidative addition of dihydrogen is more strongly exothermic (ca. 30 kcal/mol) than the oxidative addition of C-H bonds for all four examples.[208] The latter reaction is exothermic for electron-rich dmpp complexes, and endothermic for electron-poor dppp complexes. This is because the dppp ligand withdraws electron density from the metal center through π back-donation. The π-acidic phenyl ligand competes for the metal's electron density through the same pathway. Compared with the case of methane, oxidative addition of benzene is more exothermic for dmpp complexes, whereas it is more endothermic for dppp complexes. The supporting ligands greatly influence the thermodynamics of these reactions since they are *trans* to the incoming ligands. The supporting ligands' effects appear more important than the choice of metal, iron vs. ruthenium, as a result.

Carboxylation converts the stronger σ-donating hydride/carbon ligand into a more poorly donating carboxylate ligand. The metal's influence is strongest for the carboxylation of

hydride ligands. For the methyl and phenyl hydride complexes, carboxylation is more favored where the metal center is more electron-rich, than where it is poorer (i.e. together with the π-acidic dppp ligand).

Like the case for oxidative addition, reductive elimination has a greater dependence on the identity of the supporting ligand than on the metal; the strongly π-acidic dppp ligand causes reductive elimination to be less endothermic (10-20 kcal/mol), whereas it is much more so with the dmpp ligand (30-40 kcal/mol). In this model, the exothermic dimerization of the reductively eliminated carboxylic acids has been accounted for. If necessary, this step may be made less endothermic by coupling it with an exothermic acid-base reaction. As a point of reference, the aqueous neutralization of a strong acid with a strong base is exothermic by ca. 13 kcal/mol.

The lessons learned studying the *trans*-L_2M system are generally applicable toward the *cis*-L_2M system. The effect of the supporting L ligand is stronger than the effect of the metal center, whereas the reverse was true for the *trans*-L_2M system. This is because the L ligands are *trans* (and *cis*) to the substrate ligands, and they interact to a greater extent through the metal d orbitals than when the L ligands are merely *cis*.

The metal-carboxylate distances at the optimized geometries show that the M-O distance remains relatively unchanged (elongation by 0.005-0.010 Å) when the dmpp ligand is replaced by the bulky dppp ligand indicate that steric effects are not significant (Table VI-5). These changes in bond distances could be attributed to the electronics of the dppp ligand. For comparison, the sum of typical covalent radii are 2.12 and 1.98 Å for Ru-H and Ru-O respectively.[205]

Table VI-5. Metal-carboxylate distances (Å) of the *cis*-$L_2MH(O_2CY)$ complexes at their optimized geometries.

L	Ru-O (formate)	Ru-O (acetate)	Ru-O (benzoate)	Fe-O (formate)	Fe-O (acetate)	Fe-O (benzoate)
dmpp	2.194	2.208	2.207	2.062	2.084	2.079
dppp	2.199	2.213	2.213	2.080	2.084	2.095

Since the two factors (metal and supporting ligand) that control the thermodynamics of each step in the catalytic cycle do not appear tightly coupled, there is hope of finding an ideal catalyst system that is able to provide a feasible path for carboxylic acid formation. In the systems studied, the *cis*-$Ru(dppp)_2$ system is most ideal because the most endothermic step for each series of reactions is ca. 15 kcal/mol or less. This candidate can therefore be studied to determine if kinetics favors the proposed transformations. The *cis*-$Fe(dppp)_2$ also gives somewhat favorable thermodynamics for carboxylation reactions that are best coupled to subsequent exothermic reaction.

The thermodynamics of oxidative addition and carboxylation are achievable for the *cis*-$M(dmpp)_2$ complexes, but the reductive elimination step is forbidding (ΔH = 30 to 40 kcal/mol). If the last reaction were driven forward by a more exothermic reaction (without poisoning the catalyst with a Lewis base), these candidates may be workable. As a peripheral example, recent work by Limbach *et al.* demonstrates successful *catalytic* synthesis of sodium acrylate from ethylene, carbon dioxide, and a sodium base.[209] Their process is different in that no redox occurs at the metal center.

Summary and conclusions

The results of the computations are in good agreement with experimental observations. They amply show that the thermodynamics of the CO_2 insertion reaction is dictated by the electron density on the metal center, the choice of metal having the greatest influence, followed by the choice of supporting ligand, and the identity of the X ligands.

Preliminary results also indicate that the identity of the X ligands influence the barriers for CO_2 insertion.

These calculations predict that upon replacing dmpe in these ruthenium complexes with tmeda, these CO_2 insertion processes will be more thermodynamically and kinetically favored over their dmpe counterparts. On the other hand, replacing dmpe by dppe has the opposite negative effect of retarding the insertion reaction. Additionally, these calculations assert that CO_2 insertions into the corresponding Fe-H and Fe-CH_3 derivatives are both thermodynamically and kinetically favored over their ruthenium analogs.

It may be most beneficial to use computational chemistry to screen proposed catalytic reactions for their thermodynamic feasibility, prior to a detailed study of the intricacies of the individual reaction. This has been performed for the *cis*-L_2M system (L = dppm, dppp; M = Ru, Fe), and the results indicate that the *cis*-Ru(dppp)$_2$ gives the most favorable thermodynamics for the carboxylation of dihydrogen, methane, and benzene. The kinetics of the carboxylation reaction can be now be evaluated for this catalyst system.

Computational methods

All calculations were performed with the Gaussian 09 suite of programs.[127] To determine the thermodynamics of CO_2 insertion, geometry optimizations were performed using the B3LYP functional and the Pople-style all-electron 6-31G(d',p') basis set[141-143] on all non-metal atoms except for iodine, and the SDD basis set with an effective core potential for the iron, ruthenium, and iodine atoms (BS1). Local minima were confirmed by their vibrational frequencies (no imaginary vibrational modes). Single-point energy calculations using the B3LYP,[138-140] TPSS,[210] BP86,[138,211] and M06[212] functionals were performed with the 6-311G(d,p) basis set on non-metal atoms except for iodine, and the SDD basis set[186,213-214] for iron and ruthenium atoms (BS2). Thermal corrections obtained from the B3LYP/BS1 frequency calculation were applied thereafter. Enthalpies

discussed in this chapter were obtained from the B3LYP/BS2 single-point energy calculations, apart from the comparison of different functionals.

APT atomic charges[182] on the hydride ligands were obtained from frequency calculations performed at the B3LYP/BS1 level. Further such calculations were performed using a triple zeta basis set (BS2), and using this basis set with additional polarization and diffuse functions were performed. The APT charges did not change by more than 0.01 e, indicating that the BS1 level was adequate for this purpose.

To determine the barrier heights for CO_2 insertion, geometry optimizations were performed using the B3LYP functional and the 6-311++G(d,p) basis set[128,215] on all non-metal atoms, and the SDD basis set with an effective core potential for the metal atoms (BS2++). The saddle points found were confirmed to be the correct ones by visualizing the imaginary vibrational modes with AGUI[129] or Avogadro.[130]

CHAPTER VII

CONCLUSIONS AND PERSPECTIVES ON FUTURE WORK

Carbon dioxide is an increasingly importance source of inexpensive and non-toxic carbon for chemical manufacture. These efforts valorizing carbon dioxide help make its parallel large-scale capture and storage economically palatable, potentially slowing climate change caused by atmospheric CO_2's greenhouse effect.

Computational chemistry is a powerful ally to experimental work. Skillfully applied, *in silico* studies allow myriad systems, real or imagined, to be analyzed more rapidly than experiments may be practically conducted. Continued development in electronic structure theory gives rise to more accurate models, and improvements in computing power allow complicated systems to be better modeled. Most importantly, computational chemistry permits complex catalytic systems to be broken into constituent components and defeated in detail. Coupled with experimental kinetic studies, rational catalyst development may take place. Ultimately, these efforts allow resources (labor, materials, and energy) to be most profitably applied, thereby generating the least waste in the best tradition of green chemistry.

In this dissertation, the use of computational chemistry toward understanding CO_2 utilization was presented for the CO_2-epoxide copolymerization, and for the direct synthesis of carboxylic acids. The enthalpies and free energies of the overall copolymerization processes were tabulated in Chapter II. Concurrent publication has provided the literature with high-quality reference data in lieu of experimentally determined thermochemistry. Such data clarified that the commonly held understanding, that polymer and cyclic carbonate are the kinetic and thermodynamic products respectively, is actually due to entropic and not enthalpic factors. That is to say, polymer formation is actually more exothermic than cyclic carbonate formation, but that cyclic

carbonates dominate at high temperature due to entropy. Such fundamental information is useful, for example, in showing that poly(cyclopentene carbonate) is difficult to prepare because its formation is less strongly exothermic. On the other hand, poly(cyclohexene carbonate) was not found to be especially privileged, in that cyclic carbonate does not form due to kinetics, not thermodynamics.

In the attempt to model and understand the metal-catalyzed copolymerization reactions, various metal-free pathways were examined along the way. The metal-free carbonate and alkoxide backbiting reactions that lead to cyclic carbonates were modeled to determine their barriers for reaction. Poly(cyclohexene carbonate) was found to have an ordinary barrier for the elementary carbonate backbiting reaction, but a lower-energy relaxed chair conformation for the polymeric carbonate leads to a high overall barrier. Thus, that *cis*-cyclic carbonate is hardly observed. Conversely, *trans*-cyclopentene carbonate is not produced because angle strain causes the overall alkoxide backbiting reaction to have a free energy barrier almost twice that of most other polycarbonates'. Supporting current experimental efforts to prepare poly(1,4-dihydronaphthalene carbonate), we find that this polymeric carbonate has an accessible pathway to backbite to cyclic carbonate, despite its superficial similarity to poly(cyclohexene carbonate). The planar sp^2 backbone no longer participates in the 1,3-diaxial interactions that protected poly(cyclohexene carbonate) from degradation.

The power of computational chemistry to rapidly model and explain experimental results was showcased in Chapter III, where the unusual base-catalyzed degradation of poly(cyclopentene carbonate) to epoxide and CO_2 co-monomers was examined. In this case, all polymeric alkoxides may degrade to the epoxide in analogy to the halohydrin synthesis of epoxides. However, such degradation is only observed for poly(cyclopentene carbonate) because the usually-preferable alkoxide backbiting reaction (to give cyclic carbonate) is so strongly disfavored. Computations helped lead the way toward optimizing the degradation toward epoxide, rather than the less useful

cyclic carbonate, opening the door to reclaiming this polymer via monomer to give a recycled material with uncompromised physical properties.

There is growing interest in various glycerol carbonates, as they represent an ideal combination of glycerol (from biodiesel manufacture) and CO_2 waste streams. Particularly, 1,2-glycerol carbonate has been reported to decompose to glycidol and CO_2 when catalyzed with acids or bases; glycidol is popular for making functionalized copolymers with CO_2. Discussed in Chapter IV, computational investigations determined the free energy barriers of acid- and base-catalyzed pathways (the former is easier); they were also used to explain why 3-hydroxyoxetane (isomeric with glycidol) is never observed. A speculative mechanism of decarboxylation via oligomerization was also found to be unlikely.

In Chapter V, the metal-catalyzed copolymerization reaction was approached. Benchmarking identified M06 as an appropriate density functional for such work (useful to future workers), since it gives results equivalent to high-accuracy *ab initio* methods. The copolymerization of CO_2 with epoxides, catalyzed by chromium(III) and cobalt(III) salen complexes, were studied. Thermodynamics of the binding of ligands relevant to this copolymerization were calculated, and bond dissociation energies decreased in the order, polymeric alkoxide, polymeric carbonate, and epoxide. Cyclic carbonates do not competitively bind to the metal, so they are not expected to retard the copolymerization reaction. Electron-donating and electron-withdrawing methyl and fluorine substituents on the salen backbone were found to weaken and strengthen the metal-ligand interaction, although further work as to the reasons why is warranted.

While the elementary epoxide ring-opening reaction has a moderately high barrier, it is the overall displacement of a metal-bound polymeric carbonate by an epoxide, followed by epoxide ring-opening, that is rate limiting. Carboxylation of the ensuing alkoxide has a minor barrier. Metal-bound carbonate and alkoxide backbiting is also much harder due to the terminal oxygen atoms being much less nucleophilic upon coordination to the

Lewis acidic metal. Such a result definitively confirms what many workers in this field already believe: polycarbonate degradation only occurs away from the metal catalyst.

Switching gears from CO_2-epoxide chemistry, Chapter VI describes the factors controlling how favorably CO_2 inserts into metal-hydride and metal-carbon bonds. Specifically, CO_2 insertion into the M-X ligand of *trans*-ML_2XY complexes, depends most strongly on the identity of the metal center, the supporting L ligand, and the *trans* Y ligand. On the other hand, the supporting ligands for *cis*-ML_2XY complexes are both *cis* and *trans* to the ligand undergoing carboxylation, and trends are harder to reveal due to the more complicated situation.

A systematic study was carried out to understand the hypothetical direct carboxylation of dihydrogen, methane, and benzene, catalyzed by *cis*-ML_2XY complexes. Specifically, the thermodynamics of the oxidative addition, carboxylation, and reductive elimination steps were calculated, and *cis*-Fe$(dppp)_2XY$ and *cis*-Ru$(dppp)_2XY$ complexes were found most suitable for this transformation, kinetics notwithstanding. These computational results should therefore be verified experimentally. The most important lesson is that individual steps in the overall catalytic cycle cannot be optimized without regard for the whole.

Viewed alongside other computational efforts toward understanding the CO_2-epoxide copolymerization, this dissertation methodically surveys a variety of epoxides of interest to the Darensbourg research group, whereas these diverse epoxides have not been addressed in the literature. Careful benchmarking has given us better confidence in the quantitative accuracy of our results. Our computational results have been successful in explaining experimental observations. The quantitative approach has opened a new dimension with regard to the previously qualitative understanding of the copolymerization process. Reflecting advances in electronic structure theory and increases in computational power, we were able to study more complete systems using better models, and these results should provide a new baseline for further studies.

The Darensbourg group's experiments with different epoxides have suggested, empirically, that the sterically congested salen complexes (decorated with tert-butyl groups) appear to do poorly toward catalyzing the copolymerization of bulkier epoxides with CO_2. This is despite the common belief that steric bulk generally improves catalyst performance. Tetramethyltetraazaannulene complexes appear to do well as catalysts for copolymerizing these epoxides, and such activity is attributed to the larger saddle-shaped binding pocket available. A near term goal beyond this dissertation could be to understand the effect of ligand size and shape vis-à-vis the structure of the catalyst system using computational chemistry. The kinetics of the individual steps in the carboxylation of hydrogen or hydrocarbons should also be evaluated to find good routes from carbon dioxide to these commodity chemicals, avoiding the use of more expensive and much more toxic carbon monoxide gas.

On an aspirational note, I hope that the work presented in this dissertation represents one of thousands of baby steps in a growing movement toward using computational chemistry for the evaluation of novel complexes for catalysis. Coupled with rational catalyst design and verified by selected experiments, these efforts potentially yield large savings in resources for research and development. They may therefore accelerate the pace at which catalysts are found and put to work to make chemicals and materials that fulfill the needs of society.

REFERENCES

1. National Energy Technology Laboratory, DOE/NETL Carbon Dioxide Capture and Storage RD&D Roadmap, http://www.netl.doe.gov/technologies/carbon_seq/refshelf/CCSRoadmap.pdf, 2010.
2. National Energy Technology Laboratory, CO_2 Utilization Focus Area, http://www.netl.doe.gov/research/coal/carbon-storage/research-and-development/co2-utilization (accessed 2014-02-10).
3. von der Assen, N.; Jung, J.; Bardow, A. *Energy Environ. Sci.* **2013**, *6*, 2721.
4. Metcalfe, I. S.; North, M.; Pasquale, R.; Thursfield, A. *Energy Environ. Sci.* **2010**, *3*, 212.
5. North, M.; Wang, B.; Young, C. *Energy Environ. Sci.* **2011**, *4*, 4163.
6. Inoue, S.; Koinuma, H.; Tsuruta, T. *J. Polym. Sci., Part B: Polym. Lett.* **1969**, *7*, 287.
7. Empower Materials, http://www.empowermaterials.com/ (accessed 2014-08-20).
8. Novomer, http://www.novomer.com/ (accessed 2014-08-20).
9. Bayer MaterialScience, Turning Dreams into Value, http://www.news.bayer.com/baynews/baynews.nsf/id/98UBA6-Turning-dreams-into-value, 2013.
10. Darensbourg, D. J.; Holtcamp, M. W. *Coord. Chem. Rev.* **1996**, *153*, 155.
11. Coates, G. W.; Moore, D. R. *Angew. Chem., Int. Ed.* **2004**, *43*, 6618.
12. Sugimoto, H.; Inoue, S. *J. Polym. Sci., Part A: Polym. Chem.* **2004**, *42*, 5561.
13. Darensbourg, D. J.; Mackiewicz, R. M.; Phelps, A. L.; Billodeaux, D. R. *Acc. Chem. Res.* **2004**, *37*, 836.
14. Chisholm, M. H.; Zhou, Z. *J. Mater. Chem.* **2004**, *14*, 3081.
15. Darensbourg, D. J. *Chem. Rev.* **2007**, *107*, 2388.

16. Klaus, S.; Lehenmeier, M. W.; Anderson, C. E.; Rieger, B. *Coord. Chem. Rev.* **2011**, *255*, 1460.
17. Kember, M. R.; Buchard, A.; Williams, C. K. *Chem. Commun.* **2011**, *47*, 141.
18. Lu, X. B.; Darensbourg, D. J. *Chem. Soc. Rev.* **2012**, *41*, 1462.
19. Darensbourg, D. J.; Wilson, S. J. *Green Chem.* **2012**, *14*, 2665.
20. Lu, X.-B.; Ren, W.-M.; Wu, G.-P. *Acc. Chem. Res.* **2012**, *45*, 1721.
21. Darensbourg, D. J.; Holtcamp, M. W. *Macromolecules* **1995**, *28*, 7577.
22. Darensbourg, D. J.; Holtcamp, M. W.; Struck, G. E.; Zimmer, M. S.; Niezgoda, S. A.; Rainey, P.; Robertson, J. B.; Draper, J. D.; Reibenspies, J. H. *J. Am. Chem. Soc.* **1999**, *121*, 107.
23. Moore, D. R.; Cheng, M.; Lobkovsky, E. B.; Coates, G. W. *J. Am. Chem. Soc.* **2003**, *125*, 11911.
24. Jutz, F.; Buchard, A.; Kember, M. R.; Fredriksen, S. B.; Williams, C. K. *J. Am. Chem. Soc.* **2011**, *133*, 17395.
25. Hansen, K. B.; Leighton, J. L.; Jacobsen, E. N. *J. Am. Chem. Soc.* **1996**, *118*, 10924.
26. Thomas, R. M.; Widger, P. C. B.; Ahmed, S. M.; Jeske, R. C.; Hirahata, W.; Lobkovsky, E. B.; Coates, G. W. *J. Am. Chem. Soc.* **2010**, *132*, 16520.
27. Widger, P. C.; Ahmed, S. M.; Hirahata, W.; Thomas, R. M.; Lobkovsky, E. B.; Coates, G. W. *Chem. Commun.* **2010**, *46*, 2935.
28. Ahmed, S. M.; Poater, A.; Childers, M. I.; Widger, P. C.; LaPointe, A. M.; Lobkovsky, E. B.; Coates, G. W.; Cavallo, L. *J. Am. Chem. Soc.* **2013**, *135*, 18901.
29. Darensbourg, D. J.; Wilson, S. J. *J. Am. Chem. Soc.* **2011**, *133*, 18610.
30. Darensbourg, D. J.; Wilson, S. J. *Macromolecules* **2013**, *46*, 5929.
31. Byrne, C. M.; Allen, S. D.; Lobkovsky, E. B.; Coates, G. W. *J. Am. Chem. Soc.* **2004**, *126*, 11404.
32. Sonnati, M. O.; Amigoni, S.; Taffin de Givenchy, E. P.; Darmanin, T.; Choulet, O.; Guittard, F. *Green Chem.* **2013**, *15*, 283.

33. Ochoa-Gómez, J. R.; Gómez-Jiménez-Aberasturi, O.; Ramírez-López, C.; Belsué, M. *Org. Process Res. Dev.* **2012**, *16*, 389.
34. Zhang, H.; Grinstaff, M. W. *J. Am. Chem. Soc.* **2013**, *135*, 6806.
35. Geschwind, J.; Frey, H. *Macromolecules* **2013**, *46*, 3280.
36. Liu, Z.; Torrent, M.; Morokuma, K. *Organometallics* **2002**, *21*, 1056.
37. Drees, M.; Cokoja, M.; Kühn, F. E. *ChemCatChem* **2012**, *4*, 1703.
38. Fan, T.; Chen, X.; Lin, Z. *Chem. Commun.* **2012**, *48*, 10808.
39. Dadmun, M. D. *Computational Studies, Nanotechnology, and Solution Thermodynamics of Polymer Systems*; Kluwer Academic/Plenum Publishers: New York, 2001.
40. Stevens, M. P. *Polymer Chemistry: An Introduction*; Oxford University Press: New York, 1999.
41. Duda, A.; Kowalski, A. Thermodynamics and Kinetics of Ring-Opening Polymerization. In *Handbook of Ring-Opening Polymerization*; Wiley-VCH Verlag GmbH & Co. KGaA, 2009, p 1-51.
42. East, A. L. L. Entropy from Quantum Chemical Computations. In *Encyclopedia of Computational Chemistry*; John Wiley & Sons, Ltd, 2002.
43. Dainton, F. S.; Ivin, K. J. *Q. Rev. Chem. Soc.* **1958**, *12*, 61.
44. Blanksby, S. J.; Ellison, G. B. *Acc. Chem. Res.* **2003**, *36*, 255.
45. Benson, S. W. *J. Chem. Educ.* **1965**, *42*, 502.
46. Benson, S. W.; Buss, J. H. *J. Chem. Phys.* **1958**, *29*, 546.
47. Benson, S. W.; Cruickshank, F. R.; Golden, D. M.; Haugen, G. R.; O'Neal, H. E.; Rodgers, A. S.; Shaw, R.; Walsh, R. *Chem. Rev.* **1969**, *69*, 279.
48. Cohen, N.; Benson, S. W. *Chem. Rev.* **1993**, *93*, 2419.
49. Price, C. J.; Reich, B. J. E.; Miller, S. A. *Macromolecules* **2006**, *39*, 2751.
50. Brothers, E. N.; Izmaylov, A. F.; Rusakov, A. A.; Scuseria, G. E. *J. Phys. Chem. B* **2007**, *111*, 13869.
51. Kržan, A. *J. Mol. Struct. Theochem* **2009**, *902*, 49.
52. Goodman, J. M. *J. Chem. Inf. Model.* **1997**, *37*, 876.

53. Luttschwager, N. O.; Wassermann, T. N.; Mata, R. A.; Suhm, M. A. *Angew. Chem., Int. Ed. Engl.* **2013**, *52*, 463.
54. Byrd, J. N.; Bartlett, R. J.; Montgomery, J. A., Jr. *J. Phys. Chem. A* **2014**, *118*, 1706.
55. Lehenmeier, M. W.; Bruckmeier, C.; Klaus, S.; Dengler, J. E.; Deglmann, P.; Ott, A. K.; Rieger, B. *Chem. - Eur. J.* **2011**, *17*, 8858.
56. Chen, H.-Y.; Zhang, J.; Lin, C.-C.; Reibenspies, J. H.; Miller, S. A. *Green Chem.* **2007**, *9*, 1038.
57. Kazakov, A. F.; Muzny, C. D.; Chirico, R. D.; Diky, V.; Frenkel, M. *NIST/TRC Web Thermo Tables - Professional Edition NIST Standard Reference Subscription Database 3*; Thermodynamics Research Center: Boulder, CO, 2002.
58. Linstrom, P. J.; Mallard, W. G. *NIST Standard Reference Database Number 69*; National Institute of Standards and Technology: Gaithersburg, MD, 2005.
59. Marshall, E. L.; Gibson, V. C.; Rzepa, H. S. *J. Am. Chem. Soc.* **2005**, *127*, 6048.
60. Dove, A. P.; Gibson, V. C.; Marshall, E. L.; Rzepa, H. S.; White, A. J. P.; Williams, D. J. *J. Am. Chem. Soc.* **2006**, *128*, 9834.
61. Wang, L.; Kefalidis, C. E.; Sinbandhit, S.; Dorcet, V.; Carpentier, J. F.; Maron, L.; Sarazin, Y. *Chem. - Eur. J.* **2013**, *19*, 13463.
62. Miranda, M. O.; DePorre, Y.; Vazquez-Lima, H.; Johnson, M. A.; Marell, D. J.; Cramer, C. J.; Tolman, W. B. *Inorg. Chem.* **2013**, *52*, 13692.
63. Darensbourg, D. J.; Yeung, A. D. *Macromolecules* **2013**, *46*, 83.
64. Lehenmeier, M. W.; Kissling, S.; Altenbuchner, P. T.; Bruckmeier, C.; Deglmann, P.; Brym, A. K.; Rieger, B. *Angew. Chem., Int. Ed. Engl.* **2013**, *52*, 9821.
65. Buchard, A.; Jutz, F.; Kember, M. R.; White, A. J. P.; Rzepa, H. S.; Williams, C. K. *Macromolecules* **2012**, *45*, 6781.
66. Pan, X.; Liu, Z.; Cheng, R.; Jin, D.; He, X.; Liu, B. *J. Organomet. Chem.* **2014**, *753*, 63.
67. Luinstra, G. A.; Molnar, F. *Macromol. Symp.* **2007**, *259*, 203.

68. Rokicki, A. Making poly(alkylene carbonates) of controlled molecular weight. US Patent 4943677 A, 1990.
69. Jacobsen, E. N. *Acc. Chem. Res.* **2000**, *33*, 421.
70. Sun, K.; Li, W.-X.; Feng, Z.; Li, C. *Chem. Phys. Lett.* **2009**, *470*, 259.
71. Ford, D. D.; Nielsen, L. P.; Zuend, S. J.; Musgrave, C. B.; Jacobsen, E. N. *J. Am. Chem. Soc.* **2013**, *135*, 15595.
72. Cozzi, P. G. *Chem. Soc. Rev.* **2004**, *33*, 410.
73. Fang, J.; Walshe, A.; Maron, L.; Baker, R. J. *Inorg. Chem.* **2012**, *51*, 9132.
74. Curet-Arana, M. C.; Meza, P.; Irizarry, R.; Soler, R. *Top. Catal.* **2012**, *55*, 260.
75. Darensbourg, D. J.; Rokicki, A.; Darensbourg, M. Y. *J. Am. Chem. Soc.* **1981**, *103*, 3223.
76. Darensbourg, D. J.; Rokicki, A. *Organometallics* **1982**, *1*, 1685.
77. Darensbourg, D. J.; Hanckel, R. K.; Bauch, C. G.; Pala, M.; Simmons, D.; White, J. N. *J. Am. Chem. Soc.* **1985**, *107*, 7463.
78. Darensbourg, D. J.; Grotsch, G. *J. Am. Chem. Soc.* **1985**, *107*, 7473.
79. Darensbourg, D. J.; Wiegreffe, P.; Riordan, C. G. *J. Am. Chem. Soc.* **1990**, *112*, 5759.
80. Darensbourg, D. J.; Wiegreffe, H. P.; Wiegreffe, P. W. *J. Am. Chem. Soc.* **1990**, *112*, 9252.
81. Adhikari, D.; Nguyen, S. T.; Baik, M. H. *Chem. Commun.* **2014**, *50*, 2676.
82. Na, S. J.; S, S.; Cyriac, A.; Kim, B. E.; Yoo, J.; Kang, Y. K.; Han, S. J.; Lee, C.; Lee, B. Y. *Inorg. Chem.* **2009**, *48*, 10455.
83. Darensbourg, D. J.; Yarbrough, J. C.; Ortiz, C.; Fang, C. C. *J. Am. Chem. Soc.* **2003**, *125*, 7586.
84. Darensbourg, D. J.; Bottarelli, P.; Andreatta, J. R. *Macromolecules* **2007**, *40*, 7727.
85. Darensbourg, D. J.; Wei, S.-H. *Macromolecules* **2012**, *45*, 5916.
86. Luinstra, G. A.; Haas, G. R.; Molnar, F.; Bernhart, V.; Eberhardt, R.; Rieger, B. *Chem. - Eur. J.* **2005**, *11*, 6298.
87. North, M.; Pasquale, R.; Young, C. *Green Chem.* **2010**, *12*, 1514.

88. Decortes, A.; Castilla, A. M.; Kleij, A. W. *Angew. Chem., Int. Ed. Engl.* **2010**, *49*, 9822.
89. Sun, H.; Zhang, D. *J. Phys. Chem. A* **2007**, *111*, 8036.
90. Guo, C. H.; Wu, H. S.; Zhang, X. M.; Song, J. Y.; Zhang, X. *J. Phys. Chem. A* **2009**, *113*, 6710.
91. Ma, J.; Liu, J.; Zhang, Z.; Han, B. *Green Chem.* **2012**, *14*, 2410.
92. Castro-Gomez, F.; Salassa, G.; Kleij, A. W.; Bo, C. *Chem. - Eur. J.* **2013**, *19*, 6289.
93. Ren, Y.; Guo, C.-H.; Jia, J.-F.; Wu, H.-S. *J. Phys. Chem. A* **2011**, *115*, 2258.
94. Wang, J.-Q.; Dong, K.; Cheng, W.-G.; Sun, J.; Zhang, S.-J. *Catal. Sci. Tech.* **2012**, *2*, 1480.
95. Foltran, S.; Mereau, R.; Tassaing, T. *Catal. Sci. Tech.* **2014**, *4*, 1585.
96. Whiteoak, C. J.; Kielland, N.; Laserna, V.; Castro-Gomez, F.; Martin, E.; Escudero-Adan, E. C.; Bo, C.; Kleij, A. W. *Chem. - Eur. J.* **2014**, *20*, 2264.
97. Chen, F.; Li, X.; Wang, B.; Xu, T.; Chen, S. L.; Liu, P.; Hu, C. *Chem. - Eur. J.* **2012**, *18*, 9870.
98. Paddock, R. L.; Nguyen, S. T. *J. Am. Chem. Soc.* **2001**, *123*, 11498.
99. Guo, C.-H.; Song, J.-Y.; Jia, J.-F.; Zhang, X.-M.; Wu, H.-S. *Organometallics* **2010**, *29*, 2069.
100. Suh, H.-W.; Schmeier, T. J.; Hazari, N.; Kemp, R. A.; Takase, M. K. *Organometallics* **2012**, *31*, 8225.
101. Vogdanis, L.; Martens, B.; Uchtmann, H.; Hensel, F.; Heitz, W. *Makromol. Chem.* **1990**, *191*, 465.
102. Curtiss, L. A.; Redfern, P. C.; Raghavachari, K. *J. Chem. Phys.* **2007**, *126*, 084108.
103. Montgomery, J. A.; Frisch, M. J.; Ochterski, J. W.; Petersson, G. A. *J. Chem. Phys.* **1999**, *110*, 2822.
104. Ochterski, J. W.; Petersson, G. A.; Montgomery, J. A. *J. Chem. Phys.* **1996**, *104*, 2598.
105. Montgomery, J. A.; Frisch, M. J.; Ochterski, J. W.; Petersson, G. A. *J. Chem. Phys.* **2000**, *112*, 6532.

106. Curtiss, L. A.; Redfern, P. C.; Raghavachari, K.; Rassolov, V.; Pople, J. A. *J. Chem. Phys.* **1999**, *110*, 4703.
107. Verevkin, S. P.; Emel'yanenko, V. N.; Toktonov, A. V.; Chernyak, Y.; Schäffner, B.; Börner, A. *J. Chem. Thermodyn.* **2008**, *40*, 1428.
108. Parthiban, S.; de Oliveira, G.; Martin, J. M. L. *J. Phys. Chem. A* **2001**, *105*, 895.
109. Andruzzi, F.; Suradi, S.; Pilcher, G. *Makromol. Chem.* **1982**, *183*, 2183.
110. Pruckmayr, G.; Dreyfuss, P.; Dreyfuss, M. P. Polyethers, Tetrahydrofuran and Oxetane Polymers. In *Kirk-Othmer Encyclopedia of Chemical Technology*; John Wiley & Sons, Inc., 2000.
111. Darensbourg, D. J.; Moncada, A. I. *Macromolecules* **2009**, *42*, 4063.
112. Chan, S. I.; Zinn, J.; Fernandez, J.; Gwinn, W. D. *J. Chem. Phys.* **1960**, *33*, 1643.
113. Chan, S. I.; Zinn, J.; Gwinn, W. D. *J. Chem. Phys.* **1961**, *34*, 1319.
114. Chan, S. I.; Borgers, T. R.; Russell, J. W.; Strauss, H. L.; Gwinn, W. D. *J. Chem. Phys.* **1966**, *44*, 1103.
115. Lewars, E. G. *Computational Chemistry*; Springer Netherlands, 2011.
116. Bachrach, S. M. Organic Reactions of Anions. In *Computational Organic Chemistry*; John Wiley: Hoboken, N.J., 2007, p 279-347.
117. Petersson, G. Complete Basis Set Models for Chemical Reactivity: from the Helium Atom to Enzyme Kinetics. In *Quantum-Mechanical Prediction of Thermochemical Data*; Cioslowski, J., Ed.; Springer Netherlands, 2002; Vol. 22, p 99-130.
118. Haynes, W. M. *CRC Handbook of Chemistry & Physics*; 92nd ed.; CRC Press, 2011.
119. Darensbourg, D. J.; Moncada, A. I.; Wei, S.-H. *Macromolecules* **2011**, *44*, 2568.
120. Matsuo, J.; Aoki, K.; Sanda, F.; Endo, T. *Macromolecules* **1998**, *31*, 4432.
121. Jung, M. E.; Piizzi, G. *Chem. Rev.* **2005**, *105*, 1735.
122. Darensbourg, D. J.; Kyran, S. J.; Yeung, A. D. **2014**, in preparation.
123. Østergaard, J.; Larsen, C. *Molecules* **2007**, *12*, 2396.
124. Limpanuparb, T.; Punyain, K.; Tantirungrotechai, Y. *J. Mol. Struct. Theochem* **2010**, *955*, 23.

125. Darensbourg, D. J.; Yeung, A. D.; Wei, S.-H. *Green Chem.* **2013**, *15*, 1578.
126. Wheeler, S. E.; Moran, A.; Pieniazek, S. N.; Houk, K. N. *J. Phys. Chem. A* **2009**, *113*, 10376.
127. Gaussian 09. Frisch, M. J.; Trucks, G. W.; Schlegel, H. B.; Scuseria, G. E.; Robb, M. A.; Cheeseman, J. R.; Scalmani, G.; Barone, V.; Mennucci, B.; Petersson, G. A.; Nakatsuji, H.; Caricato, M.; Li, X.; Hratchian, H. P.; Izmaylov, A. F.; Bloino, J.; Zheng, G.; Sonnenberg, J. L.; Hada, M.; Ehara, M.; Toyota, K.; Fukuda, R.; Hasegawa, J.; Ishida, M.; Nakajima, T.; Honda, Y.; Kitao, O.; Nakai, H.; Vreven, T.; Montgomery, J. A., Jr.; Peralta, J. E.; Ogliaro, F.; Bearpark, M.; Heyd, J. J.; Brothers, E.; Kudin, K. N.; Staroverov, V. N.; Kobayashi, R.; Normand, J.; Raghavachari, K.; Rendell, A.; Burant, J. C.; Iyengar, S. S.; Tomasi, J.; Cossi, M.; Rega, N.; Millam, J. M.; Klene, M.; Knox, J. E.; Cross, J. B.; Bakken, V.; Adamo, C.; Jaramillo, J.; Gomperts, R.; Stratmann, R. E.; Yazyev, O.; Austin, A. J.; Cammi, R.; Pomelli, C.; Ochterski, J. W.; Martin, R. L.; Morokuma, K.; Zakrzewski, V. G.; Voth, G. A.; Salvador, P.; Dannenberg, J. J.; Dapprich, S.; Daniels, A. D.; Farkas, Ö.; Foresman, J. B.; Ortiz, J. V.; Cioslowski, J.; Fox, D. J. Gaussian Inc., Wallingford CT, 2009.
128. Krishnan, R.; Binkley, J. S.; Seeger, R.; Pople, J. A. *J. Chem. Phys.* **1980**, *72*, 650.
129. Ampac GUI 9. Semichem, Inc., 2008.
130. Hanwell, M. D.; Curtis, D. E.; Lonie, D. C.; Vandermeersch, T.; Zurek, E.; Hutchison, G. R. *J. Cheminf.* **2012**, *4*, 17.
131. Marenich, A. V.; Cramer, C. J.; Truhlar, D. G. *J. Phys. Chem. B* **2009**, *113*, 6378.
132. Liu, J.; Ren, W.-M.; Liu, Y.; Lu, X.-B. *Macromolecules* **2013**, *46*, 1343.
133. Al-Salem, S. M.; Lettieri, P.; Baeyens, J. *Waste Manage. (Oxford, U. K.)* **2009**, *29*, 2625.
134. Darensbourg, D. J.; Wei, S.-H.; Yeung, A. D.; Ellis, W. C. *Macromolecules* **2013**, *46*, 5850.
135. Iqbal, S. M.; Owen, L. N. *J. Chem. Soc.* **1960**, 1030.
136. Darensbourg, D. J.; Wilson, S. J.; Yeung, A. D. *Macromolecules* **2013**, *46*, 8102.

137. Heston, B. O.; Dermer, O. C.; Woodside, J. A. *Proc. Okl. Acad. Sci.* **1942**, *23*, 67.
138. Becke, A. D. *J. Chem. Phys.* **1993**, *98*, 5648.
139. Lee, C.; Yang, W.; Parr, R. G. *Phys. Rev. B* **1988**, *37*, 785.
140. Vosko, S. H.; Wilk, L.; Nusair, M. *Can. J. Phys.* **1980**, *58*, 1200.
141. Petersson, G. A.; Bennett, A.; Tensfeldt, T. G.; Al-Laham, M. A.; Shirley, W. A.; Mantzaris, J. *J. Chem. Phys.* **1988**, *89*, 2193.
142. Petersson, G. A.; Al-Laham, M. A. *J. Chem. Phys.* **1991**, *94*, 6081.
143. Petersson, G. A.; Tensfeldt, T. G.; Montgomery, J. A. *J. Chem. Phys.* **1991**, *94*, 6091.
144. Christoph, R.; Schmidt, B.; Steinberner, U.; Dilla, W.; Karinen, R. Glycerol. In *Ullmann's Encyclopedia of Industrial Chemistry*; Wiley-VCH Verlag GmbH & Co. KGaA, 2006.
145. Aresta, M. Carbon Dioxide Utilization: Greening Both the Energy and Chemical Industry: An Overview. In *Utilization of Greenhouse Gases*; American Chemical Society, 2003; Vol. 852, p 2-39.
146. Ray, W. C., III; Grinstaff, M. W. *Macromolecules* **2003**, *36*, 3557.
147. Parzuchowski, P. G.; Jaroch, M.; Tryznowski, M.; Rokicki, G. *Macromolecules* **2008**, *41*, 3859.
148. Simon, J.; Olsson, J. V.; Kim, H.; Tenney, I. F.; Waymouth, R. M. *Macromolecules* **2012**, *45*, 9275.
149. Hilf, J.; Frey, H. *Macromol. Rapid Commun.* **2013**, *34*, 1395.
150. Łukaszczyk, J.; Jaszcz, K.; Kuran, W.; Listoś, T. *Macromol. Biosci.* **2001**, *1*, 282.
151. Zhou, Q.; Gu, L.; Gao, Y.; Qin, Y.; Wang, X.; Wang, F. *J. Polym. Sci., Part A: Polym. Chem.* **2013**, *51*, 1893.
152. Mun, N.-Y.; Kim, K.-H.; Park, D.-W.; Choe, Y.; Kim, I. *Korean J. Chem. Eng.* **2005**, *22*, 556.
153. Ren, W.-M.; Liang, M.-W.; Xu, Y.-C.; Lu, X.-B. *Polym. Chem.* **2013**, *4*, 4425.
154. Geschwind, J.; Frey, H. *Macromol. Rapid Commun.* **2013**, *34*, 150.
155. Hilf, J.; Phillips, A.; Frey, H. *Polym. Chem.* **2014**, *5*, 814.

156. Malkemus, J. D.; Currier, V. A.; Bell, J. B., Jr. Method for prepraring glycidol. US Patent 2,856,413, 1958.
157. Yoo, J.-W.; Mouloungui, Z.; Gaset, A. Method for producing an epoxide, in particular of glycidol, and installation for implementation. US Patent 6316641 B1, 2001.
158. Dibenedetto, A.; Angelini, A.; Aresta, M.; Ethiraj, J.; Fragale, C.; Nocito, F. *Tetrahedron* **2011**, *67*, 1308.
159. Seki, Y.; Sasa, T.; Takeuchi, H.; Uno, M.; Namba, M. Process for producing glycidol. US Patent 7868192 B1, 2011.
160. Bolívar-Diaz, C. L.; Calvino-Casilda, V.; Rubio-Marcos, F.; Fernández, J. F.; Bañares, M. A. *Appl. Catal., B* **2013**, *129*, 575.
161. Ochoa-Gómez, J. R.; Gómez-Jiménez-Aberasturi, O.; Ramírez-López, C.; Maestro-Madurga, B. *Green Chem.* **2012**, *14*, 3368.
162. Gumlich, K.; Merten, R.; Teles, J. H. Process for preparing glycidyl esters. US Patent 8236974 B2, 2012.
163. Choi, J. S.; Simanjuntaka, F. S. H.; Oh, J. Y.; Lee, K. I.; Lee, S. D.; Cheong, M.; Kim, H. S.; Lee, H. *J. Catal.* **2013**, *297*, 248.
164. Parameswaram, G.; Srinivas, M.; Babu, B. H.; Prasad, P. S. S.; Lingaiah, N. *Catal. Sci. Tech.* **2013**, *3*, 3242.
165. Iaych, K.; Dumarçay, S.; Fredon, E.; Gérardin, C.; Lemor, A.; Gérardin, P. *J. Appl. Polym. Sci.* **2011**, *120*, 2354.
166. Muniz Filho, R. C.; de Sousa, S. A.; Pereira Fda, S.; Ferreira, M. M. *J. Phys. Chem. A* **2010**, *114*, 5187.
167. Darensbourg, D. J.; Chung, W.-C. *Polyhedron* **2013**, *58*, 139.
168. Hunter, E. P.; Lias, S. G. Proton Affinity Evaluation. In *NIST Chemistry WebBook, NIST Standard Reference Database Number 69*; Linstrom, P. J., Mallard, W. G., Eds.; National Institute of Standards and Technology: Gaithersburg, MD.
169. Ariga, T.; Takata, T.; Endo, T. *Macromolecules* **1997**, *30*, 737.

170. Rokicki, G.; Rakoczy, P.; Parzuchowski, P.; Sobiecki, M. *Green Chem.* **2005**, *7*, 529.
171. Tomczyk, K. M.; Guńka, P. A.; Parzuchowski, P. G.; Zachara, J.; Rokicki, G. *Green Chem.* **2012**, *14*, 1749.
172. Rokicki, G. *Prog. Polym. Sci.* **2000**, *25*, 259.
173. Darensbourg, D. J.; Yeung, A. D. *Polym. Chem.* **2014**, *5*, 3949.
174. Cramer, C. J.; Truhlar, D. G. *Phys. Chem. Chem. Phys.* **2009**, *11*, 10757.
175. Ohkawara, T.; Suzuki, K.; Nakano, K.; Mori, S.; Nozaki, K. *J. Am. Chem. Soc.* **2014**, *136*, 10728.
176. Darensbourg, D. J.; Wildeson, J. R.; Yarbrough, J. C.; Reibenspies, J. H. *J. Am. Chem. Soc.* **2000**, *122*, 12487.
177. Sinnokrot, M. O.; Valeev, E. F.; Sherrill, C. D. *J. Am. Chem. Soc.* **2002**, *124*, 10887.
178. Zhao, Y.; Truhlar, D. G. *Theor. Chem. Acc.* **2008**, *120*, 215.
179. Arunan, E.; Gutowsky, H. S. *J. Chem. Phys.* **1993**, *98*, 4294.
180. Gonzales, J. M.; Cox, R. S.; Brown, S. T.; Allen, W. D.; Schaefer, H. F. *J. Phys. Chem. A* **2001**, *105*, 11327.
181. Darensbourg, D. J.; Chung, W. C.; Wilson, S. J. *ACS Catal.* **2013**, *3*, 3050.
182. Cioslowski, J. *J. Am. Chem. Soc.* **1989**, *111*, 8333.
183. Cao, T.-P.-A.; Buchard, A.; Le Goff, X. F.; Auffrant, A.; Williams, C. K. *Inorg. Chem.* **2012**, *51*, 2157.
184. Darensbourg, D. J.; Fitch, S. B. *Inorg. Chem.* **2007**, *46*, 5474.
185. Stewart, J. J. *J. Mol. Model.* **2007**, *13*, 1173.
186. Dolg, M.; Wedig, U.; Stoll, H.; Preuss, H. *J. Chem. Phys.* **1987**, *86*, 866.
187. Zhao, Y.; Truhlar, D. G. *J. Chem. Phys.* **2006**, *125*, 194101.
188. Schaftenaar, G.; Noordik, J. H. *J. Comput.-Aided Mol. Des.* **2000**, *14*, 123.
189. Macrae, C. F.; Bruno, I. J.; Chisholm, J. A.; Edgington, P. R.; McCabe, P.; Pidcock, E.; Rodriguez-Monge, L.; Taylor, R.; van de Streek, J.; Wood, P. A. *J. Appl. Crystallogr.* **2008**, *41*, 466.

190. Darensbourg, D. J.; Kudaroski, R. A. *Adv. Organomet. Chem.* **1983**, *22*, 129.
191. Gibson, D. H. *Chem. Rev.* **1996**, *96*, 2063.
192. Gibson, D. H. *Coord. Chem. Rev.* **1999**, *185-186*, 335.
193. Riduan, S. N.; Zhang, Y. *Dalton Trans.* **2010**, *39*, 3347.
194. Aresta, M.; Dibenedetto, A. *Dalton Trans.* **2007**, 2975.
195. Louie, J. *Curr. Org. Chem.* **2005**, *9*, 605.
196. Braunstein, P.; Fryzuk, M. D.; Le Dall, M.; Naud, F.; Rettig, S. J.; Speiser, F. *J. Chem. Soc., Dalton Trans.* **2000**, 1067.
197. Michel, O.; Törnroos, K. W.; Maichle-Mössmer, C.; Anwander, R. *Eur. J. Inorg. Chem.* **2012**, *2012*, 44.
198. Leitner, W. *Coord. Chem. Rev.* **1996**, *153*, 257.
199. Jessop, P. G.; Joó, F.; Tai, C.-C. *Coord. Chem. Rev.* **2004**, *248*, 2425.
200. Jessop, P. G.; Ikariya, T.; Noyori, R. *Chem. Rev.* **1995**, *95*, 259.
201. Allen, O. R.; Dalgarno, S. J.; Field, L. D.; Jensen, P.; Willis, A. C. *Organometallics* **2009**, *28*, 2385.
202. Aresta, M.; Dibenedetto, A.; Angelini, A. *Chem. Rev.* **2014**, *114*, 1709.
203. Jessop, P. G.; Ikariya, T.; Noyori, R. *Nature* **1994**, *368*, 231.
204. Darensbourg, D. J.; Kyran, S. J.; Yeung, A. D.; Bengali, A. A. *Eur. J. Inorg. Chem.* **2013**, 4024.
205. Cordero, B.; Gomez, V.; Platero-Prats, A. E.; Reves, M.; Echeverria, J.; Cremades, E.; Barragan, F.; Alvarez, S. *Dalton Trans.* **2008**, 2832.
206. Field, L. D.; Lawrenz, E. T.; Shaw, W. J.; Turner, P. *Inorg. Chem.* **2000**, *39*, 5632.
207. Allen, O. R.; Dalgarno, S. J.; Field, L. D.; Jensen, P.; Turnbull, A. J.; Willis, A. C. *Organometallics* **2008**, *27*, 2092.
208. Labinger, J. A.; Bercaw, J. E. *Organometallics* **1988**, *7*, 926.
209. Lejkowski, M. L.; Lindner, R.; Kageyama, T.; Bodizs, G. E.; Plessow, P. N.; Muller, I. B.; Schafer, A.; Rominger, F.; Hofmann, P.; Futter, C.; Schunk, S. A.; Limbach, M. *Chem. - Eur. J.* **2012**, *18*, 14017.
210. Tao, J.; Perdew, J.; Staroverov, V.; Scuseria, G. *Phys. Rev. Lett.* **2003**, *91*, 146401.

211. Perdew, J. P. *Phys. Rev. B* **1986**, *33*, 8822.
212. Lynch, B. J.; Truhlar, D. G. *J. Phys. Chem. A* **2001**, *105*, 2936.
213. Igel-Mann, G.; Stoll, H.; Preuss, H. *Mol. Phys.* **1988**, *65*, 1321.
214. Andrae, D.; Häußermann, U.; Dolg, M.; Stoll, H.; Preuß, H. *Theor. Chim. Acta* **1990**, *77*, 123.
215. McLean, A. D.; Chandler, G. S. *J. Chem. Phys.* **1980**, *72*, 5639.